AD_____

Award Number: DAMD17-98-1-8298

TITLE: Mechanisms for Breast Cancer Cell Resistance to Doxorubicin and Solutions to Resistance and Side Effects

PRINCIPAL INVESTIGATOR: Tad H. Koch, Ph.D.

CONTRACTING ORGANIZATION: University of Colorado
Boulder, Colorado 80309-0019

REPORT DATE: October 2001

TYPE OF REPORT: Final

PREPARED FOR: U.S. Army Medical Research and Materiel Command
Fort Detrick, Maryland 21702-5012

NOTICE

USING GOVERNMENT DRAWINGS, SPECIFICATIONS, OR OTHER DATA INCLUDED IN THIS DOCUMENT FOR ANY PURPOSE OTHER THAN GOVERNMENT PROCUREMENT DOES NOT IN ANY WAY OBLIGATE THE U.S. GOVERNMENT. THE FACT THAT THE GOVERNMENT FORMULATED OR SUPPLIED THE DRAWINGS, SPECIFICATIONS, OR OTHER DATA DOES NOT LICENSE THE HOLDER OR ANY OTHER PERSON OR CORPORATION; OR CONVEY ANY RIGHTS OR PERMISSION TO MANUFACTURE, USE, OR SELL ANY PATENTED INVENTION THAT MAY RELATE TO THEM.

LIMITED RIGHTS LEGEND

Award Number: DAMD17-98-1-8298
Organization: University of Colorado

Those portions of the technical data contained in this report marked as limited rights data shall not, without the written permission of the above contractor, be (a) released or disclosed outside the government, (b) used by the Government for manufacture or, in the case of computer software documentation, for preparing the same or similar computer software, or (c) used by a party other than the Government, except that the Government may release or disclose technical data to persons outside the Government, or permit the use of technical data by such persons, if (i) such release, disclosure, or use is necessary for emergency repair or overhaul or (ii) is a release or disclosure of technical data (other than detailed manufacturing or process data) to, or use of such data by, a foreign government that is in the interest of the Government and is required for evaluational or informational purposes, provided in either case that such release, disclosure or use is made subject to a prohibition that the person to whom the data is released or disclosed may not further use, release or disclose such data, and the contractor or subcontractor or subcontractor asserting the restriction is notified of such release, disclosure or use. This legend, together with the indications of the portions of this data which are subject to such limitations, shall be included on any reproduction hereof which includes any part of the portions subject to such limitations.

THIS TECHNICAL REPORT HAS BEEN REVIEWED AND IS APPROVED FOR PUBLICATION.

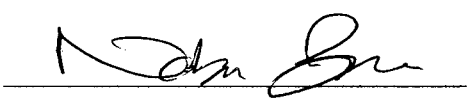

7/15/02

_____ _____

REPORT DOCUMENTATION PAGE

Form Approved
OMB No. 074-0188

1. AGENCY USE ONLY (Leave blank)	2. REPORT DATE	3. REPORT TYPE AND DATES COVERED
	October 2001	Final (15 Sep 98 - 14 Sep 01)

4. TITLE AND SUBTITLE
Mechanisms for Breast Cancer Cell Resistance to Doxorubicin and Solutions to Resistance and Side Effects

5. FUNDING NUMBERS
DAMD17-98-1-8298

6. AUTHOR(S)
Tad H. Koch, Ph.D.

7. PERFORMING ORGANIZATION NAME(S) AND ADDRESS(ES)
University of Colorado
Boulder, Colorado 80309-0019

E-Mail: tad.kcoh@colorado.edu

8. PERFORMING ORGANIZATION REPORT NUMBER

9. SPONSORING / MONITORING AGENCY NAME(S) AND ADDRESS(ES)
U.S. Army Medical Research and Materiel Command
Fort Detrick, Maryland 21702-5012

10. SPONSORING / MONITORING AGENCY REPORT NUMBER

11. SUPPLEMENTARY NOTES
Report contains color.

12a. DISTRIBUTION / AVAILABILITY STATEMENT
Distribution authorized to U.S. Government agencies only (proprietary information, Oct 01). Other requests for this document shall be referred to U.S. Army Medical Research and Materiel Command, 504 Scott Street, Fort Detrick, Maryland 21702-5012.

12b. DISTRIBUTION CODE

13. ABSTRACT *(Maximum 200 Words)*

The anthracyclines, doxorubicin and epidoxorubicin, continue to be important drugs for the treatment of breast cancer. Recent studies refocus attention to anthracycline-alkylation and crosslinking of DNA as important toxic events triggering cell death. The long term goals of the proposed research are to establish the mechanism for the crosslinking, to produce new mechanism-based anthracycline derivatives which will be active against resistant breast cancer, and to develop a delivery vehicles for the improved drugs. New derivatives have been synthesized and characterized as the formaldehyde conjugates of doxorubicin and epidoxorubicin, doxoform and epidoxoform, respectively. The following results were obtained during the grant period: 1) The crystal structure of epidoxorubicin-alkylated DNA shows the epidoxorubicin virtually crosslinking the DNA at NGC sites. 2) Flow cytometry measurements show drug-formaldehyde conjugates are taken up better by both sensitive and resistant breast cancer cells and retained longer than their clinical counterparts. 3) The nucleus of both sensitive and resistant cancer cells is the primary target for drug-formaldehyde conjugates. 4) Drug-formaldehyde conjugates are more toxic to breast cancer cells than confluent mammary epithelial cells. 5) Sensitive but not resistant breast cancer cells show anthracycline induction of formaldehyde synthesis. 6) Sensitive but not resistant breast cancer cells show measurable formaldehyde levels. 7) Apoptosis assays of drug-treated cells show similar patterns for doxorubicin and doxoform consistent with doxoform being a prodrug to the doxorubicin active metabolite. 8) Epidoxoform shows broad spectrum toxicity to human cancer cells including resistant cancer cells. 9) Epidoxoform can be formulated in DMSO/Cremaphor as a drug delivery vehicle. 10) Conjugation to glutathione is not a resistance mechanism for doxorubicin. 11) Peroxidation of unsaturated lipid is not a source of formaldehyde.

14. SUBJECT TERMS
Breast Cancer, Doxorubicin, Epidoxorubicin, Formaldehyde, Drug Mechanism, Drug Resistance

15. NUMBER OF PAGES
65

16. PRICE CODE

17. SECURITY CLASSIFICATION OF REPORT	18. SECURITY CLASSIFICATION OF THIS PAGE	19. SECURITY CLASSIFICATION OF ABSTRACT	20. LIMITATION OF ABSTRACT
Unclassified	Unclassified	Unclassified	Unlimited

Table of Contents

(4) INTRODUCTION

Preliminary experiments with deoxyoligonucleotides indicated that the anthracycline antitumor drug, doxorubicin, covalently bonds to DNA through its catalysis of formaldehyde production (1-3). Subsequently, it utilizes formaldehyde for covalent attachment to DNA from its 3'-amino group to the 2-amino group of a G-base (4-6). At a 3'-GC-5' site the combination of drug intercalation, covalent bonding to one strand and hydrogen bonding to the other strand serves to virtually crosslink the DNA (7). This mechanistic understanding prompted the synthesis of anthracycline formaldehyde conjugates as improved antitumor drugs (8, 9). The first conjugate synthesized, doxoform, proved to be highly toxic to sensitive and resistant breast cancer cells; however, doxoform rapidly hydrolyzes to doxorubicin under physiological conditions (8). The purpose and scope of the research were to design and synthesize a hydrolytically more stable anthracycline-formaldehyde conjugate, to establish that anthracyclines derive at least some of their toxicity to tumor cells from covalent bonding to DNA, to determine why anthracycline-formaldehyde conjugates overcome at least some resistance mechanisms, and to a develop drug delivery vehicle for anthracycline-formaldehyde conjugates.

(5) BODY

Research Accomplishments

During the grant period the following questions were addressed:

Can a more stable doxorubicin-formaldehyde conjugate be designed and synthesized? (Objective 7) Doxoform has a predicted half-life of less than 10 min in the vascular system with respect to hydrolysis to doxorubicin and formaldehyde. This half-life was predicted to be too short for eventual use of doxoform in humans. As a result design and synthesis of alternate formaldehyde conjugates were explored. The epimer of doxorubicin, epidoxorubicin, was reacted with formaldehyde to yield a dimeric conjugate, Epidoxoform, with a diazadioxabicyclic structure. This structure contrasts with that of doxoform which is a dimeric conjugate with a bisoxazolidinylmethane structure. The structural difference results from the stereochemistry at the 4'-position. Epidoxoform has a predicted half-life of more than 2 h in the vascular system with respect to hydrolysis to epidoxorubicin and formaldehyde. The IC50 values (concentrations which inhibit half the growth) for 3 h epidoxoform treatment of MCF-7 and MCF-7/Adr cells are 65 and 70 nmolar equiv/L relative to 200 and >10,000 for epidoxorubicin. Furthermore, preincubation of epidoxoform in cell culture medium containing 10% fetal bovine serum for 6 h at 37 °C increased the IC50 value for MCF-7/ADR treated cells only to 300 nmolar equiv/L. Although the IC50 value for doxoform is approximately 50-fold lower, doxoform loses all of its activity against MCF-7/ADR cells in less than 30 min of preincubation.

Six doxorubicin-formaldehyde N-Mannich bases were synthesized and evaluated for water solubility, hydrolytic stability, and toxicity to MCF-7 and MCF-7/Adr cells. They all demonstrated increased water solubility relative to doxoform and epidoxoform. Toxicity was inversely related to hydrolytic stability. The N-Mannich base with a half-life of 75 min was selected for further development into drugs specifically targeted to cancer cells and associated angiogenesis. A drug design for treatment of breast cancer was submitted to the Army Breast Cancer Program for a predoctoral fellowship; a second design for treatment of breast cancer and associated angiogenesis was submitted to the NIH; a design for treatment of prostate cancer was submitted to the Army Prostate Cancer Research Program; and a design for the treatment of lung cancer was submitted to the Colorado Tobacco Related Disease Research Program. All of these applications were funded except the application to the Colorado Tobacco Related Disease Research Program which just missed the funding line. Almost all of the group research efforts are now focused on synthesis and evaluation of targeted doxorubicin-formaldehyde conjugates stabilized as N-Mannich bases.

Do doxoform and epidoxoform actually form a covalent bond to DNA in sensitive and resistant breast cancer cells and how do they circumvent resistance? (Objective 3) Because of the emerging importance of

Epidoxoform, the structure of the covalent adduct from reaction of epidoxorubicn and formaldehyde with DNA was determined by crystallography. The adduct from reaction of epidoxorubicin and formaldehyde with the self complementary deoxyoligonucleotide CGCGCG was crystallized and the structure solved by molecular replacement. Comparison with the x-ray structure of the adduct from reaction of daunorubicin and formaldehyde with the same deoxyoligonucleotide showed an additional hydrogen bonding interaction from the epimeric 4'-hydroxyl group to the bonded DNA strand; however, hydrogen bonding interactions to the opposing strand appeared to be weaker.

Indirect evidence for formation of covalent bonds to DNA in cells was obtained from a tritium labeling experiment. Doxoform was synthesized from tritiated formaldehyde. Sensitive (MCF-7) and resistant (MCF-7/ADR) cells were treated with tritiated doxoform for 1 h. Treatment with doxorubicin + tritiated formaldehyde or tritiated formaldehyde for 1 h were used as controls. Cells were lysed and the contents separated into DNA, RNA, and protein fractions, and the fractions were counted in a scintillation counter. Both sensitive and resistant cells treated with tritiated doxoform showed approximately twice as many counts in DNA than cells treated with doxorubicin + tritiated formaldehyde or with tritiated formaldehyde. Hence, tritiated formaldehyde appears to reach the nucleus of both sensitive and resistant breast cancer cells.

Uptake and release of drug from doxorubicin, doxoform, epidoxorubicin, and epidoxoform treated MCF-7 and MCF-7/ADR cells was measured by flow cytometry using drug fluorescence as a measure of drug in cells. MCF-7 cells took up more of all four drugs than MCF-7/ADR cells, and both cell lines took up substantially more of the formaldehyde conjugates than the clinical drugs. Furthermore, both cell lines retained the conjugates hours after drug treatment while the clinical drugs were expelled within 1 h of drug treatment. The rate of uptake of formaldehyde conjugates appeared to parallel the rate of partial hydrolysis to monomeric forms. The half-life for this partial hydrolysis of epidoxoform is 2 h and for doxoform less than 10 min.

The location of drug in cells was studied by fluorescence microscopy. The nucleus was the primary location of drug fluorescence from treatment of MCF-7 cells with doxorubicin, Doxoform, epidoxorubicin, or Epidoxoform. Similar strong fluorescence was observed in the nuclei of MCF-7/ADR cells treated with doxoform or epidoxoform; however, drug fluorescence was very weak in MCF-7/ADR cells treated with doxorubicin or epidoxorubicin. The rate of appearance of drug fluorescence in cells treated with the formaldehyde conjugates paralleled the rate of partial hydrolysis which paralleled the rate of drug uptake observed by flow cytometry.

The conclusions from the structural determination, tritium labeling experiment, flow cytometry measurements, and fluorescence microscopy are that drug-formaldehyde conjugates are more toxic to both sensitive and resistant breast cancer cells because more of the conjugates reach the nucleus and are retained longer. Further, dimeric conjugates must partially hydrolyze to monomeric conjugates before drug uptake occurs. A structural difference which may permit higher levels of drug uptake is the lack of positive charge on the conjugates in their monomeric form. Conjugation with formaldehyde is predicted to change the pKa such that the drugs are not protonated at physiological pH.

How toxic are doxoform and epidoxoform to non-malignant cells? (Objectives 1 and 2) Doses of doxoform and doxorubicin which killed 50% of breast cancer cells (MCF-7) and human mammary epithelial cells (HME) (LC50) were established. The measurement with HME cells was performed at confluence and with MCF-7 cells, at non-confluence to reflect their natural states. The LC50 for HME cells treated with doxorubicin was 12-fold greater than for MCF-7 cells; correspondingly, the LC50 for HME cells treated with doxoform was 6-fold greater than for MCF-7 cells. Similar results were observed in a comparison of epidoxoform with epidoxorubicin. Hence, these cell experiments showed similar selectivity for the anthracycline and its formaldehyde conjugate in killing breast cancer cells over normal mammary epithelial cells.

What is the abundance of formaldehyde in sensitive tumor cells, resistant tumor cells and/or non-malignant cells with and without addition of daunorubicin or doxorubicin? The abundance of formaldehyde in sensitive MCF-7 and resistant MCF-7/Adr breast cancer cells was measured using selected ion flow tube mass spectrometry by sampling the head space above cell lysates (10). No formaldehyde above background levels was observed in the media containing growing, sensitive or resistant cells with or without drug treatment. Drug treated sensitive cells, but not resistant cells, showed formaldehyde levels above background when lysed. A lower limit for excess formaldehyde in MCF-7 cells treated with 0.5 μM daunorubicin for 24 h is 0.3 mM. This result supports a mechanism for drug cytotoxicity which involves drug induction of metabolic processes leading to formaldehyde production followed by drug utilization of formaldehyde to virtually cross-link DNA.

A new technique, which involved preconcentration of formaldehyde in cell lysates by distillation coupled with selected ion flow tube mass spectrometry, was subsequently developed to measure natural levels of formaldehyde in sensitive and resistant cancer cells. This showed 1.5 μM formaldehyde in sensitive MCF-7 cells and only background levels in MCF-7/Adr cells (0.1 μM). This result is consistent with MCF-7/Adr cells overexpressing enzymes which neutralize oxidative stress leading to formaldehyde production.

Does doxoform cause tumor cell death by apoptosis? (Objectives 4 and 5) We originally proposed to establish that doxoform caused topoisomerase mediated lesions with assistance from Professor David Kroll of the University of Colorado Health Sciences Center (Objective 4). Experiments were started but were not completed because Professor Kroll moved his lab to Duke University. We also proposed in Objective 5 to determine if Doxoform affected protein kinase C with help from Professor Katheryn Resing. These experiments were started but not completed because Professor Resing changed her research direction away from protein kinase C and was no longer able to provide the required assistance. These events led us to answer a different but related question: does doxoform cause tumor cell death by mechanisms analogous to that of doxorubicin. Three different apoptosis assays were used to compare doxorubicin and doxoform with respect to induction of programmed cell death. The assays were formation of a DNA ladder, the TUNNEL assay, and annexin V/propidium iodide staining. The assays were performed with Hela S_3, MCF-7 and MCF-7/Adr cells. Doxoform was used at 10-fold lower dose because of the 10-fold higher cytotoxicity of Doxoform. At these relative doses doxorubicin and doxoform gave the same response with all three cell lines: apoptotic death of Hela S_3 cells and non-apoptotic death of MCF-7 and MCF-7/Adr cells. This result supports the hypothesis that doxoform is a prodrug to the active metabolite of doxorubicin.

How does epidoxoform compare with epidoxorubicin and doxorubicin in the NCI tumor cell screen? (Objective 7) Epidoxoform (EPIF) was submitted to the National Cancer Institute Developmental Therapeutics Program for screening in their 60 human tumor cell assay. The log of the concentration of drug which inhibited 50% of the growth is compared in Table 1 with values for doxorubicin (DOX) and epidoxorubicin (EPI). Values which measure tumor cell resistance mechanisms, rhodamine efflux, multidrug resistance gene (*mdr-1*), multidrug resistance protein (MRP), and lung resistance protein (LRP), are compared for some cell lines. The mean values for the three drugs show that epidoxoform is approximately 0.5 log more cytotoxic than doxorubicin and 1 log more cytotoxic than epidoxorubicin. Further, epidoxoform is active against cells which express all three resistance proteins: MDR, MRP, and LRP.

Table 1. National Cancer Institute (NCI) In-Vitro Human Tumor Cell Screen and Tumor Cell Resistance Parameters

Panel/Cell Line	**log GI50 (M)**			**rhodamine[d] efflux**	***mdr-1*[d]**	**MRP[d]**	**LRP[d]**
	EPIF[a]	**DOX[b]**	**EPI[c]**				
Leukemia							
CCRF-CEM	-8.52	-7.46	-7.35	35	0.4	1.2	0.0
HTL-60 (TB)	-8.57	-7.29	-7.24				

MOLT-4	-8.60	-7.96	-7.77				
RPMI-8226	-8.31	-7.35	-7.26				
Non Small Cell Lung Carcinoma (NSCLC)							
A549/ATCC	-7.89	-7.14	-7.10				
EKVX	-7.07	-6.17	-6.52				
HOP-62	-7.66	-7.30	-6.82	62	3.4	1.3	1.7
HOP-92	-7.82	-7.09	-6.51				
NCI-H226	-7.44	-7.29	-7.36				
NCI-H23	-7.92	-6.96	-7.12				
NCI-H322M	-7.55	-6.31	-6.04				
NCI-H460	-8.35	-8.33	-7.60				
NCI-H522	-8.17	-7.22	-6.72				
Colon Cancer							
COLO 205	-7.90	-6.67	-6.30				
HCC-2998	-7.12	-6.63	-6.51	-5	0.1	1.1	2.0
HCT-116	-7.78	-7.18	-7.17	26	5.8	1.8	2.5
HCT-15	-6.93	-5.88	-5.41	414	457	1.6	0.1
HT29	-7.70	-6.73	-6.51				
KM12	-7.34	-6.56	-6.43				
SW-620	-7.98	-7.12	-6.91	31	19.4	0.8	0.3
Central Nervous System Cancer							
SF-268	-8.20	-6.96	-6.66				
SF-295	-7.51	-7.04	-6.68	91	8.3	1.6	0.8
SF-539	-8.26	-7.16	-6.71				
SNB-19	-7.82	-7.31	-7.04				
SNB-75	-8.12	-7.04	-6.60				
U251	-8.11	-7.39	-7.07	-19	2.7	1.1	0.1
Melanoma							
MALME-3M	-7.80	-7.16	-6.85				
M14	-7.30	-6.66	-6.37				
SK-MEL-2	-7.64	-6.63	-6.70	11	2.8	0.8	0.1
SK-MEL-28	-7.31	-6.56	-6.23				
SK-MEL-5	-7.35	-7.17	-6.95	12	13	2.3	1.6
UACC-257	-7.28	-6.66	-6.47				
UACC-62	-8.30	-7.19	-6.82				
Ovarian Cancer							
IGROV1	-7.76	-6.87	-6.57				
OVCAR-3	-7.33	-6.40	-6.33				
OVCAR-4	-6.98	-6.19	-5.92	-4	0.1	2.0	1.0
OVCAR-5	-7.05	-6.28	-6.14				
OVCAR-8	-7.75	-6.88	-6.70				
SK-OV-3	-6.88	-6.66	-6.39				
Renal Cancer							
786-0	-8.10	-7.31	-7.00	-44	18.4	0.5	1.5
A498	-8.42	-6.98	-	108	71	-	-
ACHN	-8.09	-7.21	-6.57	120	31	0.0	1.5
CAKI-1	-7.76	-6.77	-6.57	171	177	0.4	2.3
SN12C	-7.80	-7.04	-6.77	-86	2.2	0.4	1.5

TK-10	-6.63	-6.39	-6.14				
UO-31	-6.84	-6.13	-5.72	244	749	1.8	2.4
Prostate Cancer							
PC-3	-7.30	-6.70	-6.62				
DU-145	-7.92	-6.83	-6.57				
Breast Cancer							
MCF-7/ADR-RES	-6.49	-4.78	-				
MDA-MB-231/ATCC	-7.32	-6.41	-6.02				
HS-578T	-7.21	-6.71	-8.00				
MDA-MB-435	-7.19	-6.51	-6.21				
MDA-N	-7.28	-6.58	-6.86				
BT-549	-6.93	-6.62	-6.36				
T-47D	-7.16	-7.04	-7.03				
Mean							
	-7.64	**-6.87**	**-6.70**				

[a]Single determination with log maximum concentration (M) = -4.6.

[b]Average of multiple determinations with log maximum concentration (M) = -4.6.

[c]Single determination with log maximum concentration (M) = -4.0.

[d]Values obtained from the NCI Developmental Therapeutics Program web site: http://dtp.nci.nih.gov/; MRP (multidrug resistant protein), LRP, lung resistant protein.

Why is doxorubicin more cytotoxic than epidoxorubicin, and doxoform more cytotoxic than epidoxoform? (Objective 7) An important cytotoxicity factor appears to be the rate of release of drug from the nucleus. This was measured for drug release from MCF-7/Adr cells by flow cytometry using drug fluorescence as a measure of drug in cells. MCF-7/Adr cells overexpress P-170 efflux pump and hence will excrete drug as soon as it is released from the nucleus by hydrolysis of drug DNA covalent adducts and drug DNA virtual crosslinks. The kinetics were fit to a biexponential rate law consistent with the kinetics of release of drug from DNA (1, 11). With doxorubicin and doxoform the half-life for the more rapid release was 2 h and for the slow release 29 h and with epidoxorubicin and Epidoxoform, 4 h and 13 h, respectively. The important factor is likely the slow component of release which is proposed to result from hydrolysis of drug-DNA virtual crosslinks.

Can doxoform and epidoxoform be stabilized with respect to hydrolysis in a liposome as a drug delivery vehicle? (Objective 6) The stability of both doxoform and epidoxoform was measured in several drug delivery vehicles: mono lamellar liposomes, multi lamellar liposomes, and surfactants. The drug delivery vehicle which gave the best stabilization with respect to hydrolysis and dissolved the most drug was DMSO/Cremaphor EL. When a solution of epidoxoform in 40% DMSO / 60% Cremaphor EL was added to a pH 7.4 buffer at 37 °C, no precipitation of drug occurred and only a trace amount of hydrolysis to epidoxorubicin was observed even after 90 min. Both liposomal delivery systems were less effective primarily because they dissolved much less drug.

Is conjugation of anthracycline anit-tumor drugs to glutathione a resistance mechanism? (Additional Relevant Study) One of the proposed mechanisms for multidrug resistance relies on the ability of resistant tumor cells to efficiently promote glutathione S-transferase (GST)-catalyzed glutathione (GSH) conjugation of the antitumor drug. This type of conjugation, observed in several families of drugs, has never been documented satisfactorily for anthracyclines. Doxorubicin-resistant human breast cancer MCF-7/Adr cells, presenting a comparable GSH concentration, but a 14-fold increase of the GST P1-1 activity relative to the sensitive MCF-7 cells, were treated with doxorubicin in the presence of verapamil, an inhibitor of the P-170 glycoprotein drug transport protein, and scrutinized for any production of GSH-

doxorubicin conjugates. HPLC analysis of cell content and culture broth using synthetic standards of potential conjugates showed unequivocally that no GSH-conjugates were present either inside the cell or in the culture broth. The only anthracycline present inside cells after 24 hr of incubation was >98% pure doxorubicin. Confocal laser scanning microscopic observation showed that in MCR-7/Adr cells doxorubicin was localized mostly in the Golgi apparatus rather than in the nucleus, the preferred site of accumulation for sensitive MCF-7 cells. These findings rule out GSH conjugation or any other significant biochemical transformation as the basis for resistance to doxorubicin and as a ground for the anomalous localization of the drug in the resistant cells.

What is the carbon source of formaldehyde produced by anthracyclines in cells? (Additional Relevant Study) We proposed spermine and spermidine, which are elevated in cancer cells, as possible carbon sources for formaldehyde in doxorubicin or daunorubicin treated cancer cells. However, the literature proposes that formaldehyde is one of many products of peroxidation of unsaturated lipids. In fact, Tamura and co-workers reported some years ago that formaldehyde is the most abundant aldehyde from iron catalyzed peroxidation of arachidonic acid, linolenic acid, oleic acid and the second most abundant for oxidation of linoleic acid (12). We have reinvestigated the Tamura experiment because it was performed in Tris buffer. Earlier we reported that iron catalyzed peroxidation of Tris yields formaldehyde (7). Our experiments now demonstrate that most if not all of the formaldehyde observed by Tamura came from peroxidation of the buffer and that the unsaturated lipids in phosphate buffer yielded only background levels of formaldehyde. This result has prompted us to reconsider doxorubicin catalyzed peroxidation of spermine and spermidine as a reaction path to formaldehyde in vivo.

Can the formaldehyde conjugate of the redox incapacitated anthracycline, 5-iminodoxorubicin, be synthesized? (Objective 8) This was not attempted because we decided that the design and synthesis of doxorubicin-formaldehyde conjugates specifically targeted to tumor cells and angiogenesis was a better strategy for overcoming cardiotoxicity of doxorubicin. Experiments have begun in this area and additional research funding was obtained from the Army Prostate Cancer Program, the Army Breast Cancer Program and the National Cancer Institute to carry it forward.

(6) KEY RESEARCH ACCOMPLISHMENTS:

Epidoxoform, the dimeric formaldehyde conjugate of epidoxorubicin, is hydrolytically more stable with respect to complete hydrolysis to the clinical drug than Doxoform, the dimeric formaldehyde conjugate of doxorubicin.

Anthracycline-formaldehyde conjugates are equally toxic to sensitive and resistant breast cancer cells.

Anthracycline-formaldehyde conjugates are taken up better and retained longer by sensitive and resistant breast cancer cells than their clinical counterparts.

The nucleus is the primary target of anthracycline-formaldehyde conjugates in sensitive and resistant breast cancer cells.

The formaldehyde of doxoform reaches DNA in cells.

Dimeric anthracycline-formaldehyde conjugates must partially hydrolyze to monomeric anthracycline-formaldehyde conjugates before they are taken up by breast cancer cells.

Doxorubicin and daunorubicin induce production of formaldehyde in sensitive breast cancer cells but not in resistant breast cancer cells.

Sensitive breast cancer cells show 10-fold higher levels of formaldehyde than resistant breast cancer cells.

Doxoform at 10-fold lower dose functions the same as doxorubicin with respect to induction of apoptosis.

Epidoxoform inhibits the growth of 60 human tumor cell lines 0.5 log better than doxorubicin and 1 log better than epidoxorubicin.

Higher toxicity of doxorubicin relative to epidoxorubicin correlates with a longer half-life for the respective drug-DNA virtual crosslink.

A promising drug delivery vehicle for epidoxoform is 40% DMSO/ 60% Cremaphor EL.

Conjugation to glutathione does not appear to be a resistance mechanism for doxorubicin.

Peroxidation of unsaturated lipid does not appear to be a pathway to formaldehyde.

A design strategy for targeting doxoform to tumor cells was achieved.

(7) REPORTABLE OUTCOMES:

- publications and manuscripts

Taatjes, D. J.; Fenick, D. J.; Koch, T. H. "Nuclear Targeting and Nuclear Retention of Anthracycline-Formaldehyde Conjugates Implicates DNA Covalent Bonding in the Cytotoxic Mechanism of Anthracyclines" *Chem. Res. Toxicol. 12,* 588-596 (1999).

Podell, E. R.; Harrington, D. J.; Taatjes, D. J.; Koch, T. H. "Crystal Structure of Epidoxoform-formaldehyde *Virtual Crosslink* of DNA and Evidence for Its Formation in Human Breast Cancer Cells" *Acta Cryst., D55*, 1516-1523 (1999).

Gaudiano, G.; Koch, T. H.; Lo Bello, M.; Nuccetelli, M.; Ravagnan, G.; Serafino, A.; Sinibaldi-Vallebona, P. "Lack of Glutathione Conjugation to Adriamycin in Human Breast Cancer MCF-7/DOX Cells. Inhibition of Glutathione S-Transferase P1-1 by Glutathione Conjugates from Anthracyclines" *Biochem. Pharmacol. 60,* 1915-1923 (2000).

Taatjes, D. J.; Koch, T. H. "Nuclear Targeting and Retention of Anthracycline Antitumor Drugs in Sensitive and Resistant Tumor Cells" *Curr. Med. Chem.,7,* 15-29 (2001).

Kato, S.; Burke, P. J.; Koch, T. H.; Bierbaum, V. M. "Formaldehyde in Human Cancer Cells: Detection by Preconcentration-Chemical Ionization Mass Spectrometry" *Anal. Chem. 73,* 2992-2997 (2001).

Burke, P. J.; Koch, T. H. "Doxorubicin-formaldehyde Conjugate, Doxoform: Induction of apoptosis Relative to Doxorubicin" *Anticancer Res. 21*, 2753-2760 (2001)

Dernell, W. S.; Powers, B. E.; Taatjes, D. J.; Cogan, P.; Gaudiano, G.; Koch, T. H. "Evaluation of the Epidoxorubicin-formaldehyde Conjugate, Epidoxoform, in a Mouse Mammary Carcinoma Model" *Cancer Invest.*, in press (2001).

- abstracts

"Nuclear Targeting and Nuclear Retention of Anthracycline-formaldehyde conjugates", T. H. Koch, D. J. Taatjes, D. J. Fenick, Era Of Hope Meeting, Atlanta, GA, June 2000.

"Anthracycline-Formaldehyde Conjugates: Growth Inhibition, Nuclear Uptake, and Retention in Breast and Prostate Cancer Cells", T. H. Koch, D. J. Taatjes, D. J. Fenick, American Chemical Society National Meeting, Anaheim, CA, March 1999.

"Evaluation of the Epidoxoform-formaldehyde Conjugate, Epidoxoform, in a Mouse Mammary Carcinoma Model", Dernell, W. S.; Powers, B.; Taatjes, D. J.; Cogan, P. ; Gaudiano, G.; Koch, T. H., Colorado Institute for Research in Biotechnology Symposium, Colorado State University, Ft. Collins, CO, September 2000.

"Evaluation of the Epidoxoform-formaldehyde Conjugate, Epidoxoform, in a Mouse Mammary Carcinoma Model", Dernell, W. S.; Powers, B.; Taatjes, D. J.; Cogan, P. ; Gaudiano, G.; Koch, T. H., Colorado Alliance for Bioengineering, University of Colorado Health Sciences Center, Aurora, CO, December 2000.

"The Anthracycline-formaldehyde conjugate, Doxoform, retains the apoptosis-inducing characteristics of doxorubicin at 10-fold lower drug levels", Burke, P. J.; Koch, T. H., American Association for Cancer Research National Meeting, New Orleans, LA, March 2001.

- presentations

"Anthracycline-Formaldehyde Conjugates: Growth Inhibition, Nuclear Uptake, and Retention in Breast and Prostate Cancer Cells", T. H. Koch, D. J. Taatjes, D. J. Fenick, American Chemical Society National Meeting, Anaheim, CA, March 1999.

"Cytotoxic Mechanism for Anthracycline Antitumor Drugs and New Anthracycline-formaldehyde Conjugates Toxic to Resistant Cancer Cells", T. H. Koch, D. J. Taatjes, D. J. Fenick, S. Kato, P. J. Burke, V. Bierbaum, P. Cogan, E. R. Podell, D. J. Harrington, CU Roche Symposium on Synthetic Chemistry, May 2000.

"Nuclear Targeting and Nuclear Retention of Anthracycline-formaldehyde conjugates", T. H. Koch, D. J. Taatjes, D. J. Fenick, Era Of Hope Meeting, Atlanta, GA, June 2000.

"Evaluation of the Epidoxoform-formaldehyde Conjugate, Epidoxoform, in a Mouse Mammary Carcinoma Model", Dernell, W. S.; Powers, B.; Taatjes, D. J.; Cogan, P. ; Gaudiano, G.; Koch, T. H., Colorado Institute for Research in Biotechnology Symposium, Colorado State University, Ft. Collins, CO, September 2000.

"Evaluation of the Epidoxoform-formaldehyde Conjugate, Epidoxoform, in a Mouse Mammary Carcinoma Model", Dernell, W. S.; Powers, B.; Taatjes, D. J.; Cogan, P. ; Gaudiano, G.; Koch, T. H., Colorado Alliance for Bioengineering, University of Colorado Health Sciences Center, Aurora, CO, December 2000.

"The Anthracycline-formaldehyde conjugate, Doxoform, retains the apoptosis-inducing characteristics of doxorubicin at 10-fold lower drug levels", Burke, P. J.; Koch, T. H., American Association for Cancer Research National Meeting, New Orleans, LA, March 2001.

"Improved Anti-Tumor Drugs from Mechanistic Studies of Doxorubicin and Epidoxorubicin", T. H. Koch, Dylan, Taatjes, Giorgio Gaudiano, David Fenick, P. J. Burke, Peter Cogan, Catherine Fowler, Kimberly Maleski, Michael Coleman, Array BioPharma/CU Symposium, Boulder, CO, June 2001.

- degrees

  Catherine Fowler, M.S. degree with thesis.

- new grants

  NIH, "New Drugs Targeted to Metastatic Cancer and Angiogenesis", Tad H. Koch, P.I., 7/01/01-6/30/04, $587,474 (total costs).

  U.S. Army Medical Research and Material Command, "Design, Synthesis, and Evaluation of Activated Doxorubicin Targeted to Advanced Prostate Cancer", Tad H. Koch, P.I., 6/1/01-5/30/04, $532,291 (total costs).

  U.S. Army Medical Research and Material Command, "Synthesis and Evaluation of an Activated Doxorubicin Targeted to breast Cancer", Predoctoral Fellowship to Patrick J. Burke, 6/1/01-5/30/04, $66,000 (direct costs).

(8) PERSONNEL SUPPORTED

Tad Koch, P.I., professor of chemistry and biochemistry

Giorgio Gaudiano, senior research associate

Catherine Fowler, graduate research assistant

Dylan Taatjes, postdoctoral research associate

Patrick Burke, graduate research associate

Peter Cogan, graduate research assistant

Michael Coleman, postdoctoral research associate

Glen Post, graduate research assistant

Kimberly Malesky, graduate research assistant

Elizabeth Ashley, research assistant

(9) CONCLUSIONS

The results from the research provide additional support for the hypothesis that the anthracycline antitumor drugs derive at least some of their toxicity from induction of formaldehyde synthesis and use of formaldehyde for drug-covalent bonding to DNA. Sensitive but not resistant breast cancer cells show anthracycline induction of formaldehyde synthesis. Also, resistant breast cancer cells show less natural abundance of formaldehyde than sensitive cells. Apoptosis assays show similar patterns with doxorubicin and doxoform. Relative cytotoxicity of doxorubicin and epidoxorubicin correlates with the rate of drug release from resistant cells which parallels the rate of hydrolysis of drug-DNA virtual crosslinks. At least some resistance to anthracyclines stems from resistance to drug induction of formaldehyde synthesis but from conjugation to glutathione. Peroxidation of unsaturated lipids does not appear to be a source of drug induced formaldehyde synthesis. Anthracycline-formaldehyde conjugates overcome resistance mechanisms associated with inhibition of formaldehyde synthesis and expression of MDR, MRP and LRP resistance proteins and are prodrugs of anthracycline active metabolites. Epidoxoform can be formulated in DMSO/Cremaphor as a drug delivery vehicle.

(10) REFERENCES

(1) Cullinane, C., van Rosmalen, A. and Phillips, D. R. (1994) Does adriamycin induce interstrand cross-links in DNA? *Biochemistry* 33, 4632-4638.

(2) Taatjes, D. J., Gaudiano, G., Resing, K. and Koch, T. H. (1996) Alkylation of DNA by the Anthracycline, Antitumor Drugs Adriamycin and Daunomycin. *J. Med. Chem.* 39, 4135-4138.

(3) Taatjes, D. J., Gaudiano, G. and Koch, T. H. (1997) Production of formaldehyde and DNA-adriamycin or -daunomycin adducts, initiated through redox chemistry of DTT/iron, xanthine oxidase/NADH/iron, or glutathione/iron. *Chem. Res. Toxicol.* 10, 953-961.

(4) Wang, A. H. J., Gao, Y. G., Liaw, Y. C. and Li, Y. K. (1991) Formaldehyde cross-links daunorubicin and DNA efficiently: HPLC and X-ray diffraction studies. *Biochemistry* 30, 3812-3815.

(5) Zeman, S. M., Phillips, D. R. and Crothers, D. M. (1998) Characterization of covalent adriamycin-DNA adducts. *Proc. Natl. Acad. Sci. USA* 95, 11561-11565.

(6) Podell, E. R., Harrington, D. J., Taatjes, D. J. and Koch, T. H. (1999) Crystal structure of epidoxorubicin-formaldehyde virtual crosslink of DNA and evidence for its formation in human breast-cancer cells. *Acta Cryst.* D55, 1516-1523.

(7) Taatjes, D. J., Gaudiano, G., Resing, K. and Koch, T. H. (1997) A redox pathway leading to the alkylation of DNA by the anthracycline, anti-tumor drugs, adriamycin and daunomycin. *J. Med. Chem.* 40, 1276-1286.

(8) Fenick, D. J., Taatjes, D. J. and Koch, T. H. (1997) Doxoform and Daunoform: anthracycline-formaldehyde conjugates toxic to resistant tumor cells. *J. Med. Chem.* 40, 2452-2461.

(9) Taatjes, D. J., Fenick, D. J. and Koch, T. H. (1998) Epidoxoform: a hydrolytically more stable anthracycline-formaldehyde conjugate, cytotoxic to resistant tumor cells. *J. Med. Chem.* 41, 1306-1314.

(10) Kato, S., Burke, P. J., Fenick, D. J., Taatjes, D. J., Bierbaum, V. M. and Koch, T. H. (2000) Mass spectrometric measurement of formaldehyde generated in breast cancer cells upon treatment with anthracycline antitumor drugs. *Chem. Res. Toxicol.* 13, 509-516.

(11) van Rosmalen, A., Cullinane, C., Cutts, S. M. and Phillips, D. R. (1995) Stability of adriamycin-induced DNA adducts and interstrand crosslinks. *Nucleic Acids Res.* 23, 42-50.

(12) Tamura, H.; Kitta, K.; Shibamoto (1991) Formation of reactive aldehydes from fatty acids in a Fe^{2+} /H-2-O-2- Oxidation System. *J. Agra. Food Chem. 39*, 430-442.

(11) APPENDICES:

Manuscripts published acknowledging support:

Taatjes, D. J.; Fenick, D. J.; Koch, T. H. "Nuclear Targeting and Nuclear Retention of Anthracycline-Formaldehyde Conjugates Implicates DNA Covalent Bonding in the Cytotoxic Mechanism of Anthracyclines" *Chem. Res. Toxicol. 12,* 588-596 (1999).

Podell, E. R.; Harrington, D. J.; Taatjes, D. J.; Koch, T. H. "Crystal Structure of Epidoxoform-formaldehyde *Virtual Crosslink* of DNA and Evidence for Its Formation in Human Breast Cancer Cells" *Acta Cryst., D55*, 1516-1523 (1999).

Gaudiano, G.; Koch, T. H.; Lo Bello, M.; Nuccetelli, M.; Ravagnan, G.; Serafino, A.; Sinibaldi-Vallebona, P. "Lack of Glutathione Conjugation to Adriamycin in Human Breast Cancer MCF-7/DOX Cells. Inhibition of Glutathione S-Transferase P1-1 by Glutathione Conjugates from Anthracyclines" *Biochem. Pharmacol. 60,* 1915-1923 (2000).

Taatjes, D. J.; Koch, T. H. "Nuclear Targeting and Retention of Anthracycline Antitumor Drugs in Sensitive and Resistant Tumor Cells" *Curr. Med. Chem.,7,* 15-29 (2001).

Kato, S.; Burke, P. J.; Koch, T. H.; Bierbaum, V. M. "Formaldehyde in Human Cancer Cells: Detection by Preconcentration-Chemical Ionization Mass Spectrometry" *Anal. Chem. 73,* 2992-2997 (2001).

Burke, P. J.; Koch, T. H. "Doxorubicin-formaldehyde Conjugate, Doxoform: Induction of apoptosis Relative to Doxorubicin" *Anticancer Res. 21*, 2753-2760 (2001)

Nuclear Targeting and Nuclear Retention of Anthracycline–Formaldehyde Conjugates Implicates DNA Covalent Bonding in the Cytotoxic Mechanism of Anthracyclines

Dylan J. Taatjes, David J. Fenick, and Tad H. Koch

Department of Chemistry and Biochemistry, University of Colorado, Boulder, Colorado 80309-0215, and University of Colorado Cancer Center, Denver, Colorado 80262

Chemical Research in Toxicology®

Reprinted from
Volume 12, Number 7, Pages 588–596

Nuclear Targeting and Nuclear Retention of Anthracycline−Formaldehyde Conjugates Implicates DNA Covalent Bonding in the Cytotoxic Mechanism of Anthracyclines

Dylan J. Taatjes, David J. Fenick, and Tad H. Koch*

Department of Chemistry and Biochemistry, University of Colorado, Boulder, Colorado 80309-0215, and University of Colorado Cancer Center, Denver, Colorado 80262

Received January 15, 1999

The anthracycline, antitumor drugs doxorubicin (DOX), daunorubicin (DAU), and epidoxorubicin (EPI) catalyze production of formaldehyde through induction of oxidative stress. The formaldehyde then mediates covalent bonding of the drugs to DNA. Synthetic formaldehyde conjugates of DOX, DAU, and EPI, denoted Doxoform (DOXF), Daunoform (DAUF), and Epidoxoform (EPIF), exhibit enhanced toxicity to anthracycline-sensitive and -resistant tumor cells. Uptake and retention of parent anthracycline antitumor drugs (DOX, DAU, and EPI) relative to those of their formaldehyde conjugates (DOXF, DAUF, and EPIF) were assessed by flow cytometry in both drug-sensitive MCF-7 cells and drug-resistant MCF-7/ADR cells. The MCF-7 cells took up more than twice as much drug as the MCF-7/ADR cells, and both cell lines took up substantially more of the formaldehyde conjugates than the parent drugs. Both MCF-7 and MCF-7/ADR cells retained fluorophore from DOXF, DAUF, and EPIF hours after drug removal, while both cell lines almost completely expelled DOX, DAU, and EPI within 1 h. Longer treatment with DOX, DAU, and EPI resulted in modest drug retention in MCF-7 cells following drug removal but poor retention of DOX, DAU, and EPI in MCF-7/ADR cells. Fluorescence microscopy showed that the formaldehyde conjugates targeted the nuclei of both sensitive and resistant cells, and remained in the nucleus hours after drug removal. Experiments in which [^{3}H]Doxoform was used, synthesized from doxorubicin and [^{3}H]-formaldehyde, also indicated that Doxoform targeted the nucleus. Elevated levels of ^{3}H were observed in DNA isolated from [^{3}H]Doxoform-treated MCF-7 and MCF-7/ADR cells relative to controls. The results implicate drug−DNA covalent bonding in the tumor cell toxicity mechanism of these anthracyclines.

Introduction

The anthracycline, antitumor drugs doxorubicin (DOX)[1] and daunorubicin (DAU) remain an important part of chemotherapy regimens in the clinic. Epidoxorubicin (EPI), the 4′-epimer of doxorubicin, is also a widely used chemotherapeutic agent that is marketed worldwide except in the United States (*1*). DNA is an important target for the anthracyclines, with induction of topoisomerase II-mediated strand breaks as a cytotoxic consequence (*2*, *3*). The drugs are high-affinity DNA intercalators (*4*) and are known to form unstable covalent bonds to extracellular DNA when activated under redox conditions (*5*, *6*). Two types of covalent bonding based upon differences in stability have been described: more stable drug−DNA cross-links and less stable drug−DNA adducts (*7*). With previous extracellular experiments, we established that DOX, DAU, and EPI promote the production of formaldehyde through induction of oxidative stress in the presence of ferric ion (*8*, *9*). The iron-chelating ability of the anthracyclines is proposed to be an important factor for the efficient production of formaldehyde near the drug for formation of a drug−formaldehyde conjugate at the drug's 3′-amino substituent. This intermediate is thought to be the active drug metabolite which bonds to DNA forming a covalent methylene linkage to the 2-amino group of a G-base as shown in Scheme 1. At 5′-NGC-3′ sites, drug intercalation, covalent bonding, and hydrogen bonding at the C9 hydroxyl combine to form a *virtual DNA cross-link* (Scheme 1) (*8*, *10*−*12*). This *virtual DNA cross-link* corresponds to the drug−DNA cross-link described earlier (5−7). The drug−DNA adduct is presumed to have a similar structure without the hydrogen bonding interaction from the C9 hydroxyl to the G-base on the opposing strand. Throughout this paper, the term drug−DNA adduct is used to describe both types of drug−DNA bonding. Covalent attachment of DOX, DAU, or EPI to DNA is likely to be at least partially responsible for the drugs' toxicity to tumor cells (*13*−*15*), possibly in conjuction with its effect on the topoisomerase−DNA complex.

A major problem associated with cancer chemotherapy with the anthracyclines as well as other antitumor drugs is specific resistance and multidrug resistance. Multiple

* To whom correspondence should be addressed at the University of Colorado, Boulder, CO.

[1] Abbreviations: DAPI, 4,6-diamidino-2-phenylindole; DAU, daunorubicin; DAUF, Daunoform; DMSO, dimethyl sulfoxide; DOX, doxorubicin; DOXF, Doxoform; EPI, epidoxorubicin; EPIF, Epidoxoform; FBS, fetal bovine serum; PBS, 0.1 M phosphate-buffered saline (pH 7.4); Pgp, P-170 glycoprotein; SDS, sodium dodecyl sulfate; WGA-FITC, wheat germ agglutinin fluorescein-linked isothiocyanate.

10.1021/tx990008q CCC: $18.00
Published on Web 06/15/1999

Scheme 1. Structures of Parent Drugs (DAU, DOX, and EPI), Their Conversion to Formaldehyde Conjugates (DAUF, DOXF, and EPIF), Formation of Anthracycline Active Metabolites, and Formation and Hydrolysis of a Drug–DNA Virtual Cross-Link[a]

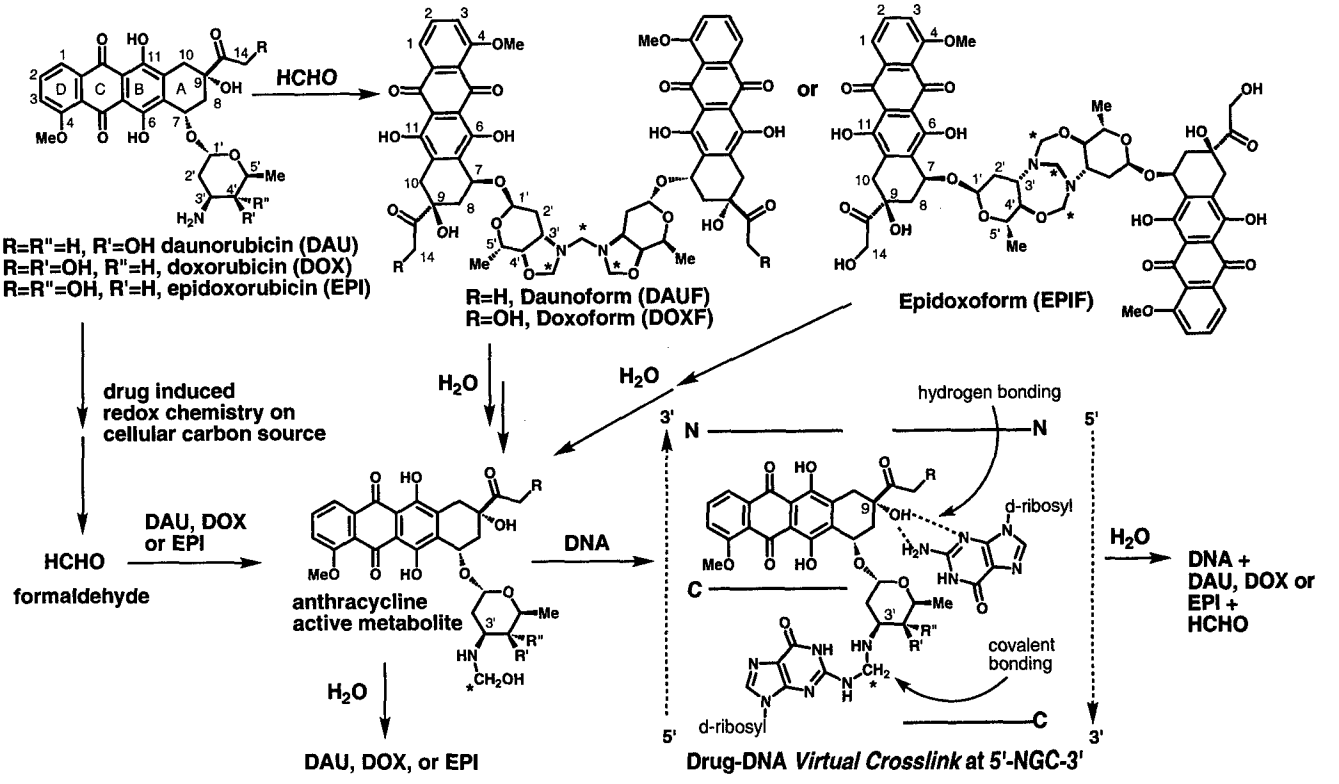

[a] Carbons coming from formaldehyde are denoted with asterisks.

resistance mechanisms have been discovered in cancer cells, with the best characterized being the overexpression of the drug efflux pump P-170 glycoprotein (Pgp) (*16, 17*). Another resistance mechanism relevant to the discussion here is the altered activity of redox enzymes involved in anthracycline-associated oxidative stress. Enzymes which produce reactive oxygen species (e.g., cytochrome P450 reductase) exhibit reduced activity, and enzymes which neutralize reactive oxygen species (e.g., superoxide dismutase and gluthathione peroxidase) exhibit increased activity (*18–20*). Both of these mechanisms are active in MCF-7/ADR cells (*18, 21*), the resistant human breast cancer cells employed in the studies described here.

Realizing the probable importance of formaldehyde in the tumor cell toxicity of DOX, DAU, and EPI, we synthesized formaldehyde conjugates of the drugs, denoted Doxoform (DOXF), Daunoform (DAUF), and Epidoxoform (EPIF) (*11, 22*). These conjugates are prodrugs to the anthracycline active metabolites, as shown in Scheme 1. Cytotoxicity experiments revealed that DOXF, DAUF, and EPIF were significantly more toxic to both sensitive (MCF-7) and resistant (MCF-7/ADR) breast cancer cells than the parent compounds DOX, DAU, and EPI (*11, 22*). Here we report the uptake, retention, and distribution of DOX, DAU, and EPI with respect to their formaldehyde conjugates in MCF-7 and MCF-7/ADR cells. Drug uptake and retention were assessed by flow cytometry, and the distribution of the drugs was visualized by fluorescence microscopy. Drug distribution was also studied by treating cells with ^{3}H-labeled DOXF and analyzing isolated DNA, RNA, and protein by scintillation counting. The results implicate DNA alkylation in the cell-killing mechanism of these drugs.

Experimental Procedures

Materials. All tissue culture materials were obtained from Gibco Life Technologies (Grand Island, NY) unless otherwise stated. MCF-7 breast cancer cells were obtained from American Type Culture Collection (Rockville, MD), and MCF-7/ADR adriamycin-resistant breast cancer cells were a gift from W. W. Wells (Michigan State University, East Lansing, MI). Daunoform (DAUF), Doxoform (DOXF), and Epidoxoform (EPIF) were synthesized from daunorubicin, doxorubicin, and epidoxorubicin, respectively, by reaction with formaldehyde as described previously (*11, 22*). These drug–formaldehyde conjugates are toxic materials and should be handled with caution especially when dissolved in DMSO which potentially makes them more permeable to the skin. Concentrations of drug–formaldehyde conjugates are given in micromolar equivalents per liter to correct for the conjugates bearing two active drug molecules per structural unit. DAPI, 4,6-diamidino-2-phenylindole, and wheat germ agglutinin fluorescein-linked (WGA–FITC) were from Sigma Chemical Co. (St. Louis, MO). TRI reagent for separation of cellular DNA, RNA, and protein was from Molecular Research Center, Inc. (Cincinnati, OH). Tritiated aqueous formaldehyde was obtained from DuPont-NEN Research Products (Boston, MA).

Maintenance of Cell Lines. MCF-7 and MCF-7/ADR cell lines were maintained in vitro by serial culture in RPMI 1640 medium supplemented with 10% fetal bovine serum (Gemini Bio-Products, Calbasas, CA), L-glutamine (2 mM), HEPES buffer (10 mM), penicillin (100 units/mL), and streptomycin (100 μg/mL). Cells were maintained at 37 °C in a humidified atmosphere of 5% CO_2 and 95% air.

Assessment of Drug Uptake and Release by Flow Cytometry. Cultured cells (MCF-7 and MCF-7/ADR) were dissociated with trypsin–EDTA and plated in six-well plates (ca. 500 000 cells/well) and allowed to adhere overnight. The cells were treated with 0.5 μmolar equiv/L drug (DOX, DAU, EPI, DOXF, DAUF, and EPIF) at 37 °C for various amounts of

time (5 min, 30 min, 1 h, 2 h, and 3 h). For each time point, the medium was removed and the cells were trypsinized and suspended in 3 mL of RPMI 1640 medium without phenol red and without FBS. The cells were transferred to 15 mL conical vials and centrifuged at 1000 rpm for 5 min at 10 °C. The supernatant was removed and replaced with 1 mL of RPMI 1640 medium without phenol red and without FBS. The cells were kept at 0 °C until analysis (up to 3 h). Control experiments exhibited no significant loss of fluorescence in samples kept at 0 °C for up to 4 h.

For drug retention analysis, cells were plated as described and treated with 0.5 μmolar equiv/L drug for 1 h (or 24 h). EPIF treatment lasted 3 h to allow for sufficient hydrolysis and drug–DNA adduct formation. Following drug treatment, the cells were incubated in fresh, drug-free medium for various time periods (0 min, 5 min, 30 min, 1 h, 3 h, and 6 h). After the alotted time had passed, the cells were prepared for flow cytometry analysis as described above.

The extent of drug uptake was determined by flow cytometry as previously described (*23*). All flow cytometry measurements were made with a Becton Dickinson (Franklin Lakes, NJ) FACScan flow cytometer, using a Hewlett-Packard 9000 series model 340 computer for data storage and analysis. Drug-treated cells were analyzed with excitation at 488 nm (15 mW Ar ion laser), with emission monitored between 570 and 600 nm. Instrument settings were held constant for all experiments, and 5000 cells were counted per measurement. The emission of drug-free cells was similarly measured to determine background fluorescence. The final data were plotted as mean fluorescence (as determined by computer data analysis) versus drug incubation time (or recovery time) for ease of data representation.

Analysis of Intracellular Drug Distribution by Fluorescence Microscopy. Cells were plated in six-well plates (ca. 300 000 cells/well). Each well contained a sterile cover slip, and the cells were allowed to adhere to the cover slip overnight. Each well contained 3 mL of RPMI 1640 medium. The drugs (DOX, DAU, EPI, DOXF, DAUF, and EPIF) were dissolved in DMSO to a concentration of 50 μmolar equiv/L (100-fold concentration). Then, 30 μL of each DMSO solution was added to the appropriate well, resulting in a 100-fold dilution (0.5 μmolar equiv/L drug and 1% DMSO). The cells were incubated with the drug for 5 min, 30 min, 1 h, 2 h, or 3 h. Following drug treatment, the medium was removed and the cells were washed with 2 mL of PBS. The cells were then fixed to the cover slips by submerging in 3 mL of cold (−20 °C) methanol and storing on ice for 5 min. The methanol was removed, and the cells were washed with 3 mL of PBS. The cover slips were then removed from the wells and inverted on a drop (30 μL) of DAPI (0.2 μg/mL in PBS) placed on Parafilm. The cover slips were kept on the DAPI solution for 5 min at ambient temperature. The cover slips were then rinsed with PBS and mounted on a microscope slide using a drop (30 μL) of mowiol mounting medium. The slides were allowed to dry in the dark overnight. Microscopic images were observed at a magnification of 1000× and recorded with a Zeiss Axioplan (Carl Zeiss, Thornwood, NY) fluorescence microscope equipped with a Photometrics Sensys (Tucson, AZ) digital CCD camera system. Images were developed using IP-LAB Spectrum Software. Drug fluorescence was observed at wavelengths above 590 nm with excitation at 546 ± 6 nm, and DAPI fluorescence was observed at wavelengths above 420 nm with excitation at 355 ± 20 nm.

MCF-7 and MCF-7/ADR cells were each treated with fluorescein-linked wheat germ agglutinin to visualize the Golgi apparatus. Fluorescein fluorescence was observed at wavelengths above 515 nm with excitation at 470 ± 20 nm.

For drug retention experiments with short periods of drug exposure, the cells were treated with drugs for 1 h except for EPIF, where cells were treated for 3 h to allow sufficient time for EPIF hydrolysis and drug–DNA adduct formation. For the assessment of retention after longer exposure, cells were treated with drugs for 24 h. After drug treatment, cells were incubated in fresh medium for various time periods (0 min, 5 min, 30 min, 1 h, 3 h, and 6 h). Cells were then fixed, stained with DAPI, and mounted as described above.

[^{3}H]Doxoform Synthesis. To a 6.7 mM solution of doxorubicin (19.4 mg in 5 mL) in pH 6 sodium cacodylate buffer (30 mM) were added 0.05 mmol of [^{3}H]H_2CO (5 mCi) and 1.62 mmol of H_2CO (3% [^{3}H]H_2CO). The mixture was stirred at room temperature for 20 min, and then extracted with 2 × 30 mL of chloroform. The chloroform extracts were dried over sodium sulfate and combined. The solvent was then removed by rotary evaporation. [^{3}H]Doxoform was crystallized by redissolving the solid in 500 μL of chloroform and transferring the mixture to a stoppered vial. To this were added 2 mL of *n*-hexane and 8 mL of ethyl acetate. The vial was stored in the dark at ambient temperature until crystal formation was complete (5 days). The crystals were washed with *n*-hexane and dried. The material was stored at ambient temperature until it was used. Scintillation counting gave 22 502 cpm for 4.46 nmol of the crystalline [^{3}H]Doxoform.

Cell Experiments with [^{3}H]Doxoform and [^{3}H]Formaldehyde. MCF-7 and MCF-7/ADR cells (approximately 10 million cells) in RPMI 1640 medium were treated for 1 h with 1 μmolar equiv/L [^{3}H]Doxoform (3% ^3H_2CO) or 1 μM doxorubicin and 1.5 μM HCHO (3% ^3H_2CO) or 1.5 μM HCHO (3% ^3H_2CO). The Doxoform concentration is reported as 1 μmolar equiv/L because it is a dimeric molecule. Doxoform and doxorubicin were introduced as DMSO solutions. All three mixtures contained 0.5% DMSO (100 μL in 20 mL of medium). Incubations were performed at 37 °C in a humidified atmosphere containing 5% CO_2 and 95% air. After 1 h, the medium was removed and stored at 4 °C until analysis. Isolation of cellular DNA, RNA, and protein was performed with TRI Reagent. For each flask containing 1 × 10^7 cells, 7 mL of TRI Reagent was added and the solution was allowed to sit at ambient temperature for 5 min. The TRI Reagent/cell lysate mixture was then transferred to a 15 mL centrifuge tube, and 700 μL of 1-bromo-3-chloropropane was added. The mixture was shaken vigorously for 15 s and allowed to stand at ambient temperature for 5 min. The solution was centrifuged at 3000 rpm for 15 min at 4 °C. After centrifugation, the solution contained an aqueous phase, an interphase, and an organic phase. The aqueous phase was removed for later isolation of RNA, and the DNA was precipitated from the interphase and the organic phase by the addition of 2.1 mL of 100% ethanol. The samples were mixed by inversion and centrifuged at 2000 rpm for 5 min at 4 °C. The supernatant was removed from the DNA pellet and stored for subsequent protein isolation. The DNA was washed twice with 7 mL of 0.1 M sodium citrate solution containing 10% ethanol. With each wash, the DNA pellet was stored in the washing solution for 30 min at 0 °C with periodic mixing. The sample was centrifuged at 2000 rpm for 5 min at 4 °C after each wash. Following the sodium citrate washes, a final wash with 7 mL of 75% ethanol was performed, with immediate centrifugation at 2000 rpm for 5 min at 4 °C. The ethanol was removed, and the DNA pellet was dissolved in 400 μL of 8 mM sodium hydroxide. RNA was precipitated from the previously extracted aqueous phase by addition of 3.5 mL of 2-propanol. The sample was mixed by inversion and stored at ambient temperature for 10 min and centrifuged at 3000 rpm for 10 min at 4 °C. The supernatant was removed, and the RNA pellet was washed with 70% ethanol followed by centrifugation at 3000 rpm for 5 min at 4 °C. The supernatant was then removed and the RNA pellet suspended in 500 μL of water (autoclaved and 0.2 μm filtered). DNA and RNA were quantitated by measuring the absorbance at 260 nm, assuming 1 OD_{260} = 50 μg of dsDNA/mL. The 260 nm/280 nm absorbance ratio for DNA isolates was >1.6; for RNA, the ratio was >1.9. The concentration of the DNA or RNA solutions for analysis by scintillation counting was ca. 300 μg/mL. Cellular proteins were precipitated from the phenol/ethanol supernatant (from the DNA precipitation) upon the addition of 8 mL of 2-propanol. The samples were stored at ambient temperature for 15 min and centrifuged at 3000 rpm for 10 min at 4 °C. The supernatant was removed, and the protein pellet was washed

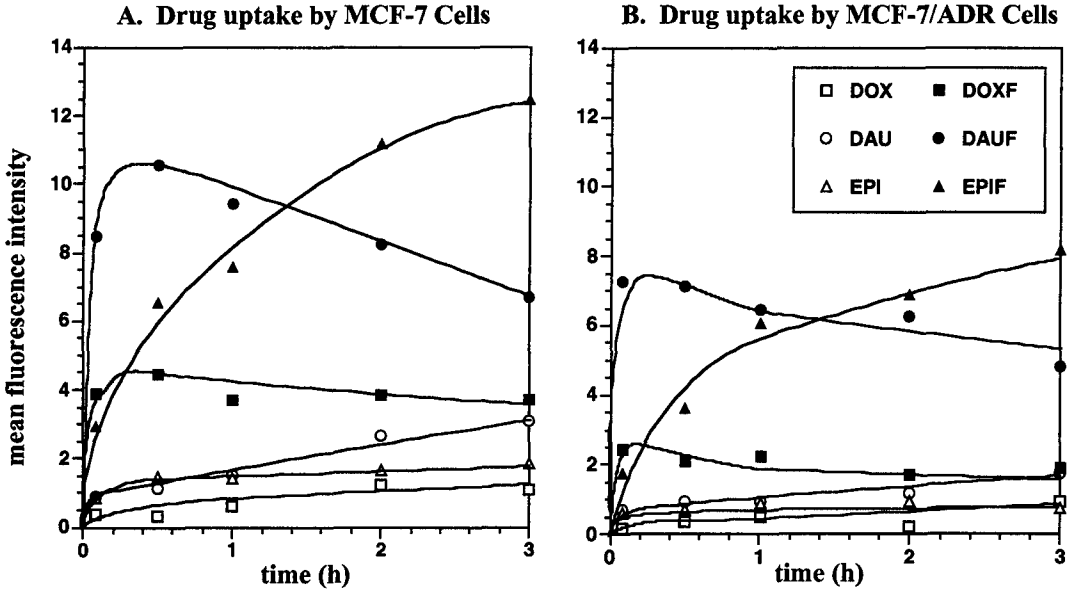

Figure 1. Uptake (A and B) of DOX, DAU, EPI, DOXF, DAUF, and EPIF by sensitive MCF-7 and resistant MCF-7/ADR tumor cells. Drug uptake by cells treated with 0.5 μmol equiv/L drug was observed as a function of time by flow cytometry by monitoring drug fluorescence at 570–600 nm upon excitation at 488 nm. Drug concentrations are given in micromolar equivalents per liter because DOXF, DAUF, and EPIF are dimeric in drug reactive intermediates.

three times with 14 mL of a 0.3 M guanidine hydrochloride solution in 95% ethanol. The samples were stored in the washing solution for 20–30 min at ambient temperature followed by centrifugation at 3000 rpm for 5 min at 4 °C. Then, the protein pellet was vortexed in 2 mL of 100% ethanol and stored at ambient temperature for 20 min. The sample was then centrifuged at 3000 rpm for 5 min at 4 °C. The supernatant was removed, and the proteins were dissolved in 2 mL of a 1% SDS solution. The protein concentration was approximately 6 mg/mL for each sample as determined by absorption at 280 nm relative to bovine serum albumin standard calibration curve. ^3H was counted with a Beckman (Fullerton, CA) LS 3801 scintillation counter. To 3 mL of scintillation fluid (Biosafe AQ–Research Products International Corp., Mount Prospect, IL) was added 300 μL of sample. Each sample was counted for 45 min.

Results

Flow Cytometry. The uptake of 0.5 μmolar equiv/L DOX, DAU, and EPI versus the uptake of their respective formaldehyde conjugates, DOXF, DAUF, and EPIF, by human breast cancer cells was assessed by flow cytometry using drug fluorescence as a measure of drug in cells. The concentration of drug is given in micromolar equivalents per liter because DOXF, DAUF, and EPIF are dimeric in active drug. Both doxorubicin-sensitive MCF-7 cells and doxorubicin-resistant MCF-7/ADR cells were studied. Drug uptake was monitored over a 3 h time period, and the results are plotted in Figure 1 (A and B). After 3 h, EPIF was taken up the most by both MCF-7 and MCF-7/ADR cells followed by DAUF, DOXF, DAU, EPI, and DOX. The sensitive cells took up at least twice as much of the drug–formaldehyde conjugate as the respective parent drug. In resistant cells, less of each drug was taken up; however, the ratio of the uptake of drug–formaldehyde conjugate to parent drug was still at least a factor of 2. The initial rate of uptake of DAUF and DOXF was substantially higher than that by EPIF.

Flow cytometry was also used to quantitate the amount of drug retained in MCF-7 and MCF-7/ADR cells as a function of time following drug treatment. For 1 h of drug treatment (3 h for EPIF), the data (Figure 2A,B) show that the parent compounds are released from both sensitive and resistant cells within 1 h of drug removal, while a significant amount of the formaldehyde conjugates remains in the cells even 6 h after drug removal. For 24 h of drug treatment, the data (Figure 2C,D) show that the parent compounds are still not retained in MCF-7/ADR cells, but are modestly retained in MCF-7 cells.

Fluorescence Microscopy. The location of drug in doxorubicin-sensitive and doxorubicin-resistant MCF-7 cells was observed by fluorescence microscopy, again relying on drug fluorescence as a measure of drug concentration. Cells were treated with 0.5 μmolar equiv/L drug for a variety of time periods as described in Experimental Procedures. All six drugs were investigated as a function of treatment time and time of recovery following drug treatment. The drug-treated cells were additionally treated with the nuclear stain 4,6-diamidino-2-phenylindole (DAPI). Fluorescence microscopy revealed that the formaldehyde conjugates targeted the nuclei of both MCF-7 and MCF-7/ADR cells, as shown with DOXF-treated MCF-7 and MCF-7/ADR cells in Figure 3 (rows a and b). The drug fluorescence mapped the fluorescence of DAPI, indicating primarily nuclear localization of DOXF, DAUF, and EPIF. Substantial amounts of DOXF and DAUF were present in the nuclei of both MCF-7 and MCF-7/ADR cells after only a 5 min drug treatment, while nuclear uptake of EPIF was considerably slower (Figure 4 and data not shown). This is due to the difference in the rates of hydrolysis of DOXF, DAUF, and EPIF to the active forms of the drugs. The parent compounds also targeted the nuclei of MCF-7 cells, but were present in smaller amounts and also were minimally present in the cytoplasm (data not shown). Additional experiments using confocal microscopy yielded results similar to those observed by fluorescence microscopy (data not shown). Control experiments with the Golgi stain, fluorescein-linked wheat germ agglutinin (*24*), established that none of the drugs was predominantly in the Golgi apparatus of either MCF-7 or MCF-

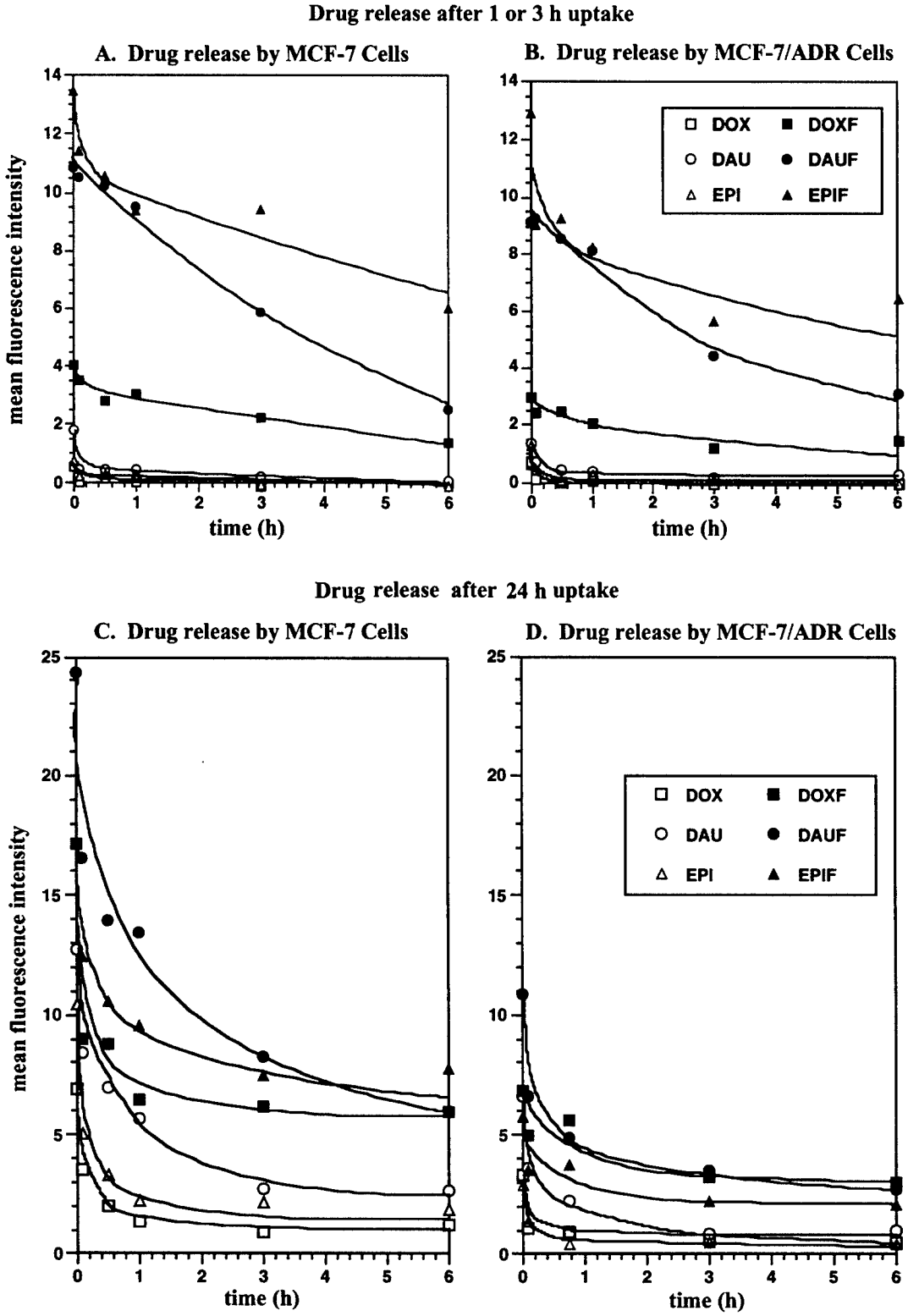

Figure 2. Release of DOX, DAU, EPI, DOXF, DAUF, and EPIF by sensitive MCF-7 (A and C) and resistant MCF-7/ADR (B and D) tumor cells after drug treatment for 1 h (except with EPIF for which drug treatment was 3 h to allow time for its hydrolysis to reactive intermediates) (A and B) and after drug treatment for 24 h (C and D). Drug release was assessed by flow cytometry.

7/ADR cells. Very little of the parent drugs was taken up by MCF-7/ADR cells, and no particular specificity for drug localization was observed (Figure 3, row c).

A major difference between the parent compounds and the formaldehyde conjugates was observed when the cells were incubated in drug-free medium following treatment with drug for 1 h (3 h with EPIF). The formaldehyde conjugates remained in the nuclei of both sensitive and resistant MCF-7 cells, even 6 h after drug removal (Figure 5 and data not shown). The parent drugs, however, were expelled from the cells within 30–60 min of drug removal as shown for DOX-treated cells in Figure 5. Similar results were observed following drug treatment for 24 h (data not shown).

Measurements of Formaldehyde Levels in Cells. Because drug–DNA adducts and drug–formaldehyde

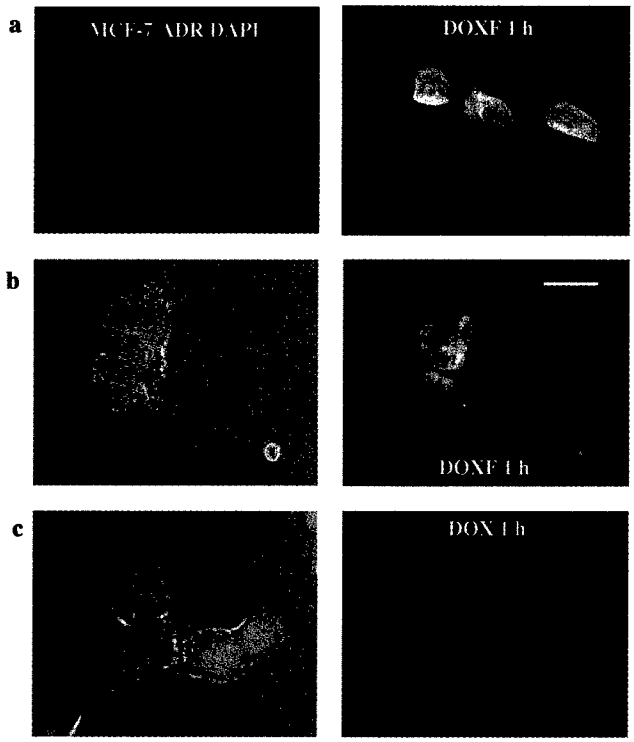

Figure 3. Fluorescence micrographs of resistant MCF-7/ADR tumor cells fixed after exposure to 0.5 μmol equiv/L DOXF (row a) and DOX (row c) for 1 h and sensitive MCF-7 tumor cells fixed after exposure to 0.5 μmol equiv/L DOXF (row b) for 1 h. Both sets of cells were also treated with the nuclear stain DAPI; in rows b and c, DAPI-stained nuclei are superimposed on whole cells. Drug fluorescence was observed at wavelengths above 590 nm with excitation at 546 nm and DAPI fluorescence at wavelengths above 420 nm with excitation at 355 nm; the bar is 25 μm long.

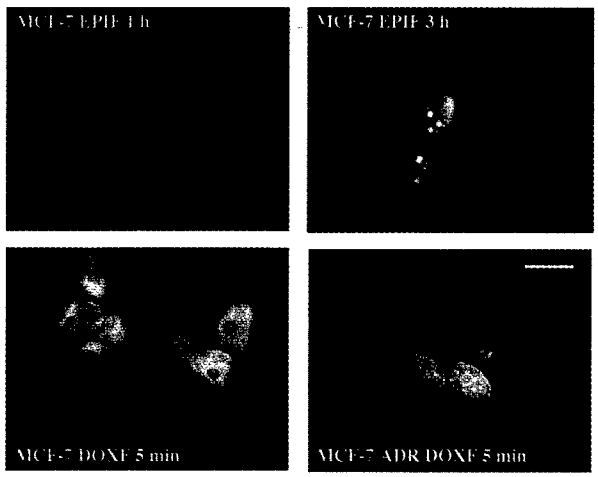

Figure 4. Fluorescence micrographs of sensitive MCF-7 cells treated with 0.5 μmol equiv/L EPIF or DOXF and MCF-7/ADR cells treated with 0.5 μmol equiv/L DOXF, all as a function of time of exposure to drug. Drug was removed from cells at the indicated time points, fixed, and stained with the nuclear stain DAPI. Fluorescence was observed as described in the legend of Figure 3; the bar is 25 μm long.

conjugates are hydrolytically unstable at elevated temperatures (*7*, *25*), most likely with release of formaldehyde, such drug-associated formaldehyde should be detectable. This was achieved using a tritium label at the formaldehyde carbon of DOXF. The distribution of formaldehyde from tritiated DOXF between DNA, RNA, and protein in MCF-7 and MCF-7/ADR cells relative to

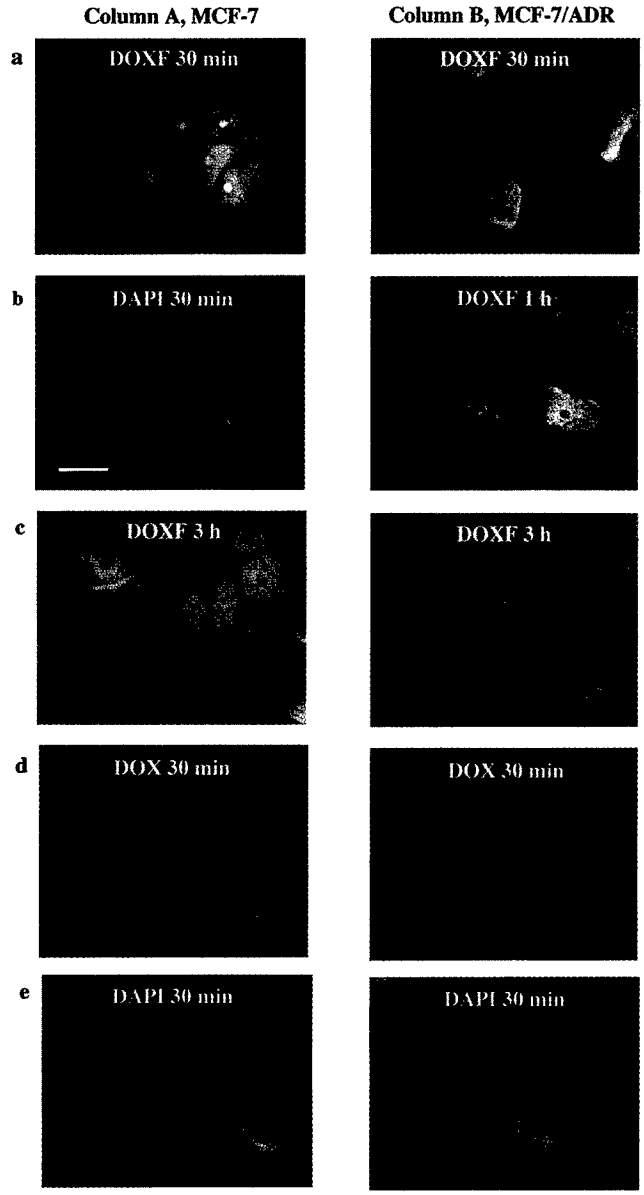

Figure 5. Fluorescence micrographs of MCF-7 cells (column A) and MCF-7/ADR cells (column B) as a function of time for drug release. Cells were treated with either 0.5 μmol equiv/L DOXF or DOX for 1 h and then placed in drug-free medium. At the indicated times in drug-free medium, cells were fixed and stained with DAPI. Fluorescence was observed as described in the legend of Figure 3; the bar is 25 μm long.

controls was determined by treating cells under a variety of conditions, followed by separation of DNA, RNA, and protein and detection by scintillation counting. Cells were treated with 1 μmolar equiv/L [^{3}H]Doxoform (3% ^3H_2CO) or 1 μM doxorubicin and 1.5 μM H_2CO (3% ^3H_2CO) or 1.5 μM H_2CO (3% ^3H_2CO) for 1 h.

Tritiated formaldehyde levels were measured with a scintillation counter for medium, DNA, RNA, and protein. The data, reported in Table 1, show the calculated counts per minute for the total amount of isolated material. In each case, the counts per minute value reported is the counts per minute value above background, which was determined to be 57.6. The counts per minute value for the total amount of isolated material was calculated by dividing the counts per minute value by the fraction of material actually used for scintillation counting. The volume of sample added to each scintillation vial was 300

Table 1. Tritium Label in Units of Counts per Minute per Milligram in DNA, RNA, and Protein of MCF-7 and MCF-7/ADR Cells Treated with either Tritiated Doxoform or Doxorubicin plus Tritiated Formaldehyde or Tritiated Formaldehyde[a]

location of label	MCF/7 with [^{3}H]DOXF	MCF-7 with DOX and ^3H_2CO	MCF-7 with ^3H_2CO	MCF-7/ADR with [^{3}H]DOXF	MCF-7/ADR with DOX and ^3H_2CO	MCF-7/ADR with ^3H_2CO
DNA	725 ± 18 (71)[b]	362 ± 10	376 ± 12	939 ± 19 (41)[b]	279 ± 10	355 ± 11
RNA	31 ± 31 (6)[b]	194 ± 12	214 ± 14	31 ± 39 (21)[b]	169 ± 11	185 ± 14
protein	41 ± 2 (35)[b]	17 ± 1	12 ± 1	23 ± 2 (13)[b]	11 ± 1	10 ± 1

[a] The data are normalized to counts in recovered cell culture media. The errors represent two standard deviations in scintillation counting. [b] The number in parentheses is one standard deviation with respect to reproducibility of the experimental measurement.

μL. This represented 1.5% of the total medium (20 mL), 75% of the DNA (400 μL), 60% of the RNA (500 μL), and 15% of the protein (2 mL). Thus, if the DNA counts per minute value were 73, the counts per minute value for the total isolated material would be 97 (73/0.75). The data in Table 1 show that the distribution of formaldehyde is quite different in [^{3}H]DOXF-treated cells. Substantially more formaldehyde was observed in the DNA of Doxoform-treated cells than in cells treated with doxorubicin and formaldehyde or formaldehyde alone.

Discussion

Covalent Bonding to Nuclear DNA. The results of fluorescence microscopy and tritium labeling experiments indicate that the chromosomal DNA of both sensitive and resistant tumor cells is the primary target for the anthracycline–formaldehyde conjugates, DOXF, DAUF, and EPIF. In particular, Figure 3 (rows a and b) shows that the drug fluorescence mostly overlaps the fluorescence of DAPI, indicating the specific nuclear localization of the fluorophore of DOXF. Only slight drug fluorescence is observed outside the nucleus, and since drug fluorescence is enhanced in lipid membranes (*26*) and partially quenched by drug–DNA intercalation (*27*, *28*), the observation of fluorescence predominantly in the nucleus more certainly identifies it as the key target. Similar results were observed with DAUF and EPIF in both MCF-7 and MCF-7/ADR cell lines (data not shown). Furthermore, elevated levels of ^{3}H were observed in the DNA of [^{3}H]DOXF-treated MCF-7 and MCF-7/ADR cells with respect to controls (Table 1). This concurs with the fluorescence microscopy data and indicates that DOXF (and by analogy DAUF and EPIF) targets the nuclei of cells. Fluorescence microscopy shows that the parent compounds DOX, DAU, and EPI also target the nuclei in MCF-7 cells. However, MCF-7/ADR cells take up very little DOX, DAU, and EPI, with drug mainly in the cytoplasm and very little in the nucleus (Figure 3, row c, and data not shown). Our observations concur with previous reports showing reduced levels of uptake and nuclear exclusion of the drugs in MCF-7/ADR cells (*29–31*).

Other differences among the six drugs reside in the rate and quantity of drug uptake and drug release. These differences are apparent from the flow cytometry and fluorescence microscopy studies. EPIF is taken up more slowly than DAUF or DOXF (Figure 1). This slower uptake parallels the observed differences in the rates of hydrolysis of DAUF and DOXF versus EPIF to the active metabolites predicted to be reactive with DNA (Scheme 1). At 37 °C, the half-lives of DAUF and DOXF with respect to formation of the active metabolites at pH 7.4 are less than 10 min (*22*), while the half-life of EPIF at 37 °C with respect to formation of the active metabolite is 2 h (*11*). Flow cytometry shows that the fluorophores of DAUF and DOXF reach the maximum levels in both sensitive and resistant cells in 15 min, while the fluorophore of EPIF continues to rise in both cell lines over a 3 h period (Figure 1A,B). Fluorescence microscopy (Figure 4) qualitatively shows the same result and indicates that the drug is predominantly in the nucleus. Hence, both flow cytometry and fluorescence microscopy indicate that hydrolysis of EPIF to the active metabolite precedes drug uptake and binding to DNA.

The observation that nuclear localization of the fluorophore of DOXF, DAUF, and EPIF is directly related to the rates of hydrolysis to the active metabolites indicates that these formaldehyde conjugates alkylate the chromosomal DNA of MCF-7 and MCF-7/ADR cells. Additional evidence for drug–DNA alkylation by DOXF, DAUF, and EPIF is provided by the drug retention analysis (Figure 2). DOXF-, DAUF-, and EPIF-treated cells placed in fresh, drug-free medium retained drug in the nucleus for hours after treatment. The observed decrease in nuclear drug levels with time is due to hydrolysis of the drug–DNA adducts. Both sensitive and resistant cells exhibited similar levels of retention, consistent with identical IC_{50} values for DOXF, DAUF, and EPIF versus sensitive and resistant cells (*11*, *22*). The parent drugs (DOX, DAU, and EPI), however, were rapidly expelled from the nucleus following treatment for 1 h in both sensitive and resistant cells, indicative of a more labile intercalative interaction with DNA. Extracellular evidence for increased stability of DNA *virtually cross-linked* by doxorubicin versus DNA intercalated by doxorubicin comes from measurements of rates of DNA exchange. DNA strand exchange was inhibited 3.9-fold by a doxorubicin intercalated in a double-stranded oligonucleotide but 637-fold by a doxorubicin *virtually cross-linked* to the oligonucleotide (*12*). When cells were treated with parent drug for 24 h, small amounts of DOX, DAU, and EPI were retained in the nuclei of MCF-7 cells (Figure 2C). This suggests the presence of drug–DNA adducts similar to those formed by DOXF, DAUF, and EPIF. The longer drug treatment (24 h vs 1 h) allows the parent drugs time to generate formaldehyde catalytically (Scheme 1) (*8*, *9*). The formaldehyde then mediates formation of the drug–DNA adducts. Retention of DOX, DAU, and EPI was not seen in resistant cells following drug treatment for 24 h (Figure 2D) due to reduced levels of drug uptake and changes in the activity of enzymes which influence formaldehyde production by these cells (*9*, *18*, *32*). Some of the DOX, DAU, and EPI retained by the MCF-7 cells after treatment for 24 h may also have resulted from drug trapped in TopoII cleavable complexes and/or transcription complexes. Formation of these adducts via in situ-generated formaldehyde is likely a key process in the cytotoxic mechanism of DOX, DAU, and EPI. As such, the formaldehyde conjugates DOXF, DAUF,

and EPIF essentially provide the active metabolites of DOX, DAU, and EPI.

The slower nuclear release of fluorophore from cells treated with DOXF with respect to cells treated with DOX is also apparent from microscopy experiments with both sensitive and resistant tumor cells as shown in Figure 5. Note that in the early stage of fluorophore release, fluorescence is observed in the cytoplasm of sensitive cells (Figure 5, column A, row a) but less in the cytoplasm of resistant cells (Figure 5, column B, row a). This no doubt reflects the increased levels of Pgp in resistant cells (*21*), which pumps cytoplasmic drug out of cells as it is released from the DNA. Similar results were seen with DAUF and EPIF with respect to DAU and EPI (data not shown). Drug–DNA adducts formed from reaction of DOXF, DAUF, and EPIF with extracellular DNA are unstable with respect to hydrolysis back to parent drug, formaldehyde, and intact DNA (*6–9, 11, 22, 25*). Consequently, the drug observed in the cytoplasm of MCF-7 cells following DOXF treatment (Figure 5, column A, row a) is probably DOX. Formation of relatively long-lived but ultimately unstable DNA lesions may afford DOXF, DAUF, and EPIF tumor cell selectivity. Cancer cells may be especially susceptible to such adducts because the cells are constantly replicating and cannot arrest their growth to allow for DNA repair. Normal cells, however, can slow their growth such that DNA repair can take place. Repair might occur by an active mechanism or simply by a passive mechanism, as observed in experiments with extracellular DNA (*6–8, 25*).

As mentioned earlier in the Discussion, the occurrence of drug–DNA alkylation is further supported by the cell experiments with [^{3}H]DOXF. The tritium label on [^{3}H]-DOXF was present on the methylene units of DOXF, as indicated in Scheme 1. Thus, the tritium label should be bound to the cellular DNA upon formation of the drug–DNA adducts (Scheme 1). As the data in Table 1 indicate, more radioactivity was present in the DNA of [^{3}H]DOXF-treated cells relative to the controls. Furthermore, elevated ^{3}H levels were observed in DNA of MCF-7/ADR cells with respect to MCF-7 cells. This somewhat contradicts the flow cytometry data, which indicate that more DOXF is taken up by sensitive cells at a concentration of 0.5 μmol equiv/L. The reason for this discrepancy is unclear. The flow cytometer measures only the drug fluorophore, while the scintillation counter measures tritiated formaldehyde from DOXF. Perhaps the difference lies in the proportion of drug–DNA binding sites occupied by intercalated drug versus intercalated and covalently bound drug. Because of relatively rapid DOXF hydrolysis to DOX (*22*) (Scheme 1), both DOX and DOXF are available for binding to DNA. If DOX occupies the binding site, the active metabolite from partial hydrolysis of DOXF cannot. Because of the activity of the drug efflux pump, Pgp, DOX will occupy less of the binding sites in MCF-7/ADR cells. Hence, a higher proportion of intercalated and covalently bound drug may be present in MCF-7/ADR cells.

DOXF, DAUF, and EPIF Overcome Some Resistance Mechanisms. The flow cytometry measurements indicate that resistant cells take up less of the parent drugs than the sensitive cells but take up significant amounts of the respective formaldehyde conjugates. This is consistent with resistance resulting in part from overexpression of Pgp (*18*). The drug–formaldehyde conjugates may overcome efflux by Pgp because they rapidly bind DNA (*11, 22*). Once covalently bound to DNA, the anthracycline–formaldehyde conjugates are no longer substrates for Pgp efflux. Conjugation with formaldehyde also dramatically lowers the pK_a of the protonated amine functional group (*33*) such that the nitrogens of the conjugates are unprotonated at physiological pH. This makes the conjugates poorer substrates for Pgp, since anthracycline efflux by Pgp correlates with the presence of positive charge (*34*).

Overexpression of Pgp is an important resistance mechanism in MCF-7/ADR cells (*18, 21*). Indeed, the data in Figure 1 are consistent with diminished uptake of DOX, DAU, and EPI by MCF-7/ADR cells as a resistance mechanism for these cells. Another mechanism of resistance observed in MCF-7/ADR cells involves changes in activity of redox enzymes involved in oxidative stress and, presumably, formaldehyde production. Xenografts of MCF-7/ADR cells in nude mice have higher activity levels of superoxide dismutase and glutathione peroxidase (*32*). Both enzymes neutralize oxidative stress. Further, the level of cytochrome P450 reductase activity was lower in the xenografts. Cytochrome P450 reductase induces oxidative stress by reducing the anthracyclines in the presence of molecular oxygen to initiate redox cycling. The formaldehyde conjugates are effective against this resistance mechanism as well because they do not require drug induction of oxidative stress for production of formaldehyde.

In conclusion, we have shown that the anthracycline–formaldehyde conjugates, Daunoform, Doxoform, and Epidoxoform, target the nuclei of both sensitive and resistant MCF-7 tumor cells with formation of unstable drug–DNA adducts. Important factors in the toxicity to tumor cells are likely the quantity of drug taken up and the longevity of drug association with nuclear DNA. Although a longer residence time with DNA increases toxicity to tumor cells, an overly long residence time with irreversible DNA damage may result in the loss of selectivity for tumor cells. Possibly one or more of these anthracycline–formaldehyde conjugates has the correct reactivity with DNA for specific toxicity to anthracycline-sensitive and -resistant tumor cells with little or no toxicity to normal cells. Animal experiments are currently in progress to address this question.

Acknowledgment. This work was supported by Grants CA24665 and CA78756 from NIH, RPG-98-110-01-ROG from the American Cancer Society, and DAMD17-98-1-8298 from the U.S. Army Breast Cancer Program and a predoctoral fellowship to D.J.T. from the Division of Medicinal Chemistry of the American Chemical Society and Wyeth-Ayerst, Inc. We thank Pharmacia-Upjohn (Milan, Italy) and Gensia-Sicor (Milan, Italy) for samples of epidoxorubicin and Nexstar Pharmaceuticals (San Dimas, CA) and Pharmacia-Upjohn for generous samples of doxorubicin and daunorubicin. We thank Dr. William W. Wells for MCF-7/ADR cells, Mark Winey for help with flow cytometry, Natalie Ahn and Paul Shapiro for help with fluorescence microscopy, and Rob Kuchta for help with the tritium labeling experiment.

References

(1) Sweatman, T. W., and Israel, M. (1997) Anthracyclines. In *Cancer Therapeutics, Experimental and Clinical Agents* (Teicher, B. A., Ed.) pp 113–135, Humana Press, Totowa, NJ.

(2) Tewey, K. M., Rowe, T. C., Yang, L., Halligan, B. D., and Liu, L. F. (1984) Adriamycin-induced DNA damage mediated by mammalian DNA topoisomerase II. *Science* **226**, 466–468.
(3) Pommier, Y. (1995) DNA topoisomerases and their inhibition by anthracyclines. In *Anthracycline Antibiotics: New Analogues, Methods of Delivery, and Mechanisms of Action* (Priebe, W., Ed.) pp 183–203, American Chemical Society, Washington, DC.
(4) Chaires, J. B., Satyanarayana, S., Suh, D., Fokt, I., Przewloka, T., and Priebe, W. (1996) Parsing the free energy of anthracycline antibiotic binding to DNA. *Biochemistry* **35**, 2047–2053.
(5) Cullinane, C., Cutts, S. M., van Rosmalen, A., and Phillips, D. R. (1994) Formation of adriamycin–DNA adducts in vitro. *Nucleic Acids Res.* **22**, 2296–2303.
(6) Cullinane, C., van Rosmalen, A., and Phillips, D. R. (1994) Does adriamycin induce interstrand cross-links in DNA? *Biochemistry* **33**, 4632–4638.
(7) van Rosmalen, A., Cullinane, C., Cutts, S. M., and Phillips, D. R. (1995) Stability of adriamycin-induced DNA adducts and interstrand crosslinks. *Nucleic Acids Res.* **23**, 42–50.
(8) Taatjes, D. J., Gaudiano, G., Resing, K., and Koch, T. (1997) A redox pathway leading to the alkylation of DNA by the anthracycline, anti-tumor drugs, adrimaycin and daunomycin. *J. Med. Chem.* **40**, 1276–1286.
(9) Taatjes, D. J., Gaudiano, G., and Koch, T. H. (1997) Production of formaldehyde and DNA-adriamycin or -daunomycin adducts, initiated through redox chemistry of DTT/iron, xanthine oxidase/NADH/iron, or glutathione/iron. *Chem. Res. Toxicol.* **10**, 953–961.
(10) Wang, A. H. J., Gao, Y. G., Liaw, Y. C., and Li, Y. k. (1991) Formaldehyde cross-links daunorubicin and DNA efficiently: HPLC and X-ray diffraction studies. *Biochemistry* **30**, 3812–3815.
(11) Taatjes, D. J., Fenick, D. J., and Koch, T. H. (1998) Epidoxoform: a hydrolytically more stable anthracycline-formaldehyde conjugate, cytotoxic to resistant tumor cells. *J. Med. Chem.* **41**, 2452–2461.
(12) Zeman, S. M., Phillips, D. R., and Crothers, D. M. (1998) Characterization of covalent Adriamycin-DNA adducts. *Proc. Natl. Acad. Sci. U.S.A.* **95**, 11561–11565.
(13) Skladanowski, A., and Konopa, J. (1993) Adriamycin and Daunomycin induce programmed cell death (apoptosis) in tumour cells. *Biochem. Pharmacol.* **46**, 375–382.
(14) Skladanowski, A., and Konopa, J. (1994) Relevance of interstrand DNA crosslinking induced by anthracyclines for their biological activity. *Biochem. Pharmacol.* **47**, 2279–2287.
(15) Skladanowski, A., and Konopa, J. (1994) Interstrand DNA crosslinking induced by anthracyclines in tumour cells. *Biochem. Pharmacol.* **47**, 2269–2278.
(16) Kartner, N., and Ling, V. (1989) Multidrug resistance in cancer. *Sci. Am.* **260**, 44–51.
(17) Gottesmann, M. M., and Pastam, I. (1993) Biochemistry of multidrug resistance mediated by the multidrug transporter. *Annu. Rev. Biochem.* **62**, 385–427.
(18) Sinha, B. K., and Mimnaugh, E. G. (1990) Free radicals and anticancer drug resistance: oxygen free radicals in the mechanisms of drug cytotoxicity and resistance by certain tumors. *Free Radical Biol. Med.* **8**, 567–581.
(19) Zwelling, L. A., Slovak, M. L., Doroshow, J. H., Hinds, M., Chan, D., Parker, E., Mayes, J., Sie, K. L., Meltzer, P. S., and Trent, J. M. (1990) HT1080/DR4: A P-glycoprotein-negative human fibrosarcoma cell line exhibiting resistance to topoisomerase II-reactive drugs despite the presence of a drug-sensitive topoisomerase II. *J. Natl. Cancer Inst.* **82**, 1553–1561.
(20) Cole, S. P. C., Downes, H. F., Mirski, S. E. L., and Clements, D. J. (1998) Alterations in glutathione and glutathione-related enzymes in a multidrug resistant small cell lung cancer cell line. *Mol. Pharmacol.* **37**, 192–197.
(21) Fairchild, C. R., Ivy, S. P., Kao-Shan, C. S., Whang-Peng, J., Rosen, N., Israel, M. A., Melera, P. W., Cowan, K. H., and Goldsmith, M. E. (1987) Isolation of amplified and overexpressed DNA sequences from adriamycin-resistant human breast cancer cells. *Cancer Res.* **47**, 5141–5148.
(22) Fenick, D. J., Taatjes, D. J., and Koch, T. H. (1997) Doxoform and Daunoform: anthracycline-formaldehyde conjugates toxic to resistant tumor cells. *J. Med. Chem.* **40**, 2452–2461.
(23) Durand, R. E., and Olive, P. L. (1981) Flow cytometry studies of intracellular adriamycin in single cells in vitro. *Cancer Res.* **41**, 3489–3494.
(24) Molinari, A., Cianfriglia, M., Meschini, S., Calcabrini, A., and Arancia, G. (1994) P-Glycoprotein expression in the golgi apparatus of multidrug-resistant cells. *Int. J. Cancer* **59**, 789–795.
(25) Leng, F., Savkur, R., Fokt, I., Przewloka, T., Priebe, W., and Chaires, J. B. (1996) Base specific and regiospecific chemical crosslinking of Daunorubicin to DNA. *J. Am. Chem. Soc.* **118**, 4731–4738.
(26) Gallois, L., Fiallo, M., Laigle, A., Priebe, W., and Garnier-Sullerot, A. (1996) The overall partitioning of anthracyclines into phosphatidyl-containing model membranes depends neither on the drug charge nor the presence of anionic phospholipids. *Eur. J. Biochem.* **241**, 879–887.
(27) Crooke, S. T., and DuVernay, V. H. (1980) Fluorescence quenching of anthracyclines by subcellular fractions. In *Anthracyclines Current Status and New Developments* (Crooke, S. T., and Reich, S. D., Eds.) pp 151–155, Academic Press, New York.
(28) Roche, C. J., Thomson, J. A., and Crothers, D. M. (1994) Site selectivity of daunomycin. *Biochemistry* **33**, 926–935.
(29) Gervasoni, J. E., Jr., Fields, S. Z., Krishna, S., Baker, M. A., Rosado, M., Thuraisamy, K., Hindenburg, A. A., and Taub, R. N. (1991) Subcellular distribution of daunorubicin in P-glycoprotein-positive and -negative drug-resistant cell lines using laser-assisted confocal microscopy. *Cancer Res.* **51**, 4955–4963.
(30) Coley, H. M., Amos, W. B., Twintyman, P. R., and Workman, P. (1993) Examination by laser confocal fluorescence imaging microscopy of the subcellular localisation of anthracyclines in parent and multidrug resistant cell lines. *Br. J. Cancer* **67**, 1316–1323.
(31) Serafino, A., Sinibaldi-Vallebona, P., Gaudiano, G., Koch, T. H., Rasi, G., Garaci, E., and Ravagnan, G. (1998) Cytoplasmic localization of anthracycline antitumor drugs conjugated with reduced glutathione: a possible correlation with multidrug resistance. *Anticancer Res.* **18**, 1159–1166.
(32) Mimnaugh, E. G., Fairchild, C. R., Fruehauf, J. P., and Sinha, B. K. (1991) Biochemical and pharmacological characterization of MCF-7 drug-sensitive and Adr multidrug-resistant human breast tumor xenografts in athymic nude mice. *Biochem. Pharmacol.* **42**, 391–402.
(33) Inouye, S. (1968) On the prediction of pK_a values of amino sugars. *Chem. Pharm. Bull.* **16**, 1134–1137.
(34) Lampidis, T. J., Kolonias, D., Podona, T., Israel, M., Safa, A. R., Lothstein, L., Savaraj, N., Tapiero, H., and Priebe, W. (1997) Circumvention of P-GP MDR as a function of anthracycline lipophilicity and charge. *Biochemistry* **36**, 2679–2685.

TX990008Q

Acta Crystallographica Section D
Biological Crystallography
ISSN 0907-4449

Crystal structure of epidoxorubicin–formaldehyde virtual crosslink of DNA and evidence for its formation in human breast-cancer cells

Elaine R. Podell,[a,b] Daniel J. Harrington,[a,b] Dylan J. Taatjes[a] and Tad H. Koch[a,c]*

[a]Department of Chemistry and Biochemistry, University of Colorado, Boulder, Colorado 80309-0215, USA, [b]Howard Hughes Medical Institute, University of Colorado, Boulder, Colorado 80309-0215, USA, and [c]University of Colorado Cancer Center, Denver, CO 80262, USA

Correspondence e-mail: tad.koch@colorado.edu

Received 22 January 1999
Accepted 15 June 1999

PDB Reference: epidoxorubicin–CH_2–d(CGCGCG), 1qda.

Epidoxorubicin and daunorubicin are proposed to be cytotoxic to tumor cells by catalyzing production of formaldehyde through redox cycling and using the formaldehyde for covalent attachment to DNA at G bases. The crystal structure of epidoxorubicin covalently bound to a d(CGCGCG) oligomer was determined to 1.6 Å resolution. The structure reveals slightly distorted B-form DNA bearing two molecules of epidoxorubicin symmetrically intercalated at the termini, with each covalently attached from its N3′ to N2 of a G base *via* a CH_2 group from the formaldehyde. The structure is analogous to daunorubicin covalently bound to d(CGCGCG) determined previously, except for additional hydrogen bonding from the epimeric O4′ to O2 of a C base. The role of drug–DNA covalent bonding in cells was investigated with synthetic epidoxorubicin–formaldehyde conjugate (Epidoxoform) and synthetic daunorubicin–formaldehyde conjugate (Daunoform). Uptake and location of drug fluorophore in doxorubicin-resistant human breast-cancer cells (MCF-7/ADR cells) was observed by fluorescence microscopy and flow cytometry. The fluorophore of Daunoform appeared more rapidly in cells and was released more rapidly from cells than the fluorophore of Epidoxoform over a 3 h exposure period. The fluorophore appeared predominantly in the nucleus of cells treated with both conjugates. The difference in uptake is explained in terms of the slower rate of hydrolysis of Epidoxoform to the species reactive with DNA and a proposed slower release from DNA based upon the crystal structures.

1. Introduction

Epidoxorubicin, the 4′-epimer of the clinically important antitumor drug doxorubicin, is a broad-spectrum anthracycline antitumor drug approved for human use in all countries of the world except the USA. A third relevant anthracycline, daunorubicin, is identical to doxorubicin except for the absence of the 14-hydroxyl group. Recent experiments by us and others indicate that all three of these anthracyclines derive at least some, if not most, of their antitumor activity through induction of oxidative stress leading to formaldehyde production. The drugs bind the formaldehyde at their 3′-amino substituents and use this formaldehyde moiety for covalent attachment to DNA at the 2-amino substituents of G bases (Cullinane, Cutts *et al.*, 1994; Cullinane, van Rosmalen *et al.*, 1994; Cutts *et al.*, 1996; Cutts & Phillips, 1995; Taatjes, Fenick, Gaudiano *et al.*, 1998; Taatjes, Gaudiano & Koch, 1997; Taatjes, Gaudiano, Resing *et al.*, 1997; Taatjes *et al.*, 1996; Wang *et al.*, 1991). The crystal structure of daunorubicin covalently attached to the self-complementary DNA oligomer

d(CGCGCG) *via* formaldehyde was solved even before drug-induced formaldehyde production was discovered (Wang *et al.*, 1991), and the structure was important in the elucidation of the mechanism. The drug–DNA covalent-binding mechanism then led to the synthesis of daunorubicin–, doxorubicin– and epidoxorubicin–formaldehyde conjugates, Daunoform (DAUF), Doxoform (DOXF) and Epidoxoform (EPIF), respectively, as improved antitumor drugs (Fenick *et al.*, 1997; Taatjes, Fenick & Koch, 1998). Of particular importance is that the conjugates are significantly more active against resistant cancer cells than the corresponding clinical drugs (Fenick *et al.*, 1997; Taatjes, Fenick & Koch, 1998). In each case, the formaldehyde conjugate is proposed to be a prodrug of the active metabolite of the clinical drug, with the metabolite released through partial hydrolysis of the conjugate. Structures for the clinical drugs, the formaldehyde conjugates and the active metabolites are shown in Fig. 1.

Of the three conjugates, Epidoxoform has emerged as the lead structure for further development because it is hydrolytically more stable with respect to release of formaldehyde (Fenick *et al.*, 1997; Taatjes, Fenick & Koch, 1998). Consequently, Epidoxoform or the product of its partial hydrolysis has a longer potential residence time in the vascular system. On this basis, the crystal structure of epidoxorubicin covalently attached to d(CGCGCG) *via* formaldehyde was solved and is reported here. The structure is compared with that of daunorubicin covalently attached to d(CGCGCG) (Wang *et al.*, 1991) and the structure of epidoxorubicin intercalated in d(CGATCG) (Williams *et al.*, 1990). Both structures are discussed in terms of uptake of Epidoxoform and Daunoform by resistant breast-cancer cells.

2. Materials and methods

2.1. Materials

All tissue-culture materials were obtained from Gibco Life Technologies (Grand Island, NY) unless otherwise stated. MCF-7/ADR breast-cancer cells were a gift from Dr William W. Wells (Michigan State University). Daunoform (DAUF) and Epidoxoform (EPIF) were synthesized from daunorubicin and epidoxorubicin, respectively, by reaction with formaldehyde, as described previously (Fenick *et al.*, 1997; Taatjes, Fenick & Koch, 1998). DAPI (4,6-diamidino-2-phenylindole), spermine and sodium cacodylate were from Sigma Chemical Co. DNA oligonucleotide was obtained from Integrated DNA Technologies (Coralville, IA) and purified by reverse-phase HPLC as described previously (Taatjes, Guadiano, Resing *et al.*, 1997). Formaldehyde was obtained from Mallinckrodt as a 37%(*w*/*w*) solution in water containing 10–15% methanol; barium chloride was obtained from Fisher Chemical Co.; 2-methyl-2,4-pentanediol (MPD) was from Aldrich Chemical Co. Water was distilled and purified with a Millipore Q-UF Plus purification system to 18 MΩ cm.

2.2. X-ray crystallography

Crystallization trials were based upon conditions described for daunorubicin–CH_2–d(CGCGCG) (Wang *et al.*, 1991). The crystallization mixture consisted of 1.2 m*M* d(CGCGCG), 1.2 m*M* epidoxorubicin and 9 m*M* formaldehyde in pH 6.0 buffer containing 30 m*M* sodium cacodylate, 16.1 m*M* spermine and 4.4 m*M* $BaCl_2$. Tetragonal crystals were grown in sterile 24-well plates (ICN Biomedicals, Aurora, OH) by the hanging-drop method on silanized cover slips. A 4 µl drop of

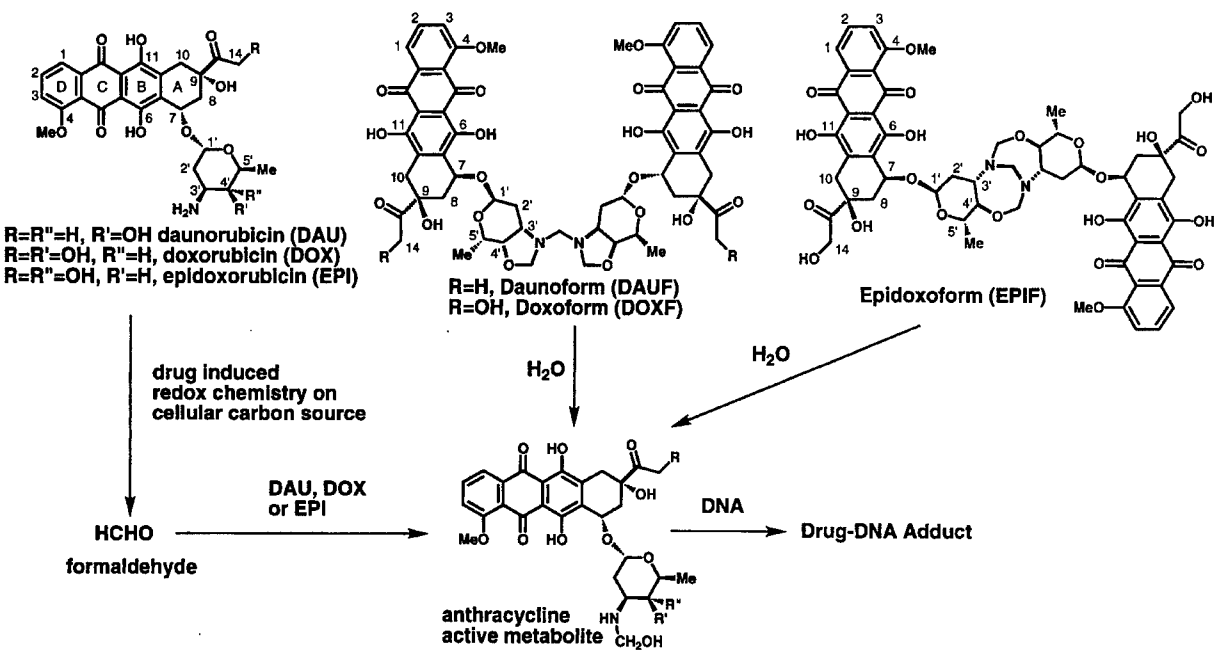

Figure 1
Structures of clinical anthracycline antitumor drugs, their metabolites and their conjugates with formaldehyde.

Table 1
Crystallographic parameters.

Data-collection and refinement statistics.

Unit-cell dimensions (Å, °)	$a = 28.11$, $b = 28.11$, $c = 52.54$; $\alpha = 90$, $\beta = 90$, $\gamma = 90$
Space group	$P4_12_12$
Temperature (K)	295
Number of collected reflections to 1.6 Å	47174
Number of unique reflections to 1.6 Å	3101
Number of reflections used for refinement [$F > 2\sigma(F)$]	2054†, 2612‡
R_{sym}§ (%)	9.9
R factor (%)	20.52†, 21.64‡
R_{free} (%)	26.78†
R.m.s. deviation of bonds from ideality (Å)	0.0197
R.m.s. deviation of angles from ideality (°)	2.087
Average B value (Å^2)	19.37
Number of observed solvent molecules	30
Overdeterminacy ratio	2.9†, 3.7‡

Number of reflections, R_{sym} and completeness by resolution.

Resolution range (Å)	No. of reflections	R_{sym} (%)	Completeness (%)
99.0–3.45	338	7.5	90.0
3.45–2.74	302	9.2	95.0
2.74–2.39	303	11.1	96.2
2.39–2.17	287	12.1	94.1
2.17–2.02	285	13.4	94.4
2.02–1.90	281	14.3	92.1
1.90–1.80	272	18.4	92.5
1.80–1.72	282	22.8	92.5
1.72–1.66	256	26.8	89.8
1.66–1.60	2482	30.9	82.7
All *hkl*	2854	9.9	92.0

† After sequestering 17.3% of the data. ‡ With all the data. § $R_{sym} = \sum[\mathrm{Abs}(I - \langle I \rangle)]/\sum I$.

the crystallization mixture was placed on a cover slip and the drop was sealed over a 1 ml well solution containing 40% MPD in water. Crystals were allowed to grow at ambient temperature; crystal formation was complete in about 6 d. The crystal was mounted and sealed in a glass capillary tube, and diffraction data were collected on an R-AXIS II image-plate system using Cu $K\alpha$ radiation from a Rigaku RU-H2R rotating-anode X-ray generator (Molecular Structures Corp., Houston, TX). The data were reduced and scaled using the *HKL* package (Gewirth, 1997; Otwinowski & Minor, 1997) and are summarized in Table 1. Epidoxorubicin–CH_2–d(CGCGCG) crystals belong to the space group $P4_12_12$, like many anthracycline–hexanucleotide complexes, and have unit-cell parameters $a = b = 28.11$, $c = 52.54$ Å, $\alpha = \beta = \gamma = 90°$. Useful diffraction was seen to a minimum Bragg spacing of 1.6 Å.

Crystallographic refinement and σ_A-weighted electron-density map calculations were carried out using *CNS* (Brünger *et al.*, 1998), with a new parameter dictionary for standard DNA nucleotides (Parkinson *et al.*, 1996). The initial model was constructed from the coordinates of daunorubicin covalently linked to d(CGCGCG) with formaldehyde (PDB entry 1d33) modified to include the position of O14 from epidoxorubicin (PDB entry 1d54). All refinement was performed on $|F_o| > 2\sigma|F_o|$. In order to obtain a statistically significant set of reflections for R_{free} calculations (Brünger & Rice, 1997), 529 reflections (17.3%) were sequestered from the data set. Initial refinement used the R_{free}, while the final series of conjugate-gradient minimizations utilized the entire data set in order to include a significant percentage (84.5%) of the theoretical data to 1.6 Å. The first set of refinement rounds consisted of torsion-angle simulated annealing with the maximum-likelihood target using amplitudes as implemented in *CNS*, followed by cycles of water picking based on positive peaks in $F_o - F_c$ difference Fourier maps. After each cycle of water picking, conjugate-gradient minimization and individual temperature-factor refinement was carried out and water positions were checked by examining $2F_o - F_c$ and $F_o - F_c$ difference Fourier maps calculated by *CNS* and displayed on a Silicon Graphics Onyx 2 workstation using *O* (Jones *et al.*, 1991). After 29 waters were picked, the model was annealed again and the cycles continued with some waters being manually repositioned into density as necessary. In the last cycle, waters with temperature factors greater than 60 Å^2 were deleted. In the final series of refinement cycles, the model was refined against all reflections using the standard crystallographic residual target and a bulk-solvent correction. As in the first set, cycles of conjugate-gradient minimization and individual temperature-factor refinement were performed, followed by scrutinizing the $F_o - F_c$ and $2F_o - F_c$ maps. Additional waters were deleted or repositioned based on the same criteria of lower temperature factors and occupied density. No other ions (Na^+, spermine or Ba^{2+}) could be unambiguously identified. The final model contained 30 waters distributed throughout the epidoxorubicin–CH_2–d(CGCGCG) asymmetric unit. Crystallographic and refinement data are reported in Table 1.

2.3. Measurement of drug uptake by flow cytometry

MCF-7/ADR cells were maintained *in vitro* by serial culture in RPMI 1640 medium supplemented with 10% fetal bovine serum (Gemini Bio-Products, Calbasas, CA), L-glutamine (2 m*M*), HEPES buffer (10 m*M*), penicillin (100 units ml^{-1}), streptomycin (100 mg ml^{-1}) and 5 µ*M* doxorubicin. Cells were maintained at 310 K in a humidified atmosphere of 5% CO_2 and 95% air. Cultured cells were dissociated with trypsin–EDTA and plated in 6-well plates (~500000 cells per well) and allowed to adhere overnight. The cells were treated with 0.25 µ*M* DAUF or EPIF at 310 K for various amounts of time (5 min, 30 min, 1 h, 2 h, 3 h). For each time point, the medium was removed and the cells were trypsinized and suspended in 3 ml of RPMI 1640 medium (−) phenol red and (−) FBS. The cells were transferred to 15 ml conical vials and centrifuged at 1000 r min^{-1} for 5 min at 283 K. The supernatant was removed and replaced with 1 ml of RPMI 1640 medium (−) phenol red and (−) FBS. The cells were kept at 273 K until analysis (up to 3 h). Control experiments showed no significant loss of fluorescence in samples kept at 273 K for up to 4 h. The extent of drug uptake was determined by flow cytometry, as previously described (Durand & Olive, 1981). All flow-

cytometry measurements were made with a Becton Dickinson FACScan flow cytometer, using a Hewlett–Packard 9000 Series Model 340 computer for data storage and analysis. Drug-treated cells were analyzed with excitation at 488 nm (15 mW argon-ion laser), with emission monitored between 570 and 600 nm. Instrument settings were held constant for all experiments and 5000 cells were counted per measurement. The emission of drug-free cells was similarly measured in order to determine background fluorescence. The final data are plotted as mean fluorescence (as determined by computer data analysis) *versus* drug incubation time (or recovery time) for ease of data representation.

2.4. Analysis of intracellular drug distribution by fluorescence microscopy

Cells were plated in 6-well plates (~300000 cells per well). Each well contained a sterile cover slip, and the cells were allowed to adhere to the cover slip overnight. Each well contained 3 ml of RPMI 1640 medium. The DAUF and EPIF were dissolved in DMSO to a concentration of 25 μM (100× solution). 30 µl of each DMSO solution was then added to the appropriate well, resulting in a 100× dilution (0.25 μM conjugate, 1% DMSO). The cells were incubated with the drug for 3 h. Following drug treatment, the medium was removed and the cells were washed with 2 ml PBS (phosphate-buffered saline). The cells were then fixed to the cover slips by submerging in 3 ml cold (253 K) methanol and storing on ice for 5 min. The methanol was then removed and the cells were washed with 3 ml PBS. The cover slips were then removed from the wells and inverted on a drop (30 µl) of DAPI (0.2 µg ml^{-1} in PBS) placed on parafilm. The cover slips were kept on the DAPI solution for 5 min at ambient temperature. The cover slips were then rinsed with PBS and mounted on a microscope slide using a drop (30 µl) of mowiol mounting medium. The slides were allowed to dry in the dark overnight. Microscopic images were observed at a magnification of 1000× and recorded with a Zeiss Axioplan fluorescence microscope equipped with a Photometrics Sensys digital CCD camera system. Images were manipulated using *IP-LAB Spectrum* software. Drug fluorescence in cells was observed at wavelengths longer than 590 nm with excitation at 546 ± 6 nm. DAPI fluorescence was observed at wavelengths longer than 420 nm with excitation at 355 ± 20 nm.

3. Results and discussion

3.1. Crystal structure of epidoxorubicin covalently bound to d(CGCGCG)

The crystallographic asymmetric unit consists of a single strand of d(CGCGCG) covalently attached to a 4′-epidoxorubicin molecule *via* a methylene group at one of the guanines and 30 ordered water molecules. Two asymmetric units form a slightly distorted B-type DNA duplex with six Watson–Crick base pairs. Fig. 2 shows [4′-epidoxorubicin–CH_2–d(CGCGCG)]$_2$ with the DNA displayed as a CPK structure and the drug as a framework structure. As observed in other anthracycline–DNA structures, the aglycon rings of epidoxorubicin are intercalated at CpG steps, with the D ring reaching into the major groove while the sugar moiety lies in the minor groove. The intercalation sites are C(1)G(2)/G(12)C(11) and C(5)G(6)/G(8)C(7). [The nucleotides labeled C(1)–G(6) are on a strand in one asymmetric unit, with C(7)–G(12) located on the complementary strand generated by twofold crystallographic symmetry]. Two methylene groups link the 3′-amino substituents of two epidoxorubicins to the 2-amino substituents of G(10) and G(4). Fig. 3 shows a stereoscopic view of the $F_o - F_c$ electron-density map superimposed on the final model of 4′-epidoxorubicin–CH_2–d(CGCGCG).

Comparison of the structure with the covalent daunorubicin–CH_2–d(CGCGCG) (Wang *et al.*, 1991) and the non-covalent 4′-epidoxorubicin–d(CGATCG) structures (Williams *et al.*, 1990) is instructive and is summarized in Table 2 and Fig. 4. The general coordinate error based on the Luzzati plot for our model is 0.20 Å. Of particular significance are hydrogen-bonding interactions between the drug and the DNA. The O9 hydroxyl groups of the drugs in all three structures are hydrogen bonded to N2 and N3 of G(8) with approximately the same bond distances (3.12–3.15 and 2.89–2.59 Å, respectively). The

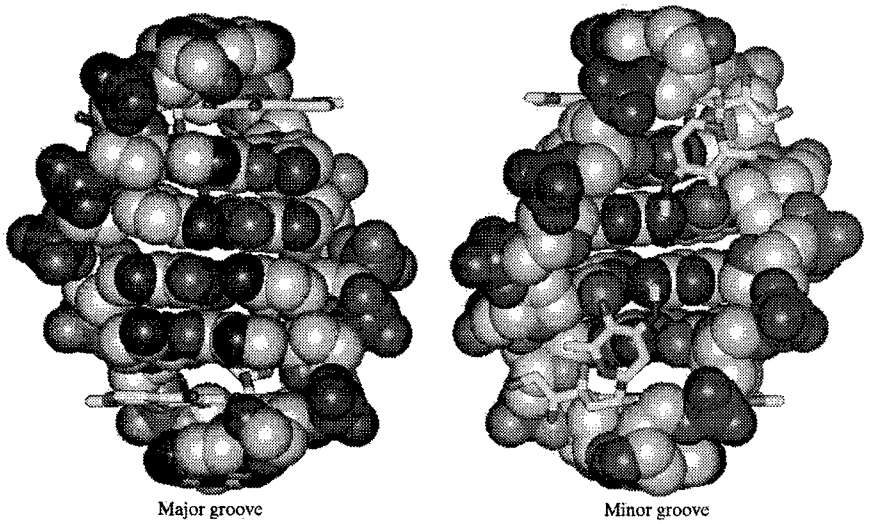

Figure 2
Epidoxorubicin–CH_2–d(CGCGCG), with DNA displayed as a CPK structure and epidoxorubicin–CH_2 displayed as a framework structure. This figure was created with *Insight*II (Biosym Technologies, San Diego, CA).

Table 2
Distances.

Drug atom	DNA atom	Water atom†	Distance (Å)		
			Epidox–CH_2–d(CG)$_3$‡	Dauno–CH_2–d(CG)$_3$	Epidox–d(CGATCG)
O9	G(8) N3		2.89	2.86	2.59
	G(8) N2		3.12	3.12	3.15
O7	G(8) N2		2.87	3.13	3.35
O14	C(9) C5′		3.70	–	–
	A(9) C5′		–	–	3.40
O4′	C(9) O2		2.70	>4.0	–
	A(9) N3		–	–	3.06
N3′	G(4) N2		2.50	2.48	–
	T(4) O2		–	–	3.37
	C(5) O2		3.33	3.24	3.27
	C(5) O4′		3.55	3.16	3.31
	CH_2		1.52	1.53	–
CH_2	G(4) N2		1.46	1.45	–
O4		W(1)	2.81	3.06	3.02
O5		W(1)	3.02	3.21	3.11
	G(6) N7	W(1)	2.69	2.72	2.83
O12		W(25)	2.90	3.81	>4.0
	G(8) N7	W(25)	3.07	3.01	2.61
O13		W(6)	2.89	3.11	3.34
	C(7) O2	W(6)	2.84	2.60	2.65

† Naming convention from epidoxorubicin–CH_2–d(CGCGCG) structure. ‡ Luzzati coordinate error = 0.20 Å.

distance between the anomeric O7 of the drug and the N2 of G(8) is shorter in epidoxorubicin–CH_2–d(CGCGCG) than in the other structures (2.87 *versus* 3.13 and 3.35 Å), suggesting that there is a stronger hydrogen bond between these atoms. The primary structural difference between epidoxorubicin and daunorubicin is the configuration of the hydroxyl at the 4′-position. This leads to a good hydrogen-bonding interaction (2.70 Å) with the O2 of C(9) on the complementary strand in the structure of epidoxorubicin–CH_2–d(CGCGCG). In epidoxorubicin–d(CGATCG), this hydrogen bonding is with the N3 of the adenine on the complementary strand. Perhaps the extra hydrogen bonding causes the aglycon A ring of the drug to lie closer to G(8) on the complementary strand in epidoxorubicin–CH_2–d(CGCGCG). The 14-hydroxyl, present in the epidoxorubicin structures but not in the daunorubicin structure, lies farther away from the C5′ of C(9) on the complementary strand in the covalent structure than in the non-covalent structure (3.70 *versus* 3.40 Å). Differences in the A ring, O7, O14 and aminosugar of the drugs in the three structures are shown *via* an overlay diagram in Fig. 5. The alignment was performed using all the common atoms, including the atoms of the nucleic acid moieties, between epidoxorubicin–CH_2–d(CGCGCG) as the reference molecule and either daunorubicin–CH_2–d(CGCGCG) or epidoxorubicin–d(CGATCG). For clarity, the superimposed DNA from the structures was omitted from Fig. 5. The O12 is within hydrogen-bonding distance (2.90 Å) of a water molecule, W(25), which is associated with the N7 of guanine G(8) (3.07 Å). [Solvent water molecules are labeled W(1)–W(30).] While the other two structures also have a water molecule near N7 of G(8) (3.01 or 2.61 Å), it is too far away from O12 (3.81 or >4.01 Å) to mediate contact between the drug and the DNA. All of these drug–DNA and drug–water molecule contacts are summarized in Table 2 and Fig. 4.

The drug–DNA adducts are hydrolytically unstable, and the drug is released at two different first-order rates, one with a half-life of 5 h and the other of 40 h (Cullinane, van Rosmalen *et al.*, 1994; van Rosmalen *et al.*, 1995). Prior to an understanding of the molecular nature of the covalent bonding, the drug released more slowly was thought to be covalently attached to both strands of the DNA at the G bases of a GC site. The crystal structure reported here and the earlier structure of daunorubicin covalently bound to d(CGCGCG) (Wang *et al.*, 1991) provide a simple explanation for slower release of drug from a GC site, even though the drug has only one covalent attachment. In addition to the covalent attachment to a G on one strand, the drug is strongly hydrogen bonded between its 9-hydroxyl and the N atoms at the 2- and 3-positions of the guanine on the complementary strand. The [epidoxorubicin–CH_2–d(CGCGCG)]$_2$ structure also suggests hydrogen bonding between O7 of the drug and N2 of G(8) and between O4′ of the drug and O2 of C(9) on the complementary strand. Because the original proposal for the structure of more stable lesions was thought to be a crosslink of DNA by the drug, we proposed the term virtual crosslink for this bonding, which is unique to the GC dinucleotide. The less stable DNA–drug adducts are then proposed to have covalent attachment to isolated G bases *via* methylene groups, and to be missing the hydrogen-bonding interactions with the opposing strand.

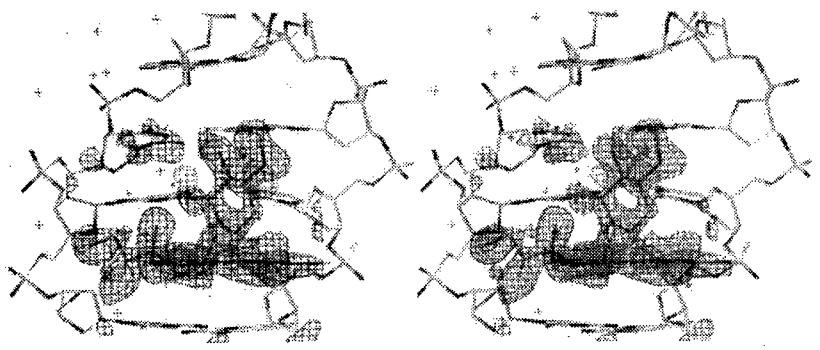

Figure 3
Stereoscopic view of an $F_o - F_c$ electron-density map superimposed on the final model of epidoxorubicin–CH_2–d(CGCGCG). All atoms of the drug were omitted during the map calculation using only the coordinates in the final model of the DNA molecule for the phase information. The density is contoured at 2σ. Bonds and atoms are colored according to atom type.

The virtual crosslink of the self-complementary hexanucleotide d(ATGCAT) at the TGC site from reaction with a single doxorubicin and formaldehyde has recently been characterized using NMR spectroscopy (Zeman *et al.*, 1998). This study also reported the effect of the virtual cross-

link on the stability of duplex DNA from measurements of the rate of DNA-strand exchange. Strand exchange was 3.9 times slower with a doxorubicin merely intercalating in an oligonucleotide but 637 times slower with a doxorubicin virtually crosslinking the oligonucleotide.

3.2. Uptake and distribution of drug in MCF-7/ADR cells

MCF-7/ADR cells are mutants of the MCF-7 human breast-cancer cell line which are highly resistant to doxorubicin (Adriamycin). They are also resistant to daunorubicin and epidoxorubicin but not to Daunoform, Epidoxoform or Doxoform (Fenick *et al.*, 1997; Taatjes, Fenick & Koch, 1998). Important resistance mechanisms are increased activity of enzymes which neutralize the effects of drug-induced oxidative stress and overexpression of the drug efflux pump, P-170 glycoprotein (Pgp) (Mimnaugh *et al.*, 1991; Sinha & Mimnaugh, 1990). This cell line, therefore, is particularly useful for studying the effect of the conjugation of the drug with formaldehyde, because daunorubicin and epidoxorubicin are maintained at lower concentrations by drug efflux. The efflux pump recognizes the drugs partly because of the positive charge at the amino substitutent (Lampidis *et al.*, 1997). Formaldehyde conjugates are uncharged because of a change in pK_a resulting from the hydroxymethylene substituent and hence are predicted to be poorer substrates for Pgp. Further, formation of active metabolite by the clinical drug is enzymatically inhibited in MCF-7/ADR cells.

Uptake of Daunoform and Epidoxoform by MCF-7/ADR cells at 310 K as a function of time of exposure to 0.25 μM drug was measured by flow cytometry (Fig. 6). Drug fluorophore in cells was detected by its fluorescence in the region of 590 nm. The fluorophore in cells treated with Daunoform appeared rapidly, with the maximum level occurring after approximately 7 min, followed by a steady decrease during the remaining 3 h exposure period. In contrast, fluorophore in cells treated with Epidoxoform steadily increased over the 3 h exposure period. The rates of uptake parallel the rates of hydrolysis of conjugates to the active metabolites of the respective clinical drugs (Fig. 1). Hydrolysis of Daunoform to the active metabolite occurs with a half-life of less than 10 min in cell-culture medium at 298 K (Fenick *et al.*, 1997), while hydrolysis of Epidoxoform to the active metabolite occurs with a half-life of 2 h at 310 K in cell-culture medium (Taatjes, Fenick & Koch, 1998). Further, the half-lives for hydrolysis of the active metabolites to daunorubicin and epidoxorubicin are less than 10 min and greater than 2 h, respectively. This parallel suggests that the slow step for drug uptake by MCF-7/ADR cells is hydrolysis to the active metabolite.

The location of drug fluorophore in the nucleus of MCF-7/ADR cells treated with either Daunoform or Epidoxoform was established by fluorescence microscopy, as shown in Fig. 6. Anthracycline fluorescence was primarily in the nucleus, as indicated by co-staining with the nuclear stain DAPI. The abundance of anthracycline in the nucleus is even higher than indicated by the micrographs because DNA partially quenches the fluorescence (Crooke & DuVernay, 1980; Roche *et al.*, 1994). Since the anthracycline is predominantly in the nucleus, the release of fluorophore from cells exposed to Daunoform after 7 min of drug treatment can be explained by hydrolysis of drug covalently bound to DNA occurring faster than new covalent binding of drug metabolite. In fact, after about 30 min most of the Daunoform in the cell-culture medium has hydrolyzed to daunorubicin, which is not significantly taken up by MCF-7/ADR cells because of the Pgp efflux pump. Further, formation of the active metabolite from daunorubicin is inhibited in these cells by the increased activity of enzymes which neutralize oxidative stress. The rate of fluorophore release over the 3 h time period is most consistent with predominant hydrolysis of drug–DNA lesions at isolated G bases. This hydrolysis releases daunorubicin which is pumped out of the cell. Steady increase of fluorophore in MCF-7/ADR cells upon treatment with Epidoxoform over the 3 h time period is a consequence of much slower

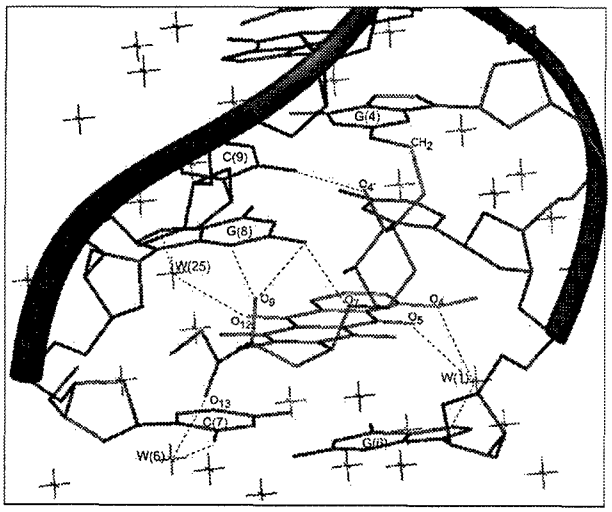

Figure 4
Hydrogen-bonding contacts between epidoxorubicin–CH_2 and d(CGCGCG). This figure was created with *Insight*II (Biosym Technologies, San Diego, CA).

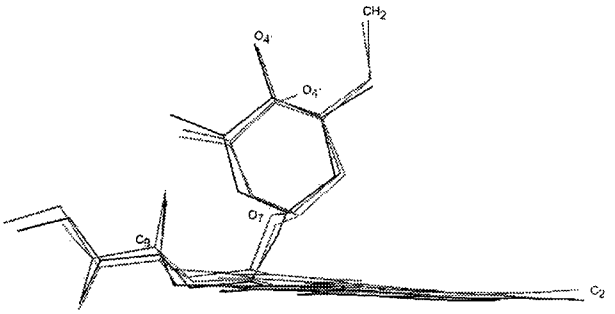

Figure 5
Overlay of epidoxorubicin (in black) and daunorubicin–CH_2 (in green) on epidoxorubicin–CH_2 (in red). R.m.s.d. in distance of all atoms common to epidoxorubicin–CH_2–d(CGCGCG) and daunorubicin–CH_2–d(CGCGCG) is 0.923 Å and between epidoxorubicin–CH_2–d(CGCGCG) and epidoxorubicin–d(CGATCG) is 0.829 Å. For clarity, the overlaid DNA strands have been omitted from the figure.

hydrolysis to the active metabolite and increased stability of the metabolite with respect to further hydrolysis to epidoxorubicin. Hence, covalent bonding of drug to DNA is occurring faster than hydrolysis of drug–DNA lesions. Additional evidence for covalent binding of drug to DNA in cells comes from a comparison of release of drug from cells treated with either parent drug or formaldehyde conjugate and from analysis of cells treated with tritiated formaldehyde conjugate (Taatjes *et al.*, 1999).

The crystal structure provides some additional insight with respect to drug uptake by MCF-7/ADR cells. The additional hydrogen-bonding interaction between the epidoxorubicin's 4′-hydroxyl and the O2 of C(9) on the complementary strand should lead to slower hydrolysis of the virtual crosslink of DNA with epidoxorubicin than with daunorubicin. This slower release from DNA gives rise to continued uptake as Epidoxoform is slowly hydrolyzing to the active metabolite. Daunoform hydrolyzes to its active metabolite very rapidly, which causes a rapid buildup of drug in the nucleus of tumor cells. The intracellular levels then also decrease because of the predicted less stable daunorubicin virtual crosslink.

In summary, the 1.6 Å crystal structure of [epidoxorubicin–CH_2–d(CGCGCG)]$_2$ shows a slightly distorted B-type DNA duplex symmetrically bearing two intercalated epidoxorubicin molecules located at the termini which are covalently attached to the DNA *via* methylene groups. Covalent attachment is from the 3′-amino group of epidoxorubicin to the 2-amino group of G(4) or G(10). The structure is analogous to the structure of [daunorubicin–CH_2–d(CGCGCG)]$_2$, except for additional hydrogen bonding from the 4′-hydroxyl group of epidoxorubicin to the O2 of C(3) or C(9). This hydrogen bonding, together with hydrogen bonding between O7 and O9 of the drug and N2 and/or N3 of G(2) or G(8) and the covalent attachment, result in a virtual crosslinking of DNA by drug. Flow cytometry and fluorescence microscopy show that daunorubicin–formaldehyde conjugate (Daunoform) and epidoxorubicin–formaldehyde conjugate (Epidoxoform) are readily taken up by doxorubicin-resistant human breast-cancer cells and locate predominantly in the nucleus. Differences in the rates of uptake are consistent with differences in the rates of hydrolysis of the conjugates to the proposed DNA-reactive form of the drugs and differences in the respective structures of the drugs covalently bound to DNA.

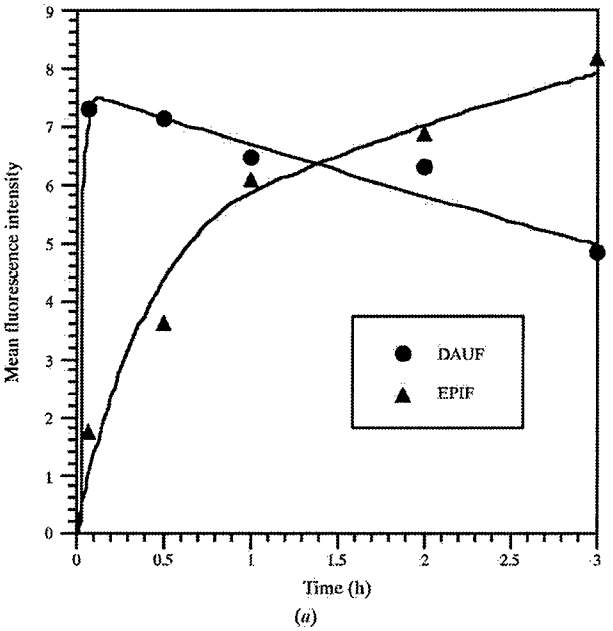

(*a*)

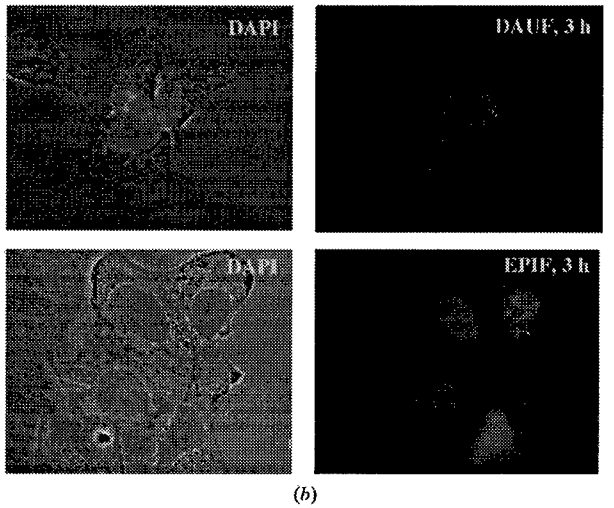

(*b*)

Figure 6
(*a*) Uptake of the fluorophore of Daunoform (DAUF) or Epidoxoform (EPIF) by MCF-7/ADR cells as a function of time of exposure to 0.25 μ*M* drug, as determined by flow cytometry measuring fluorescence intensity at 570–600 nm. (*b*) Fluorescence micrographs of MCF-7/ADR cells after treatment with either 0.25 μ*M* Daunoform or Epidoxoform for 3 h. After drug treatment, cells were fixed and stained with the nuclear stain DAPI. Each micrograph showing DAPI fluorescence in green superimposed on the whole cell image is located adjacent to the respective micrograph showing drug fluorophore emission.

This work was supported by grants from the American Cancer Society (RPG-98-110-01), the National Cancer Institute (CA78756) and the US Army Breast Cancer Research Program (DAMD17-98-1-8298) to THK and by the Howard Hughes Medical Institute to Thomas R. Cech. ERP and DJH are Research Specialists of the Howard Hughes Medical Institute. DJT thanks the Division of Medicinal Chemistry of the American Chemical Society and Wyeth-Ayerst, Inc. for a predoctoral fellowship. We thank Steve Schultz for collecting the X-ray data and for valuable discussions. We thank Gensia–Sicor (Milan, Italy) for a sample of epidoxorubicin, Nexstar Pharmaceuticals, San Dimas, CA for a sample of daunorubicin and William W. Wells for MCF-7/ADR cells.

References

Brünger, A. T., Adams, P. D., Clore, G. M., Delano, W. L., Gros, P., Grosse-Kunstleve, R. W., Fiang, J., Kuszewski, J., Niles, M., Pannu, N. S., Read, R. J., Rice, L. M., Simmonson, T. & Warren, G. L. (1998). *Acta Cryst.* **D54**, 905–921.

Brünger, A. T. & Rice, L. M. (1997). *Methods Enzymol.* **277**, 243–269.
Crooke, S. T. & DuVernay, V. H. (1980). *Anthracyclines: Current Status and New Developments*, edited by S. T. Crooke & S. D. Reich, pp. 151–155. New York: Academic Press.
Cullinane, C., Cutts, S. M., van Rosmalen, A. & Phillips, D. R. (1994). *Nucleic Acids Res.* **22**, 2296–2303.
Cullinane, C., van Rosmalen, A. & Phillips, D. R. (1994). *Biochemistry*, **33**, 4632–4638.
Cutts, S. M., Parsons, P. G., Sturm, R. A. & Phillips, D. R. (1996). *J. Biol. Chem.* **271**, 5422–5429.
Cutts, S. M. & Phillips, D. R. (1995). *Nucleic Acids Res.* **23**, 2450–2456.
Durand, R. E. & Olive, P. L. (1981). *Cancer Res.* **41**, 3489–3494.
Fenick, D. J., Taatjes, D. J. & Koch, T. H. (1997). *J. Med. Chem.* **40**, 2452–2461.
Gewirth, D. (1997). *The HKL Manual – A Description of Programs DENZO, XDISPLAYF and SCALEPACK*, 5th ed. New Haven, CT: Yale University Press.
Jones, T. A., Zou, J. Y., Cowan, S. W. & Kjeldgaard, M. (1991). *Acta Cryst.* A**47**, 110–119.
Lampidis, T. J., Kolonias, D., Podona, T., Israel, M., Safa, A. R., Lothstein, L., Savaraj, N., Tapiero, H. & Priebe, W. (1997). *Biochemistry*, **36**, 2679–2685.
Mimnaugh, E. G., Fairchild, C. R., Fruehauf, J. P. & Sinha, B. K. (1991). *Biochem. Pharmacol.* **42**, 391–402.
Otwinowski, Z. & Minor, W. (1997). *Methods Enzymol.* **276**, 307–326.
Parkinson, G., Vojtechovshy, J., Clowney, L., Brünger, A. T. & Berman, H. M. (1996). *Acta Cryst.* D**52**, 57–64.
Roche, C. J., Thomson, J. A. & Crothers, D. M. (1994). *Biochemistry*, **33**, 926–935.
Rosmalen, A. van, Cullinane, C., Cutts, S. M. & Phillips, D. R. (1995). *Nucleic Acids Res.* **23**, 42–50.
Sinha, B. K. & Mimnaugh, E. G. (1990). *Free Rad. Biol. Med.* **8**, 567–581.
Taatjes, D. J., Fenick, D. J., Gaudiano, G. & Koch, T. H. (1998). *Curr. Pharm. Des.* **4**, 203–218.
Taatjes, D. J., Fenick, D. J. & Koch, T. H. (1998). *J. Med. Chem.* **41**, 2452–2461.
Taatjes, D. J., Fenick, D. J. & Koch, T. H. (1999). *Chem. Res. Toxicol.* **12**, 588–596.
Taatjes, D. J., Gaudiano, G. & Koch, T. H. (1997). *Chem. Res. Toxicol.* **10**, 953–961.
Taatjes, D. J., Gaudiano, G., Resing, K. & Koch, T. H. (1996). *J. Med. Chem.* **39**, 4135–4138.
Taatjes, D. J., Gaudiano, G., Resing, K. & Koch, T. H. (1997). *J. Med. Chem.* **40**, 1276–1286.
Wang, A. H. J., Gao, Y. G., Liaw, Y. C. & Li, Y. K. (1991). *Biochemistry*, **30**, 3812–3815.
Williams, L. D., Frederick, C. A., Ughetto, G. & Rich, A. (1990). *Nucleic Acids Res.* **18**, 5533–5541.
Zeman, S. M., Phillips, D. R. & Crothers, D. M. (1998). *Proc. Natl Acad. Sci. USA*, **95**, 11561–11565.

Biochemical Pharmacology, Vol. 60, pp. 1915–1923, 2000.

ELSEVIER

ISSN 0006-2952/00/$–see front matter
PII S0006-2952(00)00521-9

Lack of Glutathione Conjugation to Adriamycin in Human Breast Cancer MCF-7/DOX Cells

INHIBITION OF GLUTATHIONE S-TRANSFERASE P1–1 BY GLUTATHIONE CONJUGATES FROM ANTHRACYCLINES

Giorgio Gaudiano,† Tad H. Koch,†‡ Mario Lo Bello,§ Marzia Nuccetelli,§ Giampietro Ravagnan,* Annalucia Serafino* and Paola Sinibaldi-Vallebona¶‖*

*INSTITUTE OF EXPERIMENTAL MEDICINE, NATIONAL RESEARCH COUNCIL, 00133 ROME, ITALY; †DEPARTMENT OF CHEMISTRY AND BIOCHEMISTRY, UNIVERSITY OF COLORADO, BOULDER, CO 80309-0215, U.S.A.; §DEPARTMENT OF BIOLOGY, AND ¶DEPARTMENT OF EXPERIMENTAL MEDICINE AND BIOCHEMICAL SCIENCES, UNIVERSITY OF ROME "TOR VERGATA," 00133 ROME, ITALY; AND ‖RESEARCH AREA OF ROME "TOR VERGATA" - P.B.I., NATIONAL RESEARCH COUNCIL, 00137 ROME, ITALY

ABSTRACT. One of the proposed mechanisms for multidrug resistance relies on the ability of resistant tumor cells to efficiently promote glutathione S-transferase (GST)-catalyzed GSH conjugation of the antitumor drug. This type of conjugation, observed in several families of drugs, has never been documented satisfactorily for anthracyclines. Adriamycin-resistant human breast cancer MCF-7/DOX cells, presenting a comparable GSH concentration, but a 14-fold increase of the GST P1–1 activity relative to the sensitive MCF-7 cells, have been treated with adriamycin in the presence of verapamil, an inhibitor of the 170 P-glycoprotein (P-gp) drug transport protein, and scrutinized for any production of GSH–adriamycin conjugates. HPLC analysis of cell content and culture broths have shown unequivocally that no GSH conjugates are present either inside the cell or in the culture broth. The only anthracycline present inside the cells after 24 hr of incubation was > 98% pure adriamycin. Confocal laser scanning microscopic observation showed that in MCF-7/DOX cells adriamycin was localized mostly in the Golgi apparatus rather than in the nucleus, the preferred site of accumulation for sensitive MCF-7 cells. These findings rule out GSH conjugation or any other significant biochemical transformation as the basis for resistance to adriamycin and as a ground for the anomalous localization of the drug in the cell. Adriamycin, daunomycin, and menogaril did not undergo meaningful conjugation to GSH in the presence of GST P1–1 at pH 7.2. Indeed, their synthetic C(7)-aglycon–GSH conjugates exerted a strong inhibitory effect on GST P1–1, with K_i at 25° in the 1–2 μM range, scarcely dependent on their stereochemistry at C(7). BIOCHEM PHARMACOL 60;12:1915–1923, 2000. © 2000 Elsevier Science Inc.

KEY WORDS. adriamycin; GSH conjugation; GST inhibition; multidrug resistance; MCF-7; DOX

The resistance of cancer cells acquired upon exposure to a single antitumor drug, such as ADR** (1) or DAUN (2) (Fig. 1), often extends over a range of other drugs even of a completely different chemical nature. Such ability of tumor cells to develop cross-resistance to many drugs (MDR) poses a major obstacle to successful chemotherapy [1, 2]. In spite of intense studies worldwide, the precise mechanisms of the insurgence and functioning of MDR are far from being understood clearly [1, 3–6].

The insurgence of MDR is commonly associated with the overexpression of P-gp. P-gp, encoded by the human *mdr1* gene, is an ATP-dependent membrane protein and plays a key role in drug efflux by acting as an extrusion pump that lowers the cellular drug concentration below toxic levels [1, 2, 7–9]. However, in many cases, MDR can be acquired through mechanisms other than the overexpression of P-gp or other similar membrane proteins [2, 4–6]. The hypothesis of a different mechanism for MDR first came from the observation that, independent of any overexpression of P-gp, MDR is oftentimes associated with an increase of the cellular GSH concentration and/or GST activity and expression [5, 6, 10–12]. The GSTs (EC 2.5.1.18) are a family of dimeric enzymes that conjugate a wide variety of carcinogenic, mutagenic, toxic, and pharmacologically active electrophiles to the cellular nucleophile glutathione (GSH, γ-Glu-Cys-Gly) [13]. The possible role of GSTs in MDR

‡ Corresponding author. Tel. (303) 492-6193; FAX (303) 492-5894; E-mail: tad.koch@colorado.edu

** *Abbreviations*: ADR (DOX), adriamycin (doxorubicin); ADRIGLU, adriamycin–GSH conjugate; BCNU, 1,3-bis(2-chloroethyl)-1-nitrosourea; CDNB, 1-chloro-2,4-dinitrobenzene; DAUN, daunomycin (daunorubicin); DAUNOGLU, daunomycin–GSH conjugate; DHM-3, 3,5-dimethyl-5-(hydroxymethyl)-2-oxomorpholin-3-yl; DTT, dithiothreitol; GST, glutathione S-transferase; MDR, multidrug resistance or resistant; MENOGLU, menogaril–GSH conjugate; MRP, multidrug resistance protein; PBS, phosphate-buffered saline (pH 7.4, 10 mM phosphate, 138 mM NaCl, 2.7 mM KCl); and P-gp, 170 P-glycoprotein.

Received 15 November 1999; accepted 19 June 2000.

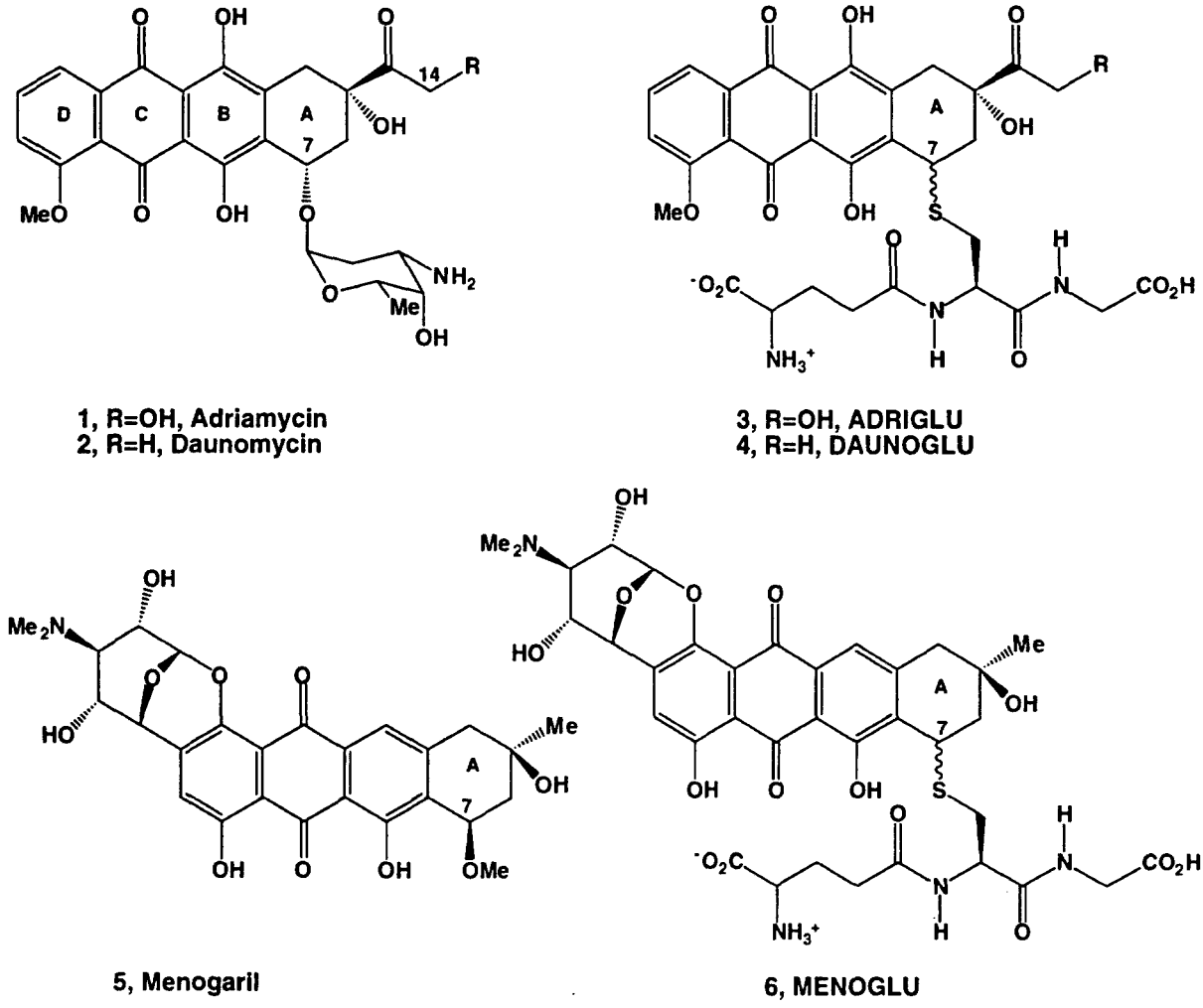

FIG. 1. Structures of the anthracycline antitumor drugs ADR (DOX), DAUN, and menogaril and their respective glutathione conjugates ADRIGLU, DAUNOGLU, and MENOGLU.

would indeed be an example of a widespread defense process in living organisms. The products of the GST-catalyzed GSH conjugation of carcinogenic, mutagenic, toxic, and pharmacologically active compounds, including antineoplastic drugs, or their metabolites, can be extruded and disposed of either as such or after enzymatic transformation [12, 14, 15]. The possibility of this type of detoxifying process being responsible for many cases of acquired MDR during chemotherapy has been investigated and often debated through the last two decades [10, 12, 14, 16–19] and critically reviewed [5, 6, 11]. Relevant to this proposed defense mechanism in MDR cells are the reports on the presence of an ATP-dependent extrusion pump (MRP) for xenobiotics and GSH conjugates, different from P-gp [15, 20–24]. However, beside the oftentimes observed increase in GSH concentration and GST activity and the reports on the presence of MRP, true evidence for a GST/GSH conjugation of anticancer drugs has been offered only for the strongly electrophilic mustard-type (chlorambucil, mephalan, cyclophosphamide, BCNU) or aziridine-type (thiotepa) drugs, with the identification of their GSH conjugates. Mitomycin C, of completely different chemical structure and properties, gives *in vitro* GSH conjugates upon enzymatic or chemical reductive activation [25, 26]. However, no clear evidence of a resistance/GSH-conjugation relationship has been offered. Concerning the anthracyclines, a family of relatively poor electrophilic drugs [27], GSH conjugates have been synthesized only upon chemical reduction of the anthracyclines **1**, **2**, and menogaril (**5**) (Fig. 1) to the corresponding more electrophilic quinone methides followed by reaction with GSH [28] or by reaction with GSH in trifluoroacetic acid [29]. So far much speculation has occurred on their possible GSH conjugation in living systems, like MDR cells, but no compelling evidence that might either prove or disprove the formation of GSH conjugates of anthracyclines has been provided by either *in vivo* or *in vitro* experiments. Indeed, beside the above-mentioned reports on the effects of variations of GSH concentration, or GST activity/expression, or MRP over-expression, on MDR, and the successful synthesis of GSH conjugates directly from GSH and anthracyclines, the only other experimental observation that might comfortably be in line with a GSH conjugation of anthracyclines has been offered by our recent report on cytoplasmic localization of

anthracyclines [30]. We have observed that in ADR-resistant MCF-7/DOX human breast cancer cells, displaying a very high GST activity, **1** and **2** seem to be localized, as suggested by fluorescence, in the same Golgi region where their synthetic GSH conjugates **3** and **4** appear to be localized. Instead, in sensitive MCF-7 cells, of relatively low GST activity, **1** and **2** localize in the nucleus, while again their GSH conjugates localize in the Golgi region. The conjugates proved to be less cytotoxic than their parent anthracyclines.

In this paper, we report clear evidence that, in spite of the previous considerations, no GSH conjugation of ADR occurs in human breast cancer MCF-7/DOX cell lines, even in the presence of the P-gp inhibitor verapamil. We also offer our *in vitro* experiments on the possible GSH conjugation of anthracyclines catalyzed by the human placenta GST, a class Pi (46 kDa) homodimeric protein identified as GST P1–1 [31]. This enzyme has been studied extensively in different laboratories because of its potential use as a marker during chemical carcinogenesis [32, 33] and its possible role in the MDR of a number of antineoplastic agents [14, 34–37]. We report that GST P1–1 did not effectively catalyze the conjugation of the antitumor anthracyclines **1, 2,** and **5** with GSH under physiological conditions, either in the presence or in the absence of dioxygen from air. Negative results were obtained even if a preliminary reduction of **1** to the corresponding, more electrophilic quinone methide [38] had been performed. Indeed, the GSH conjugates **3, 4,** and **6** [28] behaved as strong inhibitors of the enzyme.

MATERIALS AND METHODS

General

Solvents and chemicals were purchased from Janssen with the exception of 2,4-dinitrofluorobenzene and DMSO, obtained from Sigma-Aldrich. DHM-3 dimer was prepared as described earlier [39]. The uv-vis spectra were obtained with a Hewlett-Packard 8452A diode array spectrometer.

Anthracyclines and Their GSH Conjugates

ADR (**1**) and DAUN (**2**) were gifts of Pharmacia-Farmitalia. Menogaril (**5**) was a gift from Pharmacia-Upjohn. ADRIGLU (**3**) (Fig. 1) was obtained as a mixture of the epimers **3-I** and **3-II** as reported in the literature [28]. Epimers **3-I** and **3-II** then were separated and purified by submitting the mother liquors from the crude reaction mixture to preparative reverse phase HPLC. Before chromatography, the liquors were concentrated down to a 12 mM total anthracycline concentration. HPLC analysis showed 50% **1**, 25% **3-II**, and 10% **3-I** (% area monitoring at 480 nm). Preparative HPLC was performed on a Rainin semipreparative chromatograph equipped with a Dynamax model UV-1 detector and a Rainin 3 μm C18 Microsorb column, 10 mm i.d. x 50 mm. The eluting solvent was a 45/55 (v/v) mixture of methanol and a 0.3% (pH 4.0) ammonium formate-formic acid buffer, at a flow rate of 3 mL/min, isocratic. Injections were 200 μL each. Under these conditions, the retention times were 8, 11, and 14 min for **3-I, 3-II,** and **1,** respectively. The fractions containing **3-I** and **3-II** were separately combined and evaporated down to 1/20 of the original volume and again passed through the same column using a 50/50 (v/v) methanol–water mixture. The solvent from the anthracycline-containing fractions was removed under vacuum at ambient temperature to leave 99% pure **3-I** and **3-II** as dark-red powders. The two diastereoisomers displayed almost identical uv-vis spectra.

DAUNOGLU (**4-II**) (Fig. 1) was obtained through its DAUNOGLU salt (i.e. its salt with unreacted DAUN) in much the same way as **3-II** was obtained from its ADRIGLU salt ($3^{-}1^{+}$), the only noteworthy difference being the 2-fold higher concentration of the starting reactants **2** and GSH and the longer reaction time (3 days). The sample of **4-II** obtained after chloroform extraction of unreacted **2** from the basic solution of the salt showed less than 1% of unextracted **2.**

MENOGLU **I** and **II** (**6-I** and **6-II**) (Fig. 1) were used as a 1:1 mixture as obtained directly from menogaril (**5**) and GSH as reported [28]. The amount of the excess of GSH, calculated by stoichiometric relationship and confirmed by HPLC analysis, was taken into account for the calculation of the GST inhibition constant, as reported below.

Qualitative and quantitative assays of anthracyclines and their derivatives obtained by synthesis or from biological and GST inhibition tests were performed by HPLC analysis using (method A): a Waters chromatograph equipped with a model 510 two pump solvent delivery system and a uv-vis model 996 diode array detector, monitoring at 480 nm. A Supelcosil RP C18, 2.1 × 150 mm, 5 μm column was used, eluting isocratically with a 50/50 mixture of methanol and a 0.3% (pH 4.0) ammonium formate-formic acid buffer. Alternatively (method B), the HPLC analyses were performed on a Kontron chromatograph provided with a model 420 two pump solvent delivery system and a uv-vis model 430 detector, using a Supelcosil RP C18 4.6 mm × 150 mm, 5 μm column with a flow rate of 0.60 mL/min. Whenever possible, samples were analyzed containing between 1 and 20 nmol of anthracyclines. Lower amounts of anthracyclines, between 0.5 and 1 nmol, could be measured with 90% accuracy. Quantitation of the results from HPLC was done using as reference the linear Lambert-Beer region of a concentration versus peak area plot obtained from pure samples of anthracyclines and derivatives. Proof of identity in critical experiments was established by co-injection and comparison of spectra with authentic samples.

Cell Lines and Drug Treatment

The drug-sensitive human breast cancer cell line MCF-7 and its derivative MDR variant, MCF-7/DOX, were grown as a monolayer in RPMI 1640 medium (Flow) supplemented with 10% (v/v) heat-inactivated fetal bovine serum, L-glutamine (2 mM), penicillin (100 IU/mL), and streptomycin (100 μg/mL) at 37° in a humidified atmo-

sphere of 5% CO_2. Cells were passaged serially twice weekly after detachment from culture flasks with 0.05% trypsin and 0.02% EDTA in PBS. The MDR cells were grown in the presence of 10 μM ADR (**1**) and cultured for 4 weeks in drug-free medium prior to use. To analyze the anthracycline content, exponentially growing cells were cultured in 175 cm^2 flasks in RPMI 1640 medium (50 mL) without phenol red for 24 hr before exposure to **1** (1 μg/mL) or **3-II** (6 μg/mL). After exposure to drugs for 2 or 24 hr, the medium was collected, and the cells were rinsed with PBS without Ca^{2+} and Mg^{2+}. The cells were detached with a rubber spatula and collected by centrifugation. The pellet was resuspended in 500 μL of distilled water, and the cells were lysed by three freeze–thaw cycles. The cell lysate was clarified by centrifugation at 13,600 *g* for 10 min, and both pellet and supernatant were stored at −20°.

To study the intracellular distribution of drugs, cells were cultured at 37° for 24 hr before exposure to ADR, ADRIGLU, DAUN, and DAUNOGLU at concentrations ranging from 0.1 to 6 μg/mL for different periods of time. After treatment, cells were washed three times with PBS free of Ca^{2+} and Mg^{2+}, and processed for confocal microscopy. For MDR reversal, MCF-7/DOX cells were pretreated for 1.5 min at 37° in regular medium containing verapamil (Sigma) at a concentration of 10 μg/mL.

Analysis of Anthracyclines from Cell Cultures

Qualitative and quantitative assays for anthracyclines after incubation with MCF-7 and MCF-7/DOX cells were performed by HPLC using method A or B (see above). The values reported for quantitative analyses are averages from analyses performed in duplicate or triplicate, with observed variations being below 15%. The samples to be analyzed were kept in the freezer at −20° throughout the time necessary for the analyses to be completed. The samples tested were (see previous subsection): (i) the supernatant culture media recovered after centrifugation at the end of the incubation, filtered through sterile Acrodisc 0.2 μm Gelman filters; (ii) the clear supernatants from centrifugation of cell lysates; and (iii) the DMSO extract (1 mL/10^6 cells) of the pellet of the cell-fragments obtained by centrifugation of lysates. To improve the accuracy of the HPLC analysis of anthracyclines in the culture media, prior to the analysis the filtered supernatant was passed through reverse phase cartridges (C18 SEP-PAK, Waters). The anthracyclines were retained completely but could be eluted promptly with a 1:1 mixture of methanol–water to obtain an eluant showing a 10-fold increased concentration. With these conditions, using 1-mL HPLC injections, amounts of conjugate as low as 0.5 μmol, corresponding to 5% of conversion, could be detected easily if present.

Confocal Laser Microscopy

Analysis of the intracellular distribution of ADR and ADRIGLU was carried out on cells grown on coverslips and observed after fixing with 2% paraformaldehyde in PBS for 10 min at room temperature. After washing with PBS, coverslips were mounted on glass microscope slides, in the presence of 4:1 glycerol/PBS and observed on a Leica TCS 4D confocal laser scanning microscope supplemented with an Argon/Krypton laser and equipped with 40 × 1.00–0.5 and 100 × 1.3–0.6 oil immersion lenses. The excitation and emission wavelengths were 488 and 510 nm, respectively. Acquisitions were recorded employing the pseudocolor representation.

GST P1–1 Production and Purification

Human native enzyme GST P1–1 was produced in *Escherichia coli* cells as previously described [36, 37]. The purification of this recombinant enzyme was accomplished by affinity chromatography on immobilized glutathione [40]. After affinity purification, the enzyme was homogeneous as judged by SDS–PAGE [41]. The protein concentration was determined by the method of Lowry *et al.* [42].

GST Activity Measurement

The enzymatic activity of GST was assayed spectrophotometrically at 25° with CDNB as co-substrate under the conditions reported below. Spectrophotometric measurements were performed in a double beam Uvicon 940 spectrophotometer (Kontron Instruments) equipped with a thermostatted cuvette compartment. Initial rates were measured at 0.1-sec intervals for a total period of 12 sec after a lag time of 5 sec. Enzymatic rates were corrected for spontaneous reaction. A suitable amount of GST P1–1 sample (typically 1 μg of protein) was added into a cuvette containing 0.1 M phosphate buffer (pH 6.5), plus 0.1 mM EDTA, in the presence of 1 mM GSH (1 mL final volume). The reaction was started by adding 1 mM CDNB and monitored at 340 nm (ϵ = 9600 M^{-1} cm^{-1}) [43].

Attempts at GSH Conjugation of Anthracyclines Catalyzed by GST

A 100 mM (pH 7.2) Tris buffer containing 1 mM of either compounds **1** or **2**, 1 mM GSH, and 0.1 mM EDTA was kept for 2 hr at 37° in the presence of GST P1–1 (0.1 mg/mL). At the end of this incubation, a suitable aliquot was analyzed by HPLC (method B). In an experiment with compound **5** instead of **1** or **2**, because of the scarce solubility in water, a 5×10^{-3} M solution of **5** was prepared in DMSO and diluted 1:5 with the buffer containing GSH/EDTA solution just before the experiment. During the 2 hr of incubation, a portion of the anthracycline precipitated. HPLC analysis was performed on both the precipitate and the solution.

In another experiment, **1** was reductively activated to its more electrophilic quinone methide by reaction with the one-electron reducing agent DHM-3 [39]. A solution containing **1**, GSH, EDTA, and GST P1–1 at pH 7.2 in 0.1 M

Tris buffer at the above concentrations was deareated with nitrogen. DHM-3 dimer was added to a 5 mM concentration. After 1 hr at ambient temperature under nitrogen, both precipitate and supernatant were analyzed by HPLC for anthracyclines.

Inhibition studies of GST P1–1 with GSH–Anthracycline Conjugates

Inhibition experiments were performed using 1-cm cuvettes with 1 mL (final volume) of 0.1 M potassium phosphate buffer (pH 6.5) containing 1 mM EDTA, GSH (from 0.1 to 3 mM), 1 mM CDNB, suitable amounts of enzyme, and in the presence of fixed inhibitor concentrations ranging from 0 to 40 μM. The enzymatic activities were determined spectrophotometrically at 25° as reported above. Kinetic parameters were determined by fitting the collected data to the Michaelis–Menten equation by non-linear regression analysis using the Graph PAD Prism computer program (Graph PAD Software). The apparent K_m values thus obtained were replotted against the corresponding inhibitor concentration (where K_i is the intercept on the x-axis of the latter plot).

Time course of GST P1–1 inactivation in the presence of ADR

In a typical experiment, GST P1–1 (0.1 mg) was incubated in 1 mL (final volume) of 10 mM Tris–HCl buffer, pH 7.2, in the presence of 0.1 mM ADR (**1**) at 37° for 2 hr. At fixed times, aliquots of sample (10 μL) were withdrawn from the mixture and assayed for GST activity. After a 120-min incubation, 10 mM DTT was added to the mixture, and aliquots of this sample were assayed for GST activity. The same experiment was run in parallel in the presence of 1 mM DTT or 10 mM GSH.

Glutathione Analysis

Glutathione in cells was assayed by a slight modification and adaptation of the method of Reed *et al.* [44]: cells collected by centrifugation from the culture medium were treated with 5% perchloric acid and centrifuged. The supernatant, about 1 mL/10^7 cells, was analyzed for GSH and GSSG by HPLC with a Waters chromatograph (see above), using a Waters μ-Bondapack-NH_2 3.9 × 300 mm column and a 1:4 A/B isocratic mixture as eluant [44], at a flow rate of 1 mL/min. Retention times were 5.5 min (GSH) and 6.8 min (GSSG). Peak areas from HPLC used for calculations were in a linear region of an area/concentration plot obtained from pure GSH.

RESULTS AND DISCUSSION

To address the question, do anthracyclines undergo GSH conjugation in MDR tumor cells, we have chosen the MCF-7/DOX cell line to see if any conjugate with ADR (**1**) forms in significant amounts. The main reason for the choice was the fact that MCF-7/DOX cells were considered to be among the best candidates for GSH conjugation both because of the very high GST activity and the above-mentioned observations on cellular localization and relative toxicity of anthracyclines. Although **1** does not show any center so clearly electrophilic to easily predict the site for a possible GST-catalyzed GSH conjugation, the benzylic C(7) and possibly the C(14) site in the side chain are the favorite candidates for such a reaction to occur on the anthracycline itself. The alternative possibility of reductive activation of **1**, well supported by both *in vivo* and *in vitro* experiments, suggests again the position C(7) as the favorite site for reaction with GSH. Indeed, both epimers **3-I** and **3-II** have been easily obtained by direct reaction of **1** with GSH under anaerobic conditions, through the anthracycline quinone methide, the product of reductive cleavage of **1** [28]. We felt the available epimer **3-II** to be the right compound to assist the search for any GSH conjugate produced in the cells treated with **1**. Easily predictable polar characteristics and chromatographic behavior, along with our personal experience with this family of compounds [38, 45], suggested the use of reverse phase HPLC as the method of choice to detect any GSH derivative that could possibly arise from the conjugation of **1**. ADR (**1**), **3-I**, **3-II**, adriamycinone and 7-deoxyadriamycinone all appear in the range of 3–16 min under the eluting conditions. Hence, no GSH conjugate of any sort or any anthracycline-like metabolite thereof should escape from HPLC observation.

Anthracycline in MCF-7 and MCF-7/DOX Cells

Both sensitive and resistant human breast cell lines were treated with either **1** or **3-II** for 2 or 24 hr. The location of the fluorophores of both compounds in cells was established by laser scanning confocal microscopy, taking advantage of the inherent fluorescence of the drugs. ADR appeared predominantly in the nucleus of MCF-7 cells and in the Golgi apparatus of MCF-7/DOX cells, as shown in Fig. 2, panels A and C, respectively, and ADRIGLU, predominantly in the Golgi apparatus of both cell lines as shown in Fig. 2, panels B and D, respectively. In a parallel experiment (same time and same drug concentration), cells were collected and lysed, and the cell debris was collected as a pellet by centrifugation and extracted with DMSO. The recovered culture media, cell lysate supernatant, and DMSO extract of the pellet were all analyzed for **1**, **3-II**, and possible anthracycline metabolites by reverse phase HPLC, and the results are reported in Table 1. The HPLC method would detect any anthracycline and/or derivative, from compounds of even higher polarity than ADRIGLU down to low-polarity compounds like 7-deoxyadriamycinone. Inside the cells, only **1** (98% pure) or **3-II** was found from cells treated with **1** or **3-II**, respectively. Most of the anthracycline was found in the DMSO extract of the cell-fragment pellets obtained by centrifugation of the cell

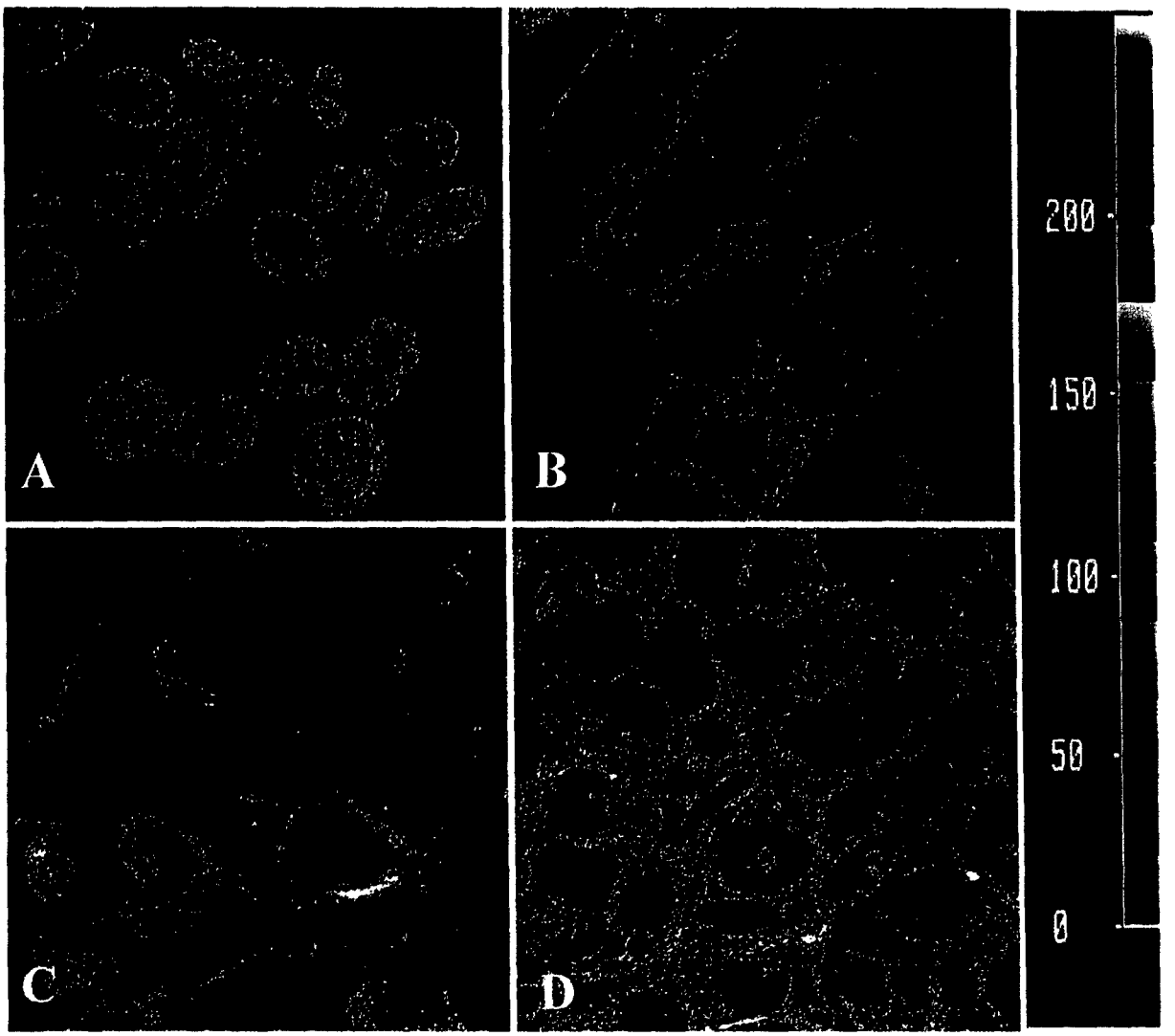

FIG. 2. Confocal fluorescence micrographs of MCF-7 (A and B) and MCF-7/DOX (C and D) cells after a 24-hr treatment with 4 μg/mL of ADR (A and C) or ADRIGLU (B and D). ADR- and ADRIGLU-exposed cells were pretreated with 10 μg/mL of verapamil. Original magnification = 100X. The color bar on the right is relative fluorescence intensity.

lysate. Only a small amount of anthracycline was found in the supernatant from centrifugation of the cell lysate. Analysis of the supernatant culture media with the anthracyclines concentrated using Sep-PAK cartridges showed mostly unchanged **1** (or, respectively, **3-II**). No traces of **3-II** or other polar anthracycline-like derivatives with retention time similar to **3-II** were found in the culture media from MCF-7/DOX cells treated with **1**. Peaks could be detected of < 1% size relative to the peak for **1**. As expected, the cellular uptake of **1** was higher in MCF-7 than in the variant MCF-7/DOX cell line, and the cellular uptake of **3-II** was lower than that of **1** for both cell lines. Basically, no ADRIGLU or any other possible anthracycline metabolite was observed in any of the components of the experiments with ADR-treated MCF-7 or MCF-7/DOX cells. Similarly, no metabolism of ADRIGLU was observed in any of the analytes from the experiments with **3-II**-treated cells.

The lack of ADRIGLU, especially in ADR-treated MCF-7/DOX cells, might have resulted from low levels of GSH or low activity of GST. Analysis for GSH showed 54 nmol/10^6 MCF-7 cells and 6.2 nmol/10^6 MCF-7/DOX cells, and as mentioned earlier, analysis for GST activity showed 14-fold higher activity in MCF-7/DOX cells than in MCF-7 cells. The higher activity of GST should have more than compensated for the lower GSH concentration in MCF-7/DOX cells. If ADR or ADRIGLU were substrates for GST, metabolites should have been observed in MCF-7/DOX and/or MCF-7 cells.

Attempts to Achieve GST-Catalyzed in vitro *GSH Conjugation*

Reaction of **1** with GSH in the presence of GST P1–1 at pH 7.2 at 37° for 2 hr gave only 4% of conjugate **3** (HPLC retention time, 5.7 min) with 95% of **1** (retention time, 7.5 min) accounted for as unreacted ADR. Identical results were obtained in a control reaction missing GST P1–1. Hence, the 4% product resulted from the previously described direct reaction of **1** with GSH [28]. Similar reac-

TABLE 1. HPLC analysis of ADR (1) and ADRIGLU II (3-II) from MCF-7 and MCF-7/DOX cells treated with 1 (1 μg/mL) and 3-II (6 μg/mL) for 2 or 24 hr*

Source	Culture medium supernatant† Area % of anthracycline peaks‡ (*ca.* area % of all peaks§)	Cell lysate supernatant‖	DMSO extract of pellet¶ Area % of anthracyclines peaks‡ (*ca.* area % of all peaks§)
MCF-7 + 1, 2 hr		Traces of 1	> 95% 1**, 1.0 μg
MCF-7 + 1, 24 hr	> 98% 1** (65%)	Traces of 1	> 95% 1**, 3.2 μg
MCF-7 + 3-II, 2 hr		0	Traces of 3-II
MCF-7 + 3-II, 24 hr	> 98% 3-II, (75%)	0	> 70% 1**, 0.5 μg
MCF-7/DOX + 1, 2 hr	> 99% 1** (85%††)	Traces of 1**	95% 1**, 0.7 μg
MCF-7/DOX + 1, 24 hr	> 98% 1** (85%††)	Traces of 1**	> 95% 1** (85%††), 0.3 μg‡‡
MCF-7/DOX + 3-II, 2 h	>98% 3-II (85%††)	0	0
MCF-7/DOX + 3-II, 24 hr	*ca.* 90% (80%††)	Traces of 3-II	Traces of 3-II

*Percent peak area of 1 or 3-II is given for samples obtained from cells treated with 1 or 3-II, respectively. HPLC profiles were obtained as described in Materials and Methods. Retention times for 3-I, 3-II, and 1 were as follows: (method A) 4.0, 4.6, and 8.5 min, respectively, and (method B) 5.0, 5.7, and 7.5 min. The percent area values reported are the averages from analyses performed in duplicate or triplicate, with observed variations being below 15%. Samples injected contained 0.5 to 20 nmol of anthracyclines.

†Cell culture medium supernatants at the end of the incubation, after filtration through sterile 0.2-μm filters, were concentrated by percolation through reverse phase C18 cartridges followed by elution with a 1:1 methanol-water mixture.

‡Anthracyclines were distinguished by their characteristic absorption in the region λ_{max} 450-550 nm.

§Percent area relative to all peaks absorbing at 480 nm.

‖Clear supernatants from centrifugation of cell lysates were 0.5 mL starting with one flask of cells.

¶DMSO extracts of cell debris pellets were *ca.* 0.5 mL starting with one flask of cells.

**No peaks corrsponding to 3-I or 3-II were detected.

††The major non-anthracycline compounds had retention times of 2.5 and 3.4 min.

‡‡In a similar experiment where verapamil had been added to the culture medium at 10 μg/mL, twice as much 1 was found in the DMSO extract of the pellet.

tions of 2 and 5 with GSH in the presence of GST P1–1 gave 100% recovery of starting anthracycline. The activity of GST P1–1 in an 8/2 (v/v) water–DMSO mixture (the mixture used for the experiment with 5) showed only a 10% decrease in comparison with pure water. When the chemical reducing agent DHM-3 was added to the reaction mixture of 1, GSH, and GST P1–1 under anaerobic conditions, the only product observed was 7-deoxyadriamycinone (retention time 12 min) [39]. 7-Deoxyadriamycinone is the major product of direct anaerobic reduction of ADR with DHM-3 and results from reduction to the hydroquinone followed by glycosidic cleavage to the electrophilic quinone methide and tautomerization of the quinone methide to the 7-deoxyaglycon [39]. Even with assistance from a chemical reducing agent, GST P1–1 conjugation of ADR to GSH does not occur.

Effect of ADR on GST P1–1 Activity

When GST P1–1 was incubated at pH 7.2 in the presence of 0.1 mM 1, a time-dependent inactivation of the enzyme was observed, as shown in Fig. 3. After 2 hr of incubation, the residual activity of GST P1–1 was about 29%. Further, the addition of DTT induced only a partial recovery of the enzymatic activity. On the contrary, when GST P1–1 was incubated in the presence of 1 mM DTT or 10 mM GSH from time zero, only a slight decrease of activity was observed (Fig. 3). As a control, we incubated GST P1–1 alone for the same time and observed at the end of the experiment a partial inactivation (11%). The time-dependent inactivation of GST P1–1 in the presence of 1 and other anthracyclines may be explained as follows: 1 and other anthracyclines produce free radical species that could interact with the side chain of some amino acid residues of proteins, affecting their biological activity. In the case of GST P1–1, potential targets are Cys 47 (amongst cysteine residues) and some tyrosyl residues such as Tyr 7, Tyr 49, and Tyr 108. Among them, Cys 47 is the most reactive species and may undergo oxidation with an intrachain disulfide bond formation with Cys 101. In fact, the inclusion of DTT after a 120-min incubation yielded only a partial recovery of GST activity, indicating that Cys 47 may have been strongly oxidized to other species that do not react with DTT or that the inactivation proceeded also via other residues. The protection afforded by GSH is easily

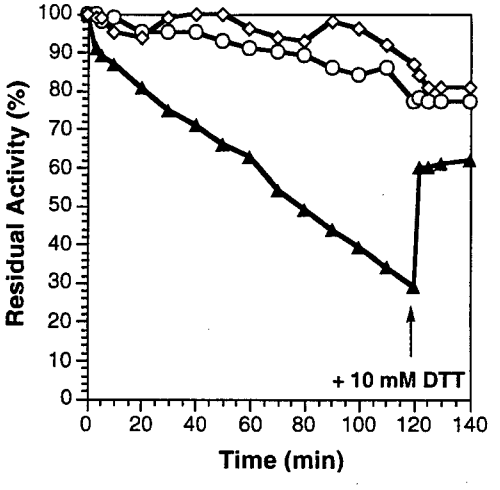

FIG. 3. Time course of GST P1–1 inactivation in the presence of ADR. The experimental conditions are reported in Materials and Methods. Key: (▲) GST P1–1 + 0.1 mM ADR; (○) GST P1–1 + 0.1 mM ADR + 1 mM DTT; and ◇ GST P1–1 + 0.1 mM ADR + 10 mM GSH.

explained by the same reason: the binding of GSH to the active site is accompanied by a conformational change that partially buries Cys 47 into a hydrophobic pocket and significantly increases the distances between Cys 47 and Cys 101 (about 18 Å).

Inhibition of GST-P1-1 by Anthracycline–GSH Conjugates

All of the anthracycline conjugates, **3-I, 3-II, 4-II,** and **6** (1:1 mixture of the two epimers **I** and **II**), were strong, competitive-type inhibitors of GST P1-1. Their K_i values, calculated under conditions described in Materials and Methods, were 2.16 ± 0.09 μM (**3-I**), 1.27 ± 0.03 μM (**3-II**), 1.36 ± 0.10 μM (**4-II**), and 1.01 ± 0.09 μM (**6**). Inhibition was not very sensitive to relatively large changes in structure (compare **4-II** with **6**), indicating primary recognition of the gluthathione group and possibly the A-ring of the anthracycline at the enzyme binding site.

In conclusion, under our conditions no GSH conjugation occurred in MCF-7/DOX cells treated with ADR. Further, no other biochemical change of ADR occurred in resistant cells because of MDR. This is consistent with the parallel unsuccessful attempts of direct GST-catalyzed conjugation of **1, 2,** and **5** and the strong competitive inhibition of GST P1-1 by ADRIGLU, DAUNOGLU, and MENOGLU. We cannot rule out the possibility that other GSTs might yield different results. Our conclusions are reinforced by the recent report that synthetic ADRIGLU and DAUNOGLU as well as the anthracyclines conjugated with GSH at the 14-position are very strong inhibitors of the MRP/GS-X efflux pump [29]. Hence, if GSH conjugates were produced by GST in cells, they would not be pumped out of the cells by the efflux pump and should have been observed either in the cell lysate supernatant or in the cell debris pellets. Co-transport of vincristine with GSH not covalently attached by MRP was recently reported; however, the phenomenon was not observed with DOX or DAUN [46]. From a general point of view, lack of evidence of any direct GSH conjugation mediated by GST P1-1 is reasonable by considering that even in the case of strongly electrophilic mustard drugs, as GST substrates, low k_{cat} values have been reported [47]. The overexpression of GST P1-1 in MCF-7/DOX cells might be explained in light of recent findings, suggesting that GST P1-1 is a component of the jun kinase stress system [48]. Therefore, the increased GST activity, as outlined by Tew and co-workers [5, 6], could be a defense against oxidative stress induced by anthracyclines, which is an important component of tumor cell cytotoxicity [49].

We thank Marco Paterno for technical assistance with the HPLC analyses. This study was supported by the Institute of Experimental Medicine, NRC, by grants to the Department of Biology, University of Rome "Tor Vergata" from Ministero della Sanità, and by grants to the University of Colorado from the American Cancer Society (RPG-98-110-01-ROG), the U.S. National Institutes of Health (CA78756), and the U.S. Department of Defense (DAMD17-98-1-8298).

References

1. Moscow JA and Cowan KH, Multidrug resistance. *J Natl Cancer Inst* **80:** 14–20, 1988.
2. Gottesman MM, How cancer cells evade chemotherapy: Sixteenth Richard and Hinda Rosenthal Foundation Award Lecture. *Cancer Res* **53:** 747–754, 1993.
3. Gottesmann MM and Pastam I, Biochemistry of multidrug resistance mediated by the multidrug transporter. *Annu Rev Biochem* **62:** 385–427, 1993.
4. Simon SM and Schindler M, Cell biological mechanism of multidrug resistance in tumors. *Proc Natl Acad Sci USA* **91:** 3497–3504, 1994.
5. O'Brien ML and Tew KD, Glutathione and related enzymes in multidrug resistance. *Eur J Cancer* **32A:** 967–978, 1996.
6. Tew KD, Glutathione-associated enzymes in anticancer drug resistance. *Cancer Res* **54:** 4313–4320, 1994.
7. Kartner N, Riordan JR and Ling V, Cell surface P-glycoprotein is associated with multidrug resistance in mammalian cell lines. *Science* **221:** 1085–1088, 1983.
8. Endicott JA and Ling V, The biochemistry of P-glycoprotein-mediated multidrug resistance. *Annu Rev Biochem* **58:** 137–171, 1989.
9. Riordan JR and Ling V, Genetic and biochemical characterization of multidrug resistance. *Pharmacol Ther* **28:** 51–75, 1985.
10. Whelan RDH, Waring CJ, Wolf CR, Hayes JD, Hosking LK and Hill BT, Over-expression of P-glycoprotein and glutathione S-transferase π in MCF-7 cells selected for vincristine resistance *in vitro*. *Int J Cancer* **52:** 241–246, 1992.
11. Tsuchida S and Sato K, Glutathione transferase and cancer. *Crit Rev Biochem Mol Biol* **27:** 337–384, 1992.
12. Sies H and Ketterer B, *Glutathione Conjugation, Mechanism and Biological Significance*. Academic Press, New York, 1988.
13. Jakoby WB and Habig WH, Glutathione transferases [in detoxification]. In: *Enzyme Basis of Detoxification* (Ed. Jakoby WB), Vol. 2, pp. 63–94. Academic Press, New York, 1980.
14. Black SM and Wolf CR, The role of glutathione-dependent enzymes in drug resistance. *Pharmacol Ther* **51:** 139–154, 1991.
15. Ishikawa T, The ATP-dependent glutathione S-conjugate export pump. *Trends Biochem Sci* **17:** 463–468, 1992.
16. Chen G and Waxman DJ, Identification of glutathione S-transferase as a determinant of 4-hydroperoxycyclophosphamide resistance in human breast cancer cells. *Biochem Pharmacol* **49:** 1691–1701, 1995.
17. Whelan RDH, Hosking LK, Townsend AJ, Cowan KH and Hill BT, Differential increases in glutathione S-transferase activities in a range of multidrug-resistant human tumor cell lines. *Cancer Commun* **1:** 359–365, 1989.
18. Hayes JD, Pickett CB and Mantle TJ, *Glutathione S-Transferases and Drug Resistance*. Taylor Frances, New York, 1990.
19. Kelley K, Engqvist-Goldstein A, Montali JA, Wheatley JB, Schmidte DE and Kauvar L, Variability of glutathione S-transferase isoenzyme patterns in matched normal and cancer human breast tissue. *Biochem J* **304:** 843–848, 1994.
20. Grant CE, Valdimarsson G, Hipfner DR, Almquist KC, Cole SPC and Deeley RG, Overexpression of multidrug resistance-associated protein (MRP) increases resistance to natural product drugs. *Cancer Res* **54:** 357–361, 1994.
21. Hayes JD and Pulford DJ, The glutathione S-transferase supergene family: Regulation of GST and the contribution of the isoenzymes to cancer chemoprotection and drug resistance. *Crit Rev Biochem Mol Biol* **30:** 445–600, 1995.
22. Jedlitschky G, Leier I, Buchholz U, Center M and Kappler D, ATP-dependent transport of glutathione S-conjugates by the multidrug resistance-associated protein. *Cancer Res* **54:** 4833–4836, 1994.

23. Awasthi S, Singhal SS, Srivastava SK, Zimniak P, Bajpai KK, Saxena M, Sharma R, Ziller SA, Frenkel EP, Singh SV, He NG and Awasthi YC, Adenosine triphosphate-dependent transport of doxorubicin, daunomycin, and vinblastine in human tissues by a mechanism distinct from the P-glycoprotein. *J Clin Invest* **93:** 958–965, 1994.
24. Cole SPC, Bhardwaj G, Gerlach JH, Mackie JE, Grant CE, Almquist KC, Stewart AJ, Kurz EU, Duncan AMV and Deeley RG, Overexpression of a transporter gene in a multidrug-resistant human lung cancer cell line. *Science* **258:** 1650–1654, 1992.
25. Siegel D, Beall H, Senekowitsch C, Kasai M, Arai H, Gibson NW and Ross D, Bioreductive activation of mitomycin-C by DT-diaphorase. *Biochemistry* **31:** 7879–7885, 1992.
26. Sharma M and Tomasz M, Conjugation of glutathione and other thiols with bioreductively activated mitomycin C. Effect of thiols on the reductive activation rate. *Chem Res Toxicol* **7:** 390–400, 1994.
27. Arcamone F, *Doxorubicin Anticancer Antibiotics*. Academic Press, New York, 1981.
28. Gaudiano G, Resing K and Koch TH, Reaction of anthracycline antitumor drugs with reduced glutathione. Formation of aglycon conjugates. *J Am Chem Soc* **116:** 6537–6544, 1994.
29. Priebe W, Krawczyk M, Kuo MT, Yamane Y, Savaraj N and Ishikawa T, Doxorubicin- and daunorubicin-glutathione conjugates, but not unconjugated drugs, competitively inhibit leukotriene C_4 transport mediated by *MRP/GS-X* pump. *Biochem Biophys Res Commun* **247:** 859–863, 1998.
30. Serafino A, Sinibaldi-Vallebona P, Gaudiano G, Koch TH, Rasi G, Garaci E and Ravagnan G, Cytoplasmic localization of anthracycline antitumor drugs conjugated with reduced glutathione: A possible correlation with multidrug resistance. *Anticancer Res* **18:** 1159–1166, 1998.
31. Mennervik B, Awasthi YC, Board PG, Hayes JD, Dillio C, Ketterer B, Listowsky I, Morgerstern R, Muramatsu M, Pearson WR, Pickett CB, Sato K, Widersten K and Wolf CR, Nomenclature for human glutathione transferases. *Biochem J* **282:** 305–306, 1992.
32. Kano T, Sakai M and Muramatsu M, Structure and expression of a human class π glutathione *S*-transferase messenger RNA. *Cancer Res* **47:** 5626–5630, 1987.
33. Tsuchida S, Sekine Y, Shineha R, Nishihira T and Sato K, Elevation of the placental glutathione *S*-transferase form (GST-π) in tumor tissues and the levels in sera of patients with cancer. *Cancer Res* **49:** 5225–5229, 1989.
34. Batist G, Tulpule A, Sinha BK, Katki AG, Myers CE and Cowan KH, Overexpression of a novel anionic glutathione transferase in multidrug-resistant human breast cancer cells. *J Biol Chem* **261:** 15544–15549, 1986.
35. Puchalski RB and Fahl WE, Expression of recombinant glutathione *S*-transferase π, Ya, or Yb_1 confers resistance to alkylating agents. *Proc Natl Acad Sci USA* **87:** 2443–2447, 1990.
36. LoBello M, Battistoni A, Mazzetti AP, Board PG, Muramatsu M, Federici G and Ricci G, Site-directed mutagenesis of human glutathione transferase P1–1. Spectral, kinetic, and structural properties of Cys-47 and Lys-54 mutants. *J Biol Chem* **270:** 1249–1253, 1995.
37. Battistoni A, Mazzetti AP, Petruzzelli R, Muramatsu M, Federici G, Ricci G and LoBello M, Cytoplasmic and periplasmic production of human placental glutathione transferase in *Escherichia coli*. *Protein Expr Purif* **6:** 579–587, 1995.
38. Gaudiano G and Koch TH, Redox chemistry of anthracycline antitumor drugs and use of captodative radicals as tools for its elucidation and control. *Chem Res Toxicol* **4:** 2–16, 1991.
39. Gaudiano G and Koch TH, Bi[3,5-dimethyl-5-(hydroxymethyl)-2-oxomorpholin-3-yl] (DHM-3 dimer), A water soluble, one electron reducing agent. *J Org Chem* **52:** 3073–3081, 1987.
40. Simmons PC and VanderJagt DL, Purification of glutathione *S*-transferases from human liver by glutathione-affinity chromatography. *Anal Biochem* **82:** 334–341, 1977.
41. Laemmli UK, Cleavage of structural proteins during the assembly of the head of bacteriophage T4. *Nature* **227:** 680–685, 1970.
42. Lowry OH, Rosebrough NJ, Farr AL and Randall RJ, Protein measurement with the Folin phenol reagent. *J Biol Chem* **193:** 265–275, 1951.
43. Habig WH, Pabst MT and Jakoby WB, Glutathione *S*-transferases: The first enzymatic step in mercapturic acid formation. *J Biol Chem* **249:** 7130–7139, 1974.
44. Reed DJ, Babson JR, Beatty PW, Brodie AE, Ellis WW and Potter DW, High-performance liquid chromatography analysis of nanomole levels of glutathione, glutathione disulfide and related thiols and disulfides. *Anal Biochem* **106:** 55–62, 1980.
45. Gaudiano G, Frigerio M, Sangsurasak C, Bravo P and Koch TH, Reduction of daunomycin and 11-deoxydaunomycin with sodium dithionite in DMSO. Formation of quinone methide sulfite adducts and the first NMR characterization of an anthracycline quinone methide. *J Am Chem Soc* **114:** 5546–5552, 1992.
46. Loe DW, Deeley RG and Cole SPC, Characterization of vincristine transport by M_r 190,000 multidrug resistance protein (MRP): Evidence for cotransport with reduced glutathione. *Cancer Res* **58:** 5130–5136, 1998.
47. Ciaccio PJ, Tew KD and LaCreta FP, Enzymatic conjugation of chlorambucil with glutathione by human glutathione *S*-transferases and inhibition by ethacrynic acid. *Biochem Pharmacol* **42:** 1504–1507, 1991.
48. Alder V, Vin Z, Fuchs SY, Benezra M, Rosario L, Tew KD, Pincus MR, Sardana M, Henderson CJ, Wolf CR, Davis RJ and Ronai Z, Regulation of JNK signaling by GSTp. *EMBO J* **18:** 1321–1334, 1999.
49. Taatjes DJ, Fenick DJ, Gaudiano G and Koch TH, A redox pathway leading to the alkylation of nucleic acids by doxorubicin and related anthracyclines: Application to the design of antitumor drugs for resistant cancer. *Curr Pharm Des* **4:** 203–218, 1998.

Nuclear Targeting and Retention of Anthracycline Antitumor Drugs in Sensitive and Resistant Tumor Cells

Dylan J. Taatjes‡ and Tad H. Koch*

Department of Chemistry and Biochemistry, University of Colorado, Boulder, CO 80309-0215, University of Colorado Cancer Center, Denver, CO 80262, USA

‡*Current address, Dept. of Molecular and Cell Biology, University of California, Berkeley, CA 94720, USA*

Abstract: Recent and new results which support a drug-DNA covalent bonding mechanism for cell toxicity of the clinical antitumor drugs, daunorubicin, doxorubicin, and epidoxorubicin, are summarized. The mechanism involves the iron complex of the drugs inducing oxidative stress to yield formaldehyde, which then mediates covalent attachment to G-bases of DNA. At NGC sites the combination of covalent and non-covalent drug interactions serve to *virtually crosslink* the DNA. Structural data for *virtual crosslinks* are compared as a function of drug structure. Elucidation of the mechanism led to the synthesis and evaluation of drug formaldehyde conjugates, Daunoform, Doxoform, and Epidoxoform, as improved chemotherapeutics. Drug uptake, nuclear targeting, drug release, and cytotoxicity of the clinical drugs by sensitive and resistant breast and prostate cancer cells are contrasted with those of the corresponding formaldehyde conjugates. Conjugates are taken up better, retained longer, and are more toxic to a wide variety of tumor cells. The kinetics of drug release from Doxoform and Epidoxoform treated MCF-7/Adr cells are biexponential and correlate with the biexponential kinetics of drug release from extracellular DNA. The results of the lead conjugate, Epidoxoform, in the National Cancer Institute 60 human tumor cell screen are presented and discussed in terms of some resistance mechanisms. Epidoxoform shows increased toxicity to all panels relative to doxorubicin and epidoxorubicin, and this enhanced toxicity is especially evident with the more resistant cell lines.

INTRODUCTION

In a recent review we have described the discovery of a mechanism by which the clinically useful anthracycline antitumor drugs, daunorubicin (DAU), doxorubicin (DOX), and epidoxorubicin (EPI), become covalently attached to DNA [1]. Our participation in the discovery was stimulated by a series of papers published by Phillips and co-workers in which they reported that reaction of Tris-buffered DNA with daunorubicin or doxorubicin under redox conditions in the presence of iron led to covalent bonding of drug to DNA [2-6]. The need for iron was intriguing because iron and its induction of oxidative stress has long been associated with cardiotoxicity [7-9]. The bonding was detected as transcription blockages and was shown to involve the 2-amino groups of G-bases. Drug-DNA covalent bonds were unstable and were lost at two different first-order rates, one with a half-life of 5 h and the other, 40 h [2,6]. Phillips proposed that the more labile covalent bonding was to an isolated G-base on one strand of DNA and that the less labile covalent bonding involved crosslinking of both strands of DNA by drug aglycon at 5'-GC-3' sites. Our interest was heightened by reports of Konopa and Skladanowski that metabolically activated doxorubicin produced unstable drug-DNA crosslinks in HeLa cells [10,11] and a report by Bartosek and Wolf that preincubation of doxorubicin with cytochrome P450 reductase and NADPH enhanced its toxicity to MCF-7 cells [12].

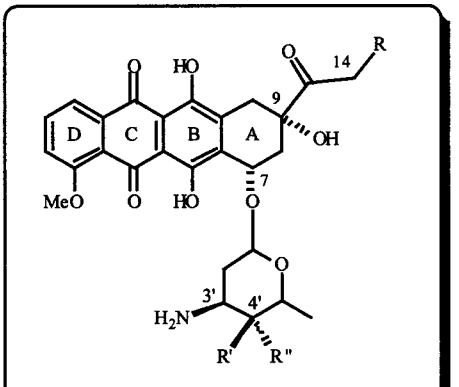

R=R"=H, R'=OH daunorubicin (DAU)
R=R'=OH, R"=H doxorubicin (DOX)
R=R"=OH, R'=H epidoxorubicin (EPI)

We employed negative ion electrospray mass spectrometry to study the bonding in the less labile site. Our experiments involved redox activated daunorubicin and doxorubicin reacting with the self-complementary oligomer

*Address correspondence to this author at the Department of Chemistry and Biochemistry, University of Colorado, Boulder, CO 80309-0215, USA; email: tad.koch@colorado.edu

0929-8673/01 $28.00+.00

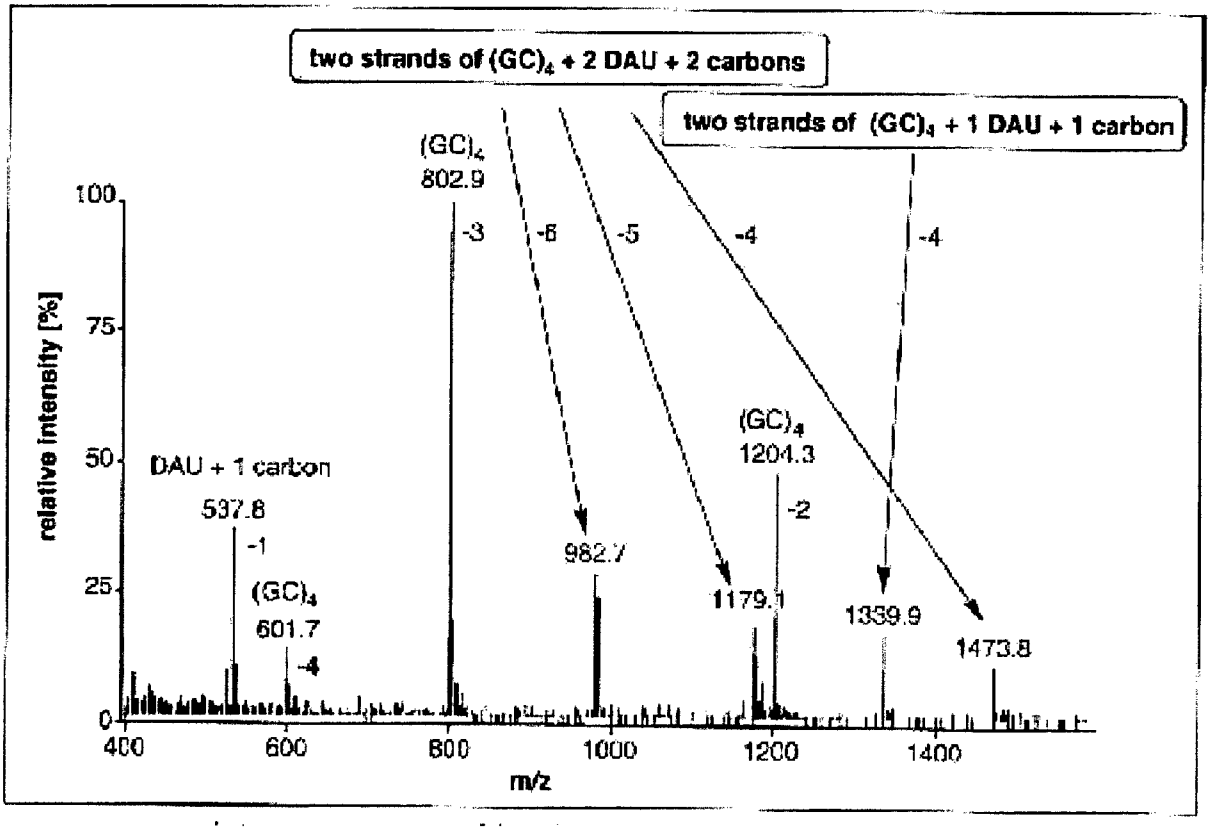

Fig. (1). Negative ion electrospray mass spectrum of the major product from reaction of daunorubicin with the self complementary deoxyoligonucleotide $(GC)_4$ under redox conditions. Charges are indicated with the assignments.

$(GC)_4$ in Tris buffer. These conditions gave as the predominant product a double stranded DNA with a molecular mass showing the presence of two drug molecules plus two extra carbons (Fig (**1**)) [13,14]. Thus, the product was neither DNA crosslinked by drug aglycon, as proposed by Phillips and co-workers [2], nor DNA bearing intercalated drug as neither of these possibilities was consistent with the mass spectrum. The source of the extra carbons was established as formaldehyde from further study of the redox reaction [15]. The structure of the product, shown schematically in Figure 2, was then proposed, based upon a crystal structure by Wang and co-workers [13,15,16]. Wang and co-workers reported some years earlier a structure with two daunorubicins each covalently bonded to $(CG)_3$ at the 2-amino group of a G-base from reaction with formaldehyde, which originated as an impurity in the crystallization solvent. Through serendipity, the model system we selected, $(GC)_4$, contained the sequence of Wang $(CG)_3$. Hence, the structural assignment in Fig. (**2**) was reasonable for the product which gave the mass spectrum in Fig.(**1**).

The carbon source for drug catalyzed formaldehyde production turned out to be Tris buffer in the Phillips experiment [15]. Tris is not present in cells; however, cell membrane lipid and natural polyamines such as spermine are candidate carbon sources in tumor cells. Spermine is oxidized to formaldehyde by the reactive oxygen species produced by the anthracyclines [15], and formaldehyde from proposed lipid oxidation has been detected in the urine of mice treated with doxorubicin [17].

The steps leading to covalent bonding of drug to DNA are summarized as follows: 1) drug complexation with iron, 2) induction of oxidative stress through iron redox chemistry, 3) reaction of reactive oxygen species (ROS) with a cellular constituent to yield formaldehyde, 4) covalent bonding of the formaldehyde to the amino group of the drug to form a Schiff base or its equivalent, and 5) intercalation of drug in DNA with covalent bonding of the Schiff base to the 2-amino group of a G-base in the minor groove of DNA. If the interaction with DNA occurs at the trinucleotide 5'-NGC-3', then the drug intercalates between N and G and covalently bonds to the G-base on one strand using formaldehyde and hydrogen bonds to the G-base on the opposing strand, as shown in Fig. (**2**). We describe the combination of intercalation, covalent bonding, and hydrogen bonding as a *virtual crosslinking* of the DNA by the drug [14].

The discovery of the *virtual crosslinking* mechanism prompted the synthesis of anthracycline formaldehyde conjugates as novel drugs, potentially less cardiotoxic and active against resistant cancer. Less cardiotoxicity was proposed because the drugs do not require production of reactive oxygen species for covalent bonding to DNA; activity against resistant cancer was predicted because

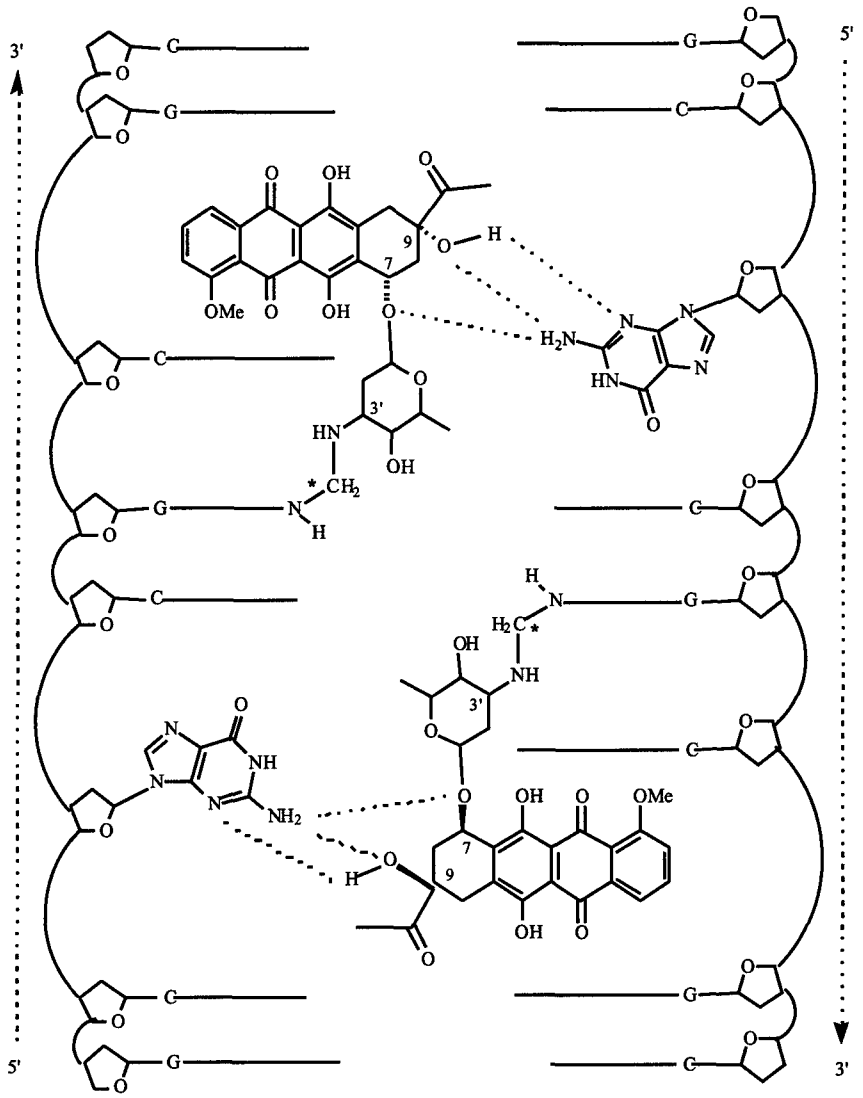

Fig. (2). Schematic representation of the structure proposed for the product with the mass spectrum shown in Fig. (**1**). Two daunorubicins are each covalently bonded to a 2-amino group of a G-base on one strand of DNA via a methylene group and hydrogen bonded to a G-base on the opposing strand, *virtually crosslinking* the DNA. The methylene group is marked with an asterisk.

inhibition of oxidative stress is a resistance mechanism [18,19]. Daunorubicin and doxorubicin, bearing a cis-1,2-aminoalcohol functionality, react with formaldehyde to yield the dimeric oxazolidine structures, Daunoform (DAUF) and Doxoform (DOXF) [20]. Epidoxorubicin, bearing a trans-1,2-aminoalcohol functionality, reacts with formaldehyde to yield a dimeric diazadioxabicyclic structure, Epidoxoform (EPIF) [21]. DAUF, DOXF, and EPIF are prodrugs with rapid to moderate hydrolysis rates to monomeric structures predicted to be the active metabolites of the clinical drugs (Fig. (**3**)). At 37 °C and pH 7.4, the half-life of DOXF with respect to hydrolysis to the active metabolite is estimated at less than 5 min [20], while the half-life of EPIF is more than 2 h [21]. All three conjugates show superior growth inhibition of both sensitive (MCF-7) and resistant (MCF-7/Adr) human breast cancer cells as summarized in Table 1. In fact, comparison of growth inhibition of the resistant cells is quite dramatic.

We now review recent experiments which further support the covalent bonding of anthracycline antitumor drugs to DNA as an important cytotoxic mechanism. These focus on structure of the *virtual crosslink*, drug uptake, localization, and retention in both sensitive and resistant tumor cells, and a mechanism by which the clinical anthracyclines may sequester iron. Results on breast cancer cells and metastatic prostate cancer cells are reported in detail, and a comparison of EPIF with DOX and EPI in the NCI 60 human tumor cell screen is presented. The intent of this paper is not to review the literature on the mechanism of action of the clinical anthracycline antitumor drugs; for such a review a recent commentary by Gewirtz is recommended [22] as well as our

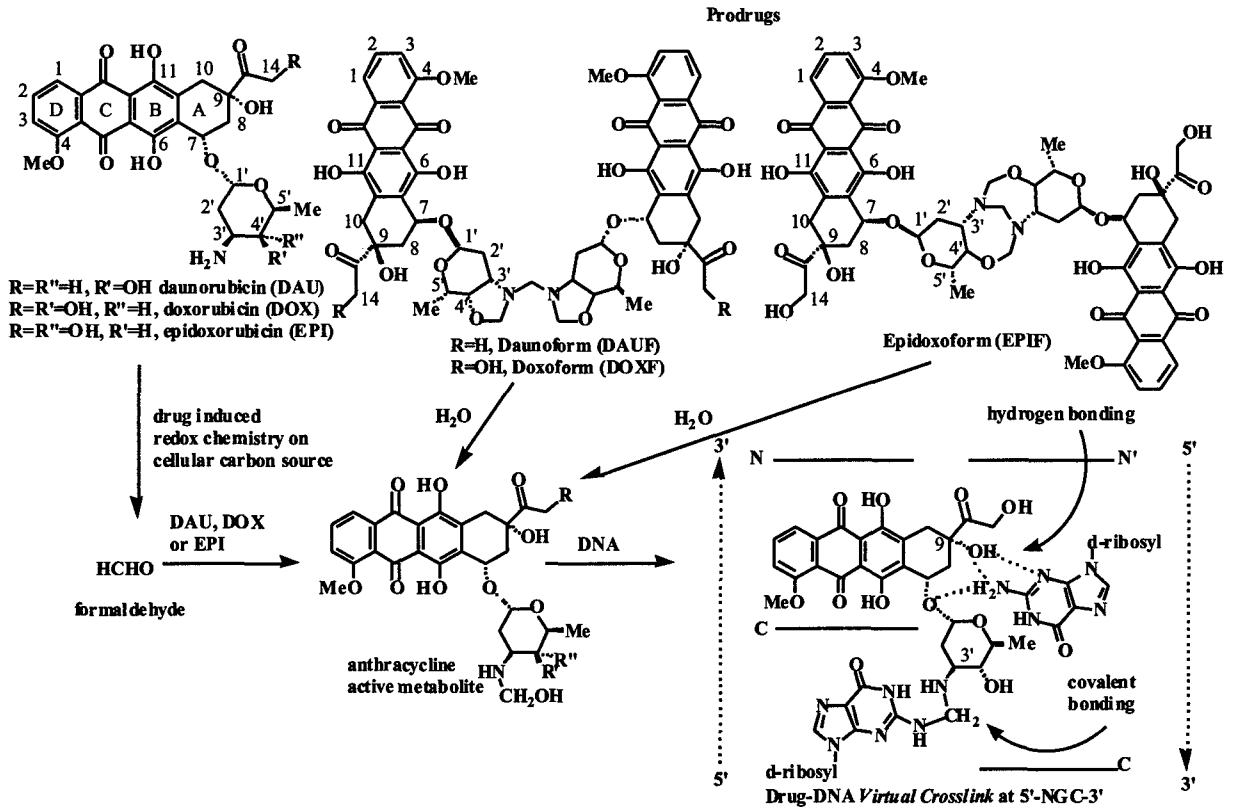

Fig. (3). Structures for the prodrugs, DAUF, DOXF, and EPIF, and proposed pathways to the respective drug-DNA *virtual crosslink* via an active metabolite. The active metabolite results from drug-induced redox chemistry on a cellular carbon source or from hydrolysis of the respective prodrug.

recent review which focuses on drug-DNA covalent bonding [1].

RESULTS AND DISCUSSION

Structure of the *Virtual Crosslink*

Wang and co-workers have reported crystal structures of both daunorubicin and doxorubicin covalently bonded to DNA through reaction with formaldehyde [16,23]. Guided by this work, we recently solved the crystal structure of epidoxorubicin covalently bonded to the Wang $(CG)_3$ sequence [24]. Our structural work was prompted by the emergence of Epidoxoform as the lead compound in our drug development program. We anticipated that a comparison of the crystal structures might provide a clue to the differences among the three conjugates with respect to drug toxicity, uptake, and retention in sensitive and resistant breast cancer cells. Significant differences in toxicity are apparent from the

Table 1. **IC_{50} values for doxorubicin, Doxoform, epidoxorubicin, Epidoxoform treated MCF-7 and MCF-7/Adr human breast cancer cells and LNCaP, PC-3, and DU-145 metastatic human prostate cancer cells. Cells were incubated with drug for 3 h in RPMI 1640 media containing 10% fetal bovine serun and 1% DMSO. Plates were developed using the crystal violet assay**

Cell Type	IC_{50} Values (nmol equiv/L)			
	Doxorubicin	Doxoform	Epidoxorubicin	Epidoxoform
MCF-7	300	2	300	65
MCF-7/Adr	10,000	1	>10,000	70
LNCaP	25	1	30	8
PC-3	48	1	40	7
DU-145	240	3	380	26

IC50 data in Table 1. Doxoform is approximately 50-fold more toxic to MCF-7 cells than Epidoxoform, with Daunoform exhibiting intermediate toxicity.

Comparison of the crystal structure of [epidoxorubicin-CH_2-d(CGCGCG)]$_2$ with the crystal structure of [daunorubicin-CH_2-d(CGCGCG)]$_2$ showed differences in hydrogen bonding (Fig. (**4**)) [24]. Most significant was the appearance of a 2.70 Å contact between the 4'-hydroxyl of epidoxorubicin and the carbonyl of a C-base on the opposing strand. In the daunorubicin structure this distance is greater than 4.0 Å [16]. In addition, the oxygen at the 7-position of epidoxorubicin is 0.25 Å closer to the nitrogen of the G-base on the opposing strand. Meanwhile, the nitrogen at the 3'-position of the daunorubicin structure is 0.4 Å closer to the $O_{4'}$ of the C-base on the bonded strand. No difference was observed in the methylene bond lengths coupling the drug to the DNA. Additional comparison of the covalent [epidoxorubicin-CH_2-d(CGCGCG)]$_2$ structure with the non-covalent [epidoxorubicin-d(CGATCG)]$_2$ structure [25] showed no remarkable effect from the hydroxyl at the 14-position. These comparisons suggest that daunorubicin (and presumably doxorubicin) is held more tightly to the bonded strand, while epidoxorubicin is held more tightly to the opposing strand. In other words, epidoxorubicin *virtually crosslinks* CGCGCG better than daunorubicin or doxorubicin. Differences in associated water molecules and hydrophobic effects probably also contribute to variation in the stability of the *virtual crosslink* [26].

In a study complementary to the crystallographic measurements, Crothers and co-workers recently reported an NMR structural characterization of the doxorubicin *virtual crosslink* of d(ATGCAT)$_2$ with *in situ* generated formaldehyde [27]. In addition, using the ^{13}C labeled 14-mer deoxyoligonucleotide d(TAATAAGCATAAAT-ATTATTCGTATTTA) which bears only one NGC site, they studied the effect of the *virtual crosslink* on DNA strand exchange. The *virtual crosslink* slowed strand exchange by 160-fold relative to DNA bearing intercalated doxorubicin and by 640-fold relative to drug-free DNA. The 160-fold difference in strand exchange rate highlights the importance of the covalent linkage in the drug-DNA interaction.

Uptake, Nuclear Targeting, and Retention in Breast Cancer Cells

Doxorubicin is a main line drug for the treatment of breast cancer in the U.S., while epidoxorubicin is a main line drug for treatment of breast cancer in Europe. Resistance mechanisms and side effects, especially cardiotoxicity,

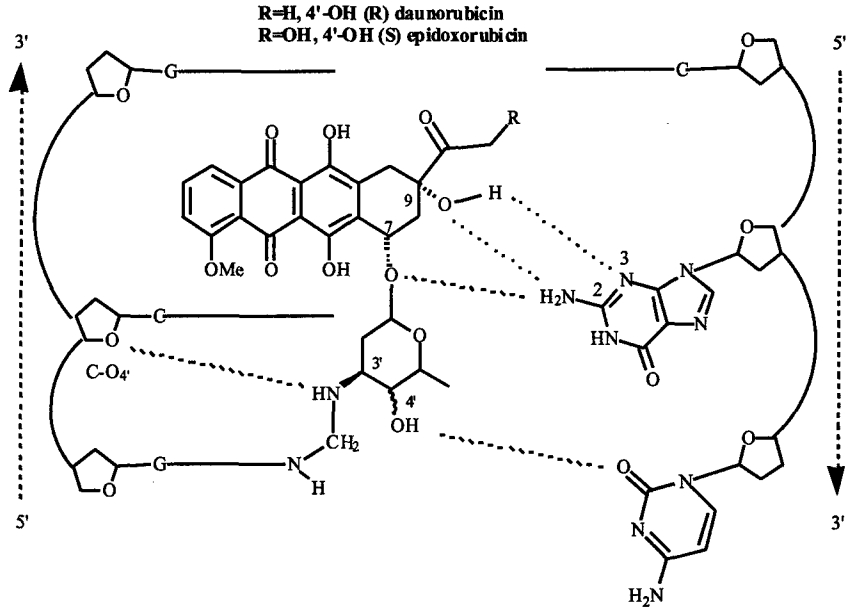

Contact drug-DNA	Distance (Å) [EPI-CH_2-d(CGCGCG)]$_2$	[DAU-CH_2-d(CGCGCG)]$_2$
O_9 - $G(N_3)$	2.89	2.86
O_9 - $G(N_2)$	3.12	3.12
O_7 - $G(N_2)$	2.87	3.13
$O_{4'}$ - $C(O_2)$	2.70	>4.0
$N_{3'}$ - $C(O_{4'})$	3.55	3.16

Fig. (4). Schematic representation of half of the crystal structures for daunorubicin and epidoxorubicin *virtually crosslinking* $(CG)_3$. Important non-bonding contacts, shown with dashed lines, are compared in the two structures.

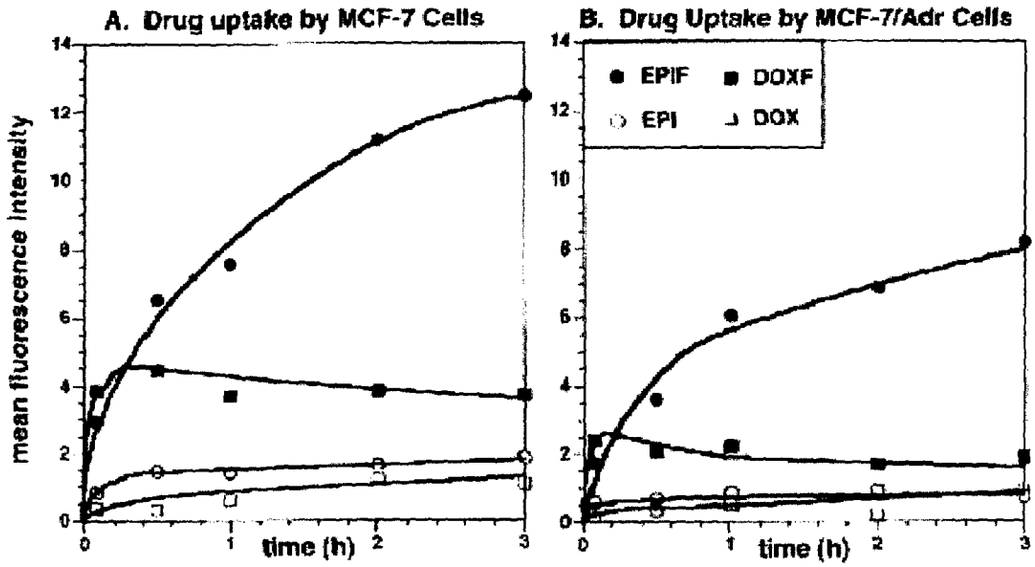

Fig. (5). Comparison of the uptake of EPIF, EPI, DOXF, and DOX by sensitive (MCF-7) and resistant (MCF-7/Adr) human breast cancer cells. Cells were treated with 0.5 mol equiv/L of drug, and drug in cells was determined by flow cytometry, measuring drug fluorescence. Concentrations are given in mol equiv/L to correct for EPIF and DOXF producing two active drug metabolites.

ultimately compromise their utility. Epidoxorubicin exhibits lower cardiotoxicity, but this is partially offset by lower antitumor activity. Reduced epidoxorubicin cardiotoxicity may result in part from its conjugation with glucuronic acid, which facilitates excretion as the glucuronide [28]. Doxoform and Epidoxoform are dramatically more toxic to resistant MCF-7/Adr cells relative to doxorubicin and epidoxorubicin, respectively, as shown in Table 1. Enhanced toxicity to resistant breast cancer cells prompted a comparison of uptake, targeting and retention of clinical drugs (DOX and EPI) with their formaldehyde conjugates (DOXF and EPIF).

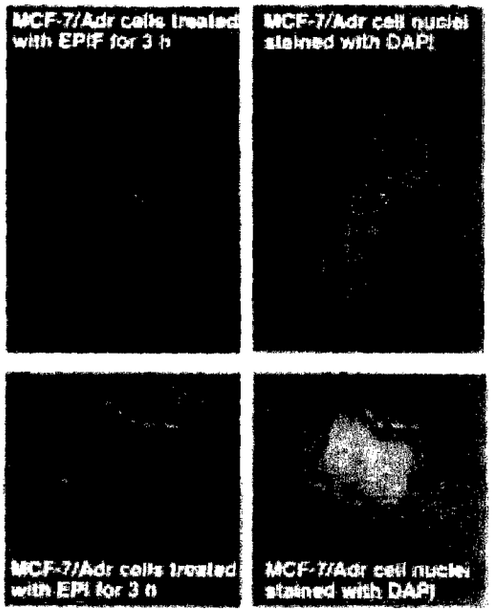

Fig. (6). Fluorescence micrographs of resistant MCF-7/Adr tumor cells treated with 0.5 mol equiv/L of EPIF (row a) or EPI (row b) for 3 h. Drug is highlighted in red, and nuclei, visualized with the nuclear stain DAPI, are highlighted in cyan. EPIF appears in the nuclei of resistant cells, but EPI is excluded from the nuclei.

The uptake of DOX, EPI, DOXF, and EPIF by sensitive MCF-7 and resistant MCF-7/Adr cells was measured over a 3 h time period by flow cytometry utilizing drug fluorescence as a measure of drug in cells (Fig. (**5**)) [29]. The data indicate that uptake of DOXF was more rapid than uptake of EPIF. The rates mimic the rates of hydrolysis of DOXF and EPIF to monomeric amino alcohols, presumed to be the active metabolites of the clinical drugs. The half-life of EPIF with respect to this hydrolysis is 2 h and of DOXF, less than 5 min. The parallel of hydrolysis and drug uptake rates indicates that EPIF (and presumably DOXF) must partially hydrolyze before drug passes through the cell membrane. In addition, Fig (**5**) shows that both sensitive and resistant cells take up significantly more drug-formaldehyde conjugate than parent drug, which correlates with drug toxicity. However, the quantity of drug taken up cannot be the only factor in toxicity since DOXF is 50-fold more toxic than EPIF to both MCF-7 and MCF-7/Adr cells, yet both cell lines take up more EPIF.

In another series of experiments, 24 h drug treatment led to enhanced uptake of the clinical drugs relative to 3 h drug treatment, especially by the sensitive MCF-7 cells (data not shown). However, this was still 2- to 3-fold below the uptake of the respective formaldehyde conjugates [29]. The enhanced uptake of the clinical drugs over 24 h is likely the result of increased time for drug-catalyzed production of formaldehyde and subsequent covalent bonding to DNA.

The 24 h drug treatment period did not lead to a similar increase of clinical drug in resistant cells. This is due to the effectiveness of the resistance mechanisms, which include overexpression of the drug efflux pump, P-170 glycoprotein, and changes in enzyme levels associated with regulation of oxidative stress [18,19].

Fluorescence microscopy studies of drug-treated cells show that the nucleus is a primary target of the drug-formaldehyde conjugates in both sensitive and resistant cells, while clinical drugs are excluded from the nuclei of resistant MCF-7/Adr cells [29]. Fig. (**6**) shows drug chromophore primarily in the nucleus of resistant cells treated with EPIF for 3 h and primarily in the Golgi/cytoplasm of resistant cells treated with EPI for 3 h [29]. The results in Fig (**6**) are even more dramatic upon realizing that DNA substantially quenches drug fluorescence [30]. Similar localization of DAU and DOX in the Golgi/cytoplasm of MCF-7/Adr cells has also been observed by laser scanning confocal microscopy [31]. Further evidence for nuclear targeting of the formaldehyde conjugates comes from labeling studies. Treatment of both MCF-7 and MCF-7/Adr cells with DOXF synthesized with tritiated formaldehyde showed significantly more tritium counts in the DNA relative to controls [29]. Indeed, 20-fold more counts per milligram of cell fraction was observed in DNA with respect to RNA or protein in DOXF-treated cells.

Release of drug chromophore from cells was also monitored by flow cytometry following drug removal from the growth medium. In addition to higher uptake and more nuclear involvement by drug-formaldehyde conjugates, drug retention was also longer, especially with 3 h drug treatment, relative to retention of the clinical drugs [29]. This most likely results from 3 h treatment limiting clinical drug-catalyzed formaldehyde production.

In a series of previously unreported experiments, the rate of release of DOX, DOXF, EPI and EPIF from MCF-7/Adr cells was measured after 24 h drug treatment. Cells were treated for 24 h to allow time for the clinical drugs, DOX and EPI, to catalyze formaldehyde production (Fig. (**7**)). MCF-7/Adr cells were selected for these measurements because only drug covalently bonded to DNA is retained in these cells once drug is removed from the medium, due to P-glycoprotein efflux. Thus, the rate of release is likely a measure of the rate of release of covalently bound drug from DNA. The extracellular experiments of Phillips and co-workers showed that doxorubicin was released with two different time constants, one for release from isolated G-bases (faster) and one for release from GC sites (slower) [2,6]. The latter sites are what we describe as *virtual crosslinking* sites [14]. Given these two release rates, the data in Fig. (**7**) were fit to a double exponential rate law with faster and slower release rates: one with a half-life of 2 h and the other with a half-life of 29 h. These are comparable with the half-lives of 5 h and 40 h for release from extracellular DNA determined by Phillips and co-workers [2,6]. The best fit non-linear least squares pre-exponential factors indicate that 60% of drug is bonded at isolated G-bases and 40% is at NGC sites (to

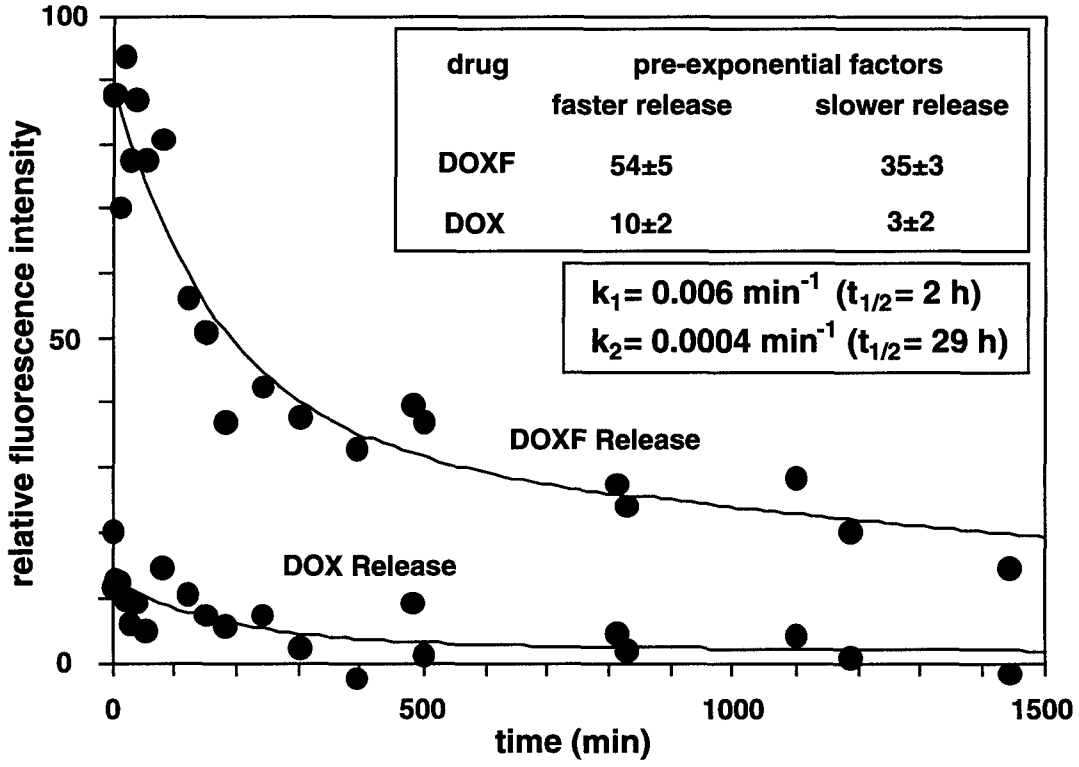

Fig. (7). Release of DOXF and DOX from resistant MCF-7/Adr tumor cells treated with 0.5 mol equiv/L of drug for 24 h. Drug in cells was determined by flow cytometry, measuring drug fluorescence. The rate of drug release was fit to a double exponential rate law by non-linear least squares analysis.

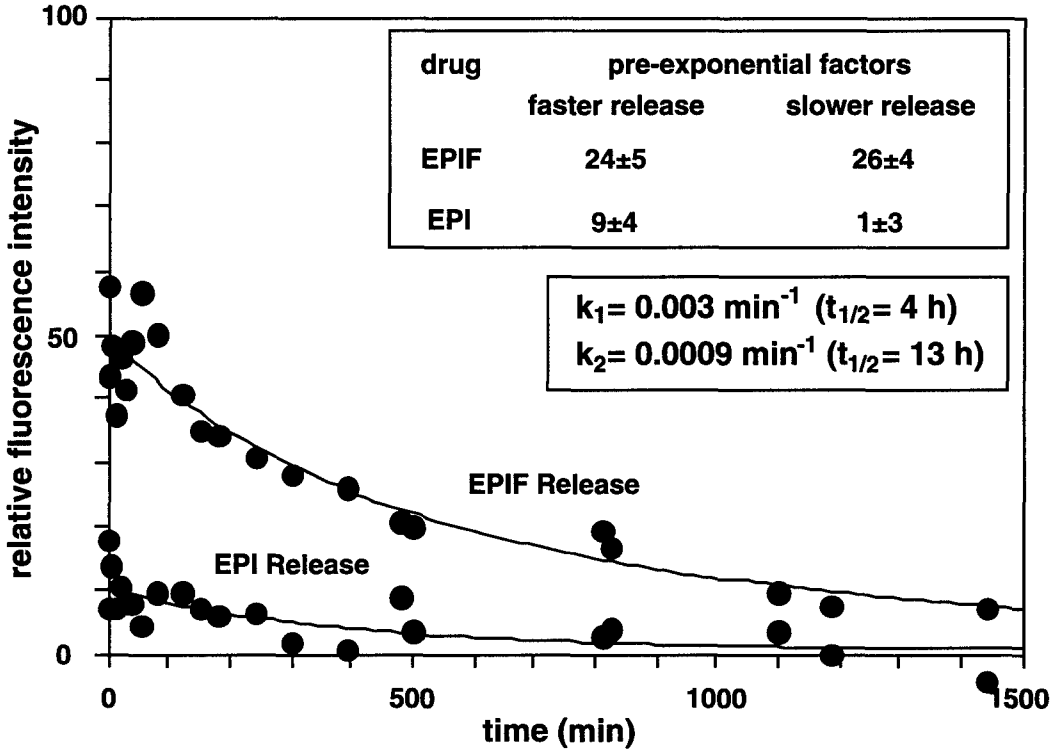

Fig. (8). Release of EPIF and EPI from resistant MCF-7/Adr tumor cells treated with 0.5 mol equiv/L of drug for 24 h. Drug in cells was determined by flow cytometry, measuring drug fluorescence. The rate of drug release was fit to a double exponential rate law by non-linear least squares analysis.

create *virtual crosslinks*) in DOXF treated cells. For DOX treated cells, more drug is also located at isolated G-bases than at NGC sites. The pre-exponential factors further indicate 7-fold more covalent bonding occurs from 24 h treatment with DOXF than from 24 h treatment with DOX.

Corresponding kinetic analysis of drug release from EPIF and EPI treated cells fit best with drug release half-lives of 4 h and 13 h, respectively, for drug bonded at isolated G-bases and at NGC sites, as shown in Fig. (**8**). EPIF gave about equal amounts of covalent bonding at isolated G-bases and *virtual crosslinking* sites; whereas, EPI gave more covalent bonding at isolated G-bases than at *virtual crosslinking* sites. In addition, EPIF gave 5-fold more covalent bonding than EPI after 24 h drug treatment. Release of non-covalently bonded DOX and EPI from cells occurs on a much faster time scale and was observed with MCF-7 cells treated with clinical drug for 3 h (data not shown). The conclusion from these studies is that covalently bound DOX is released from isolated G-bases more rapidly than EPI, but from NGC (*virtual crosslinking*) sites more slowly than EPI. Thus, the extra hydrogen bonding from the 4'-hydroxyl of EPI, shown in Fig. (**4**), may not increase the stability of EPI-DNA *virtual crosslinks* relative to DOX-DNA *virtual crosslinks*. Slower drug release from *virtual crosslinking* sites may be an explanation for the higher cytotoxicity of DOXF (Table 1).

A question, possibly relevant to drug cytotoxicity, relates to the mechanism of drug release from DNA. Upon hydrolysis of the covalent linkage between the 3'-amino group of the drug and the 2-amino group of a G-base, is the formaldehyde retained by the drug or by the DNA? The principle of microscopic reversibility predicts that the formaldehyde is retained by the drug. A recent extra cellular experiment by Hopkins and co-workers [32] supports initial hydrolysis of the bond from the 2-amino group of the G-base to the methylene group of the linkage. The experiment involved trapping the product from hydrolysis of doxorubicin-DNA adducts and *virtual crosslinks* by adding a large excess of sodium borohydride to a solution of DNA covalently bonded to doxorubicin. This presumably led to rapid reduction of the species leaving the DNA upon hydrolysis of the lesion. The sodium borohydride reductively cleaved the drug at the 7-position to release the sugar [33] and reduced the sugar-formaldehyde Schiff base both at the sugar aldehyde and the Schiff base. Gas chromatography mass spectrometry of the peracetylated reduced sugar showed the sugar to bear an N-methyl substituent. The experiment indicates that upon hydrolysis of the drug-DNA lesion, the formaldehyde is retained by the drug, leaving the DNA unmodified.

Uptake, Nuclear Localization, and Retention in Metastatic Prostate Cancer Cells

First line treatment of prostate cancer is through hormone manipulation. Upon relapse and metastasis, tumors become hormone-resistant. Doxorubicin and mitomycin C are the most effective chemotherapeutics for metastatic prostate cancer but do not increase survival [34,35]. Epidoxorubicin

gives similar palliative results to doxorubicin but with less side effects [36]. The resistance of metastatic prostate cancer to doxorubicin and epidoxorubicin, coupled with the observed toxicity of Doxoform and Epidoxoform to resistant MCF-7/Adr cells prompted a comparison of the effect of these drugs on the metastatic prostate cancer cell lines, LNCaP, PC-3, and DU-145. PC-3 and DU-145 are completely hormone resistant, while LNCaP cells are relatively hormone resistant [37-39].

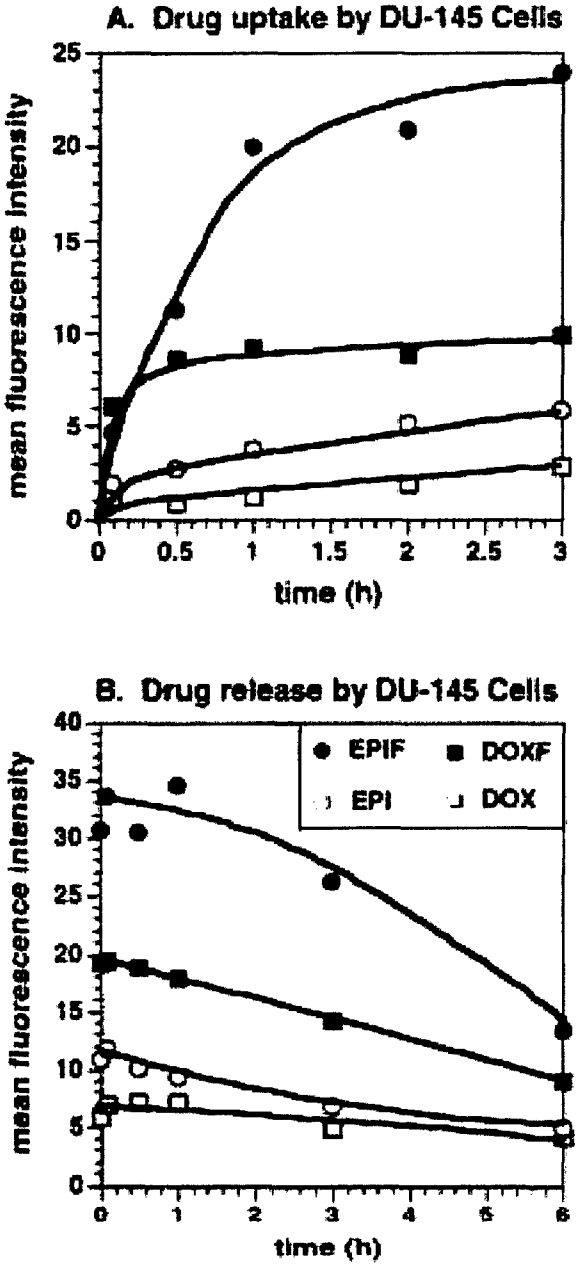

Fig. (9). Comparison of the uptake and release of EPIF, EPI, DOXF, and DOX by resistant DU-145 human prostate cancer cells. Cells were treated with 0.5 mol equiv/L of drug for 3 h, and drug in cells was determined by flow cytometry, measuring drug fluorescence.

Growth inhibition of LNCaP, PC-3, and DU-145 cells by DOXF and EPIF after a 3 h drug treatment is compared in Table 1 with growth inhibition by DOX and EPI. Doxoform inhibits the growth of PC-3 and DU-145 cells 50- and 80-fold better, respectively, than DOX, and EPIF inhibits the growth 6- and 15-fold better than EPI [40]. The improved toxicity of the conjugates is less dramatic with the less resistant LNCaP cells.

Drug uptake and release of the four drugs was monitored by flow cytometry. In general, all three cell lines took up more of the respective formaldehyde conjugate than the clinical drug and retained the drug longer [40]. Uptake during the 3 h drug treatment period followed by drug release for a 6 h period is shown for DU-145 cells in Fig. (9). As observed with breast cancer cells, EPIF is taken up more slowly, and the rate parallels the hydrolysis rate to the active metabolite. Further, drug uptake does not simply parallel cytotoxicity. DU-145 cells take up approximately twice as much EPIF chromophore as DOXF chromophore, but the IC50 value for DOXF is about 9-fold smaller than the IC50 value for EPIF. As with breast cancer cells the relative toxicity of the conjugates appears to be inversely

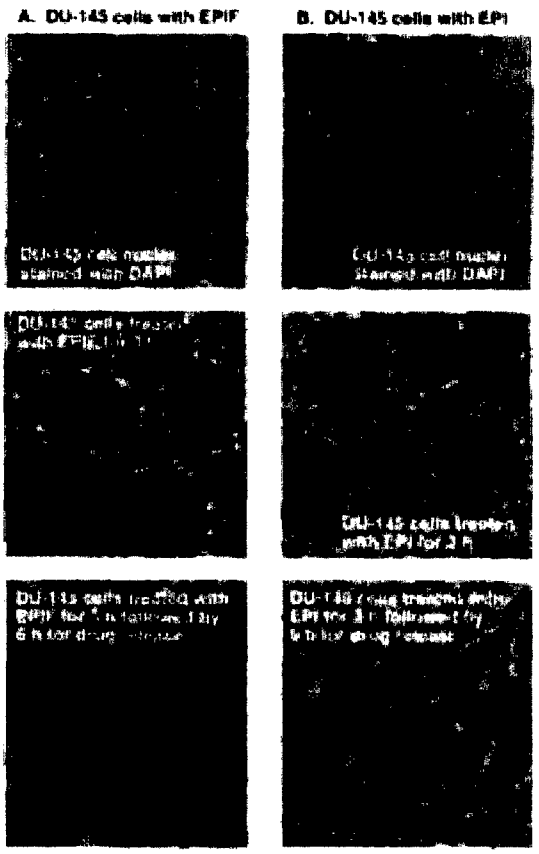

Fig. (10). Fluorescence micrographs of resistant DU-145 prostate tumor cells after treatment for 3 h with 0.5 mol equiv/L of EPIF (column A) or EPI (column B) and 6 h after drug removal. Drug is highlighted in red, and nuclei, visualized with the nuclear stain DAPI, are highlighted in cyan. Both drugs appear in the nuclei but EPIF is retained longer than EPI.

Table 2. National Cancer Institute (NCI) In-Vitro Human Tumor Cell Screen and Tumor Cell Resistance Parameters

Panel/Cell Line	log GI50 (M)			rhodamine[d]	mdr-1[d]	MRP[d]	LRP[d]
	EPIF[a]	DOX[b]	EPI[c]	efflux			
Leukemia							
CCRF-CEM	-8.52	-7.46	-7.35	35	0.4	1.2	0.0
HTL-60 (TB)	-8.57	-7.29	-7.24				
MOLT-4	-8.60	-7.96	-7.77				
RPMI-8226	-8.31	-7.35	-7.26				
Non Small Cell Lung Carcinoma (NSCLC)							
A549/ATCC	-7.89	-7.14	-7.10				
EKVX	-7.07	-6.17	-6.52				
HOP-62	-7.66	-7.30	-6.82	62	3.4	1.3	1.7
HOP-92	-7.82	-7.09	-6.51				
NCI-H226	-7.44	-7.29	-7.36				
NCI-H23	-7.92	-6.96	-7.12				
NCI-H322M	-7.55	-6.31	-6.04				
NCI-H460	-8.35	-8.33	-7.60				
NCI-H522	-8.17	-7.22	-6.72				
Colon Cancer							
COLO 205	-7.90	-6.67	-6.30				
HCC-2998	-7.12	-6.63	-6.51	-5	0.1	1.1	2.0
HCT-116	-7.78	-7.18	-7.17	26	5.8	1.8	2.5
HCT-15	-6.93	-5.88	-5.41	414	457	1.6	0.1
HT29	-7.70	-6.73	-6.51				
KM12	-7.34	-6.56	-6.43				
SW-620	-7.98	-7.12	-6.91	31	19.4	0.8	0.3
Central Nervous System Cancer							
SF-268	-8.20	-6.96	-6.66				
SF-295	-7.51	-7.04	-6.68	91	8.3	1.6	0.8
SF-539	-8.26	-7.16	-6.71				
SNB-19	-7.82	-7.31	-7.04				
SNB-75	-8.12	-7.04	-6.60				
U251	-8.11	-7.39	-7.07	-19	2.7	1.1	0.1
Melanoma							
MALME-3M	-7.80	-7.16	-6.85				
M14	-7.30	-6.66	-6.37				
SK-MEL-2	-7.64	-6.63	-6.70	11	2.8	0.8	0.1
SK-MEL-28	-7.31	-6.56	-6.23				
SK-MEL-5	-7.35	-7.17	-6.95	12	13	2.3	1.6

(Table 2). contd.....

Panel/Cell Line	log GI50 (M)			rhodamine[d] efflux	mdr-1[d]	MRP[d]	LRP[d]
	EPIF[a]	DOX[b]	EPI[c]				
UACC-257	-7.28	-6.66	-6.47				
UACC-62	-8.30	-7.19	-6.82				
Ovarian Cancer							
IGROV1	-7.76	-6.87	-6.57				
OVCAR-3	-7.33	-6.40	-6.33				
OVCAR-4	-6.98	-6.19	-5.92	-4	0.1	2.0	1.0
OVCAR-5	-7.05	-6.28	-6.14				
OVCAR-8	-7.75	-6.88	-6.70				
SK-OV-3	-6.88	-6.66	-6.39				
Renal Cancer							
786-0	-8.10	-7.31	-7.00	-44	18.4	0.5	1.5
A498	-8.42	-6.98	-	108	71		
ACHN	-8.09	-7.21	-6.57	120	31	0.0	1.5
CAKI-1	-7.76	-6.77	-6.57	171	177	0.4	2.3
SN12C	-7.80	-7.04	-6.77	-86	2.2	0.4	1.5
TK-10	-6.63	-6.39	-6.14				
UO-31	-6.84	-6.13	-5.72	244	749	1.8	2.4
Prostate Cancer							
PC-3	-7.30	-6.70	-6.62				
DU-145	-7.92	-6.83	-6.57				
Breast Cancer							
MCF-7/ADR-RES	-6.49	-4.78	-				
MDA-MB-231/ATCC	-7.32	-6.41	-6.02				
HS-578T	-7.21	-6.71	-8.00				
MDA-MB-435	-7.19	-6.51	-6.21				
MDA-N	-7.28	-6.58	-6.86				
BT-549	-6.93	-6.62	-6.36				
T-47D	-7.16	-7.04	-7.03				
Mean							
	-7.64	-6.87	-6.70				

[a]Single determination with log maximum concentration (M) = -4.6; [b]Average of multiple determinations with log maximum concentration (M) = -4.6; [c]Single determination with log maximum concentration (M) = -4.0; [d]Values obtained from the NCI Developmental Therapeutics Program web site: http://dtp.nci.nih.gov/; MRP (multidrug resistant protein), LRP, lung resistant protein.

related to the drug release rate; the EPIF chromophore is released more rapidly than the DOXF chromophore from DU-145 cells and MCF-7/Adr cells. Fluorescence microscopy shows the nucleus to be a major target for both the clinical drugs and their formaldehyde conjugates as shown with DU-145 cells in Fig. (**10**) [40]. This contrasts with the highly resistant MCF-7/Adr cells which reject the clinical drugs from the nucleus (Fig. (**6**)). The fluorescence micrographs of DU-145 cells also show qualitatively longer retention of chromophore from treatment with EPIF than from treatment with EPI (compare micrograph in column A, row c, with the micrograph in column B, row c).

NCI 60 Human Tumor Cell Screen

Epidoxoform has recently been evaluated in the National Cancer Institute human tumor cell screen which includes 60 cell lines in 8 panels: leukemia, non small cell lung carcinoma, colon cancer, central nervous system cancer, melanoma, ovarian cancer, renal cancer, prostate cancer, and breast cancer. Growth inhibition by EPIF is compared with growth inhibition by DOX and EPI in Table 2. The screen utilizes a 48 h drug treatment period instead of the 3 h drug treatment period for the measurements reported in Table 1. Values are reported as the log of the concentration which inhibits half of the growth, and no correction is included for EPIF bearing two reactive drug equivalents. Measures of four components of the multidrug-resistant (MDR) phenotype are also reported for some of the cell lines. These include two measures of P-170 glycoprotein (Pgp) efflux pump (rhodamine efflux and *mdr-1* expression) and measures of the multidrug resistance protein (MRP) and the lung resistance-related protein (LRP). Pgp and MRP are ATP dependent, membrane bound proteins which shuttle cytotoxic agents out of the cell. Pgp pumps out postively charged and hydrophobic xenobiotics [41]; whereas, MRP pumps out anionic species, often created through association with anionic glutathione [42]. LRP is expressed in many multi-drug resistant cancer cells and has been identified as the human major vault protein involved in nucleo-cytoplasmic transport [43]. The data in Table 2 show EPIF to be more active than EPI in all but one cell line and more active than DOX in 90% of the cell lines. The mean values over all 60 cell lines show EPIF to be approximately 0.7 log more toxic to tumor cells than EPI and 0.5 log more toxic than DOX, correcting for EPIF being dimeric. Not surprisingly, the most dramatic increase in toxicity appears with the more resistant cell lines. For colon HCT-15 cells, which show the highest value for rhodamine efflux (a measure of P-glycoprotein activity), the corrected log GI50 value for EPIF is 0.75 better than for DOX and 1.2 better than for EPI. For renal UO-31 cells, which show the highest value for *mdr-1* (the gene which codes for P-glycoprotein) and high values for rhodamine efflux, MRP, and LRP, the corrected log GI50 for EPIF is 0.4 better than for DOX and 0.8 better than for EPI. As discussed earlier in this paper, EPIF also significantly exceeds the toxicity of DOX and EPI with the most resistant breast cancer cell line, MCF-7/Adr, and the most resistant prostate cancer cell line, DU-145. Although resistance parameters were not available for MCF-7/Adr or DU-145 cells from NCI, expression of Pgp is reported by Kreis and co-workers as strong for MCF-7/Adr cells and slight for DU-145 cells [44]. Of the 8 panels of tumor cells, the more dramatic increases in toxicity of EPIF relative to DOX and EPI occur with leukemia, colon, renal, and prostate panels. Amongst all of the cell lines in Table 2, the largest increase in toxicity occurred with the highly resistant MCF-7/Adr breast cell line in which the clinical drugs are excluded from the nucleus as shown in Fig. (**6**). Although the origin of this nuclear exclusion is unknown, involvement of LRP is a possibility.

The data in Table 2 were submitted for COMPARE analysis [45] with the standard anticancer agent data base at the NCI Developmental Therapeutics web site (http://dtp.nci.nih.gov/). Doxorubicin and daunorubicin ranked 1 and 2 with Pearson correlation coefficients of 0.78 and 0.76, respectively. Compounds with rank of 20 or better included primarily topoisomerase II inhibitors: anthracyclines (4'-deoxydoxorubicin, Rubidazone, and Menogaril), mitoxantrone and its congeners (bisanthrene, oxanthrazole, anthrapyrazole), teniposide and etoposide. Strong similarity to doxorubicin and daunorubicin and other topo II inhibitors is consistent with Epidoxoform serving as a prodrug to the active metabolite of epidoxorubicin. The Pearson correlation coefficients are not as high as observed when doxorubicin or epidoxorubicin is similarly analyzed. This may result from Epidoxoform's ability to overcome some resistance mechanisms.

Researchers at NCI observed strong correlation of Epidoxoform with rhodamine efflux using COMPARE to relate EPIF to molecular targets; the Pearson correlation coefficient was 0.82. However, only modest correlation with rhodamine efflux and *mdr-1* expression is evident from the data in Table 2, looking at three of the cell lines used by NCI in their current MDR screen. The three cell lines in order of increasing MDR are CAKI, UO-31 and HCT-15. The GI50 values from EPIF treatment of the more resistant UO-31 and HCT-15 cells are on average 8-fold higher than for the more sensitive CAKI cells. However, the GI50 values from DOX and EPI treatment of the more resistant cells are on average 30-fold and 85-fold higher than from EPIF treatment of CAKI cells, respectively, even with correction for EPIF being dimeric. The modest correlation of GI50 values for EPIF with rhodamine efflux might actually result from hydrolysis of EPIF to EPI during the 48 h drug treatment period used in the assay. The resulting EPI would show some toxicity to CAKI cells but much less to UO-31 and HCT-15 cells. *In vivo*, the effect of the EPI from hydrolysis of EPIF would be modulated by drug clearance.

Epidoxoform Toxicity to Normal Cells

Increased toxicity in tumor cells is of little consequence if a similar increase occurs in normal cells. Preliminary mouse experiments at the National Cancer Institute show a maximum tolerated dose for EPIF in nude mice that significantly exceeds that for DOX and EPI. Several factors might contribute to an improved therapeutic index for EPIF. First, slow hydrolysis allows sufficient time for the drug to reach the tumor. Second, the absence of positive charge on EPIF (or its "active form") may limit cardiotoxicity. Indeed, high levels of DOX in heart cells have been attributed to the positively-charged drug associating with negatively charged cardiolipin in heart cells [46]. Third, since EPIF carries its own formaldehyde, it does not require damaging redox processes to generate formaldehyde. In addition, normal cells may survive the covalent bonding of EPIF to DNA upon slowing their growth to allow for repair or hydrolysis of the drug-DNA lesion. Intracellular experiments described here and extracellular experiments indicate that the *virtual crosslink* is an unstable, temporary lesion [2,6,14,15,47]. Hydrolysis of the DNA lesion created with EPIF should release EPI, which is relatively rapidly excreted as a conjugate with glucuronic acid [48].

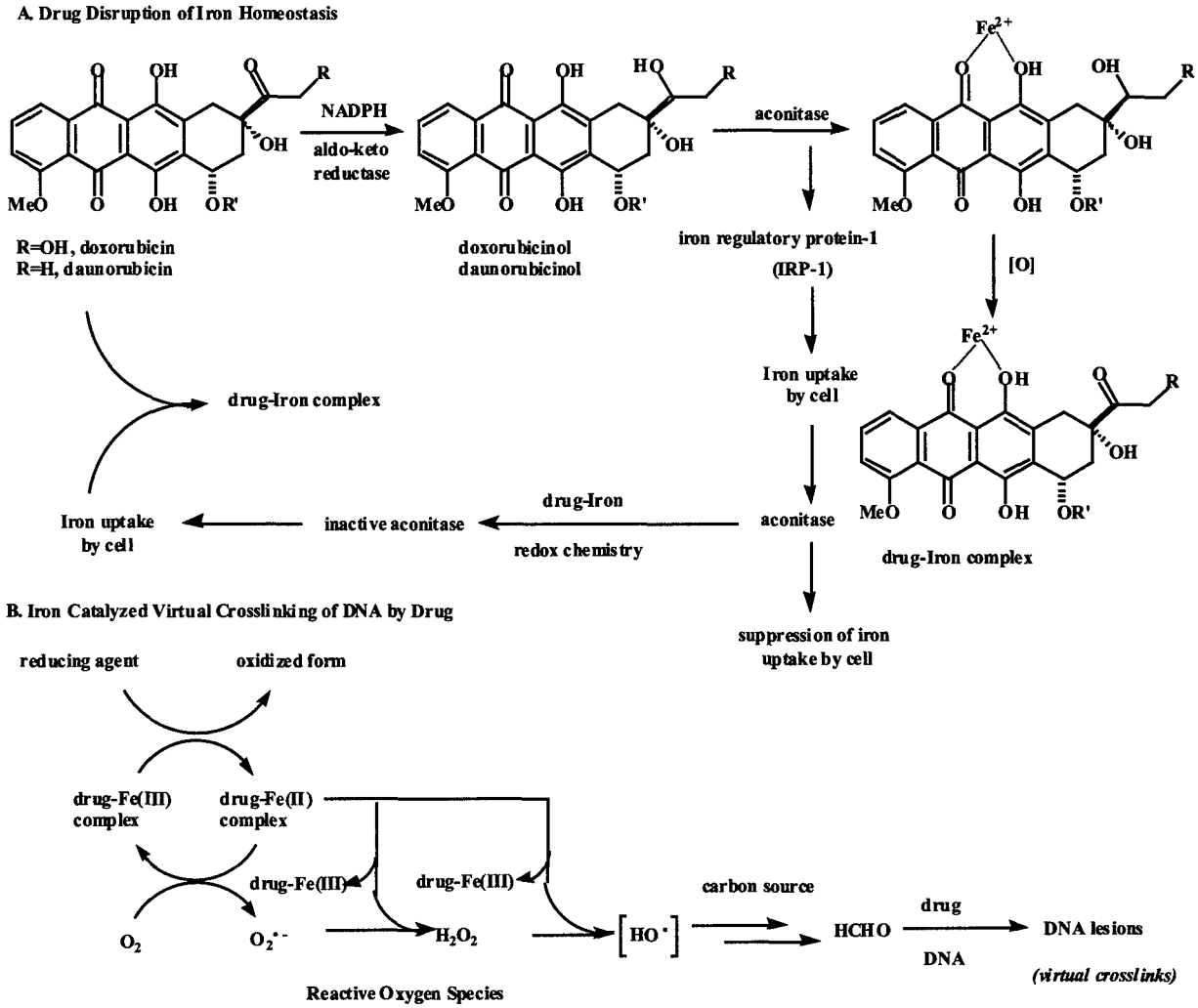

Fig. (11). A. Proposed mechanism for sequestering of iron by clinical drugs through disruption of the iron regulatory machinery. B. Proposed mechanism for clinical drug-catalyzed formaldehyde production through induction of oxidative stress by the drug iron complex resulting in *virtual crosslinking* of DNA by drug.

Anthracycline Disruption of Iron Homeostasis

A key step in the proposed anthracycline-catalyzed production of formaldehyde is drug sequestering of iron. Doxorubicin, daunorubicin, and presumably epidoxorubicin are excellent chelators of iron ions with iron co-ordinated predominantly at the oxygens at the 11- and 12-positions [49]. However, thermodynamic measurements suggested that doxorubicin and daunorubicin cannot shift iron from the iron storage and regulatory machinery of the cell [49,50].

New results point to an elaborate pathway for iron sequestration by the drugs as summarized in Fig. (**11A**) [51]. A well established metabolic reaction of doxorubicin is enzymatic reduction of the ketone at the 13-position to the alcohol, doxorubicinol. Minotti and co-workers have reported evidence which suggests that doxorubicinol is able to extract ferrous ion from the iron-sulfur cluster of aconitase. This converts aconitase to iron regulatory protein-1 (IRP-1). IRP-1 binds the iron responsive element of mRNAs for both transferrin receptor and ferritin, an iron storage protein. This results in increased synthesis of transferrin receptor and decreased synthesis of ferritin, leading to an increase in available iron. Increased iron transforms IRP-1 back to aconitase, reversing iron uptake. No substantial increase in available iron would occur by the mechanism except that the oxidative stress induced by the iron anthracycline complexes causes irreversible damage to aconitase and IRP-1, disrupting the iron regulatory machinery and iron homeostasis. This oxidative stress is also responsible for formaldehyde production leading to drug-DNA *virtual crosslinks*, as summarized in Fig. (**11B**).

Upon elucidation of the mechanism by which doxorubicinol disrupts iron homeostasis, Minotti and co-workers suggested two strategies for minimizing doxorubicin

cardiotoxicity: iron chelating agents such as Dexrazoxane (ICRF-187) and inhibitors of the reductase that reduces doxorubicin to doxorubicinol [51]. However, if our mechanism for cytotoxicity is correct, these strategies would also inhibit tumor cell toxicity of the clinical drugs. Of course, tumor cell toxicity of the anthracycline-formaldehyde conjugates might not be so inhibited because the conjugates do not require additional formaldehyde. Clinical studies indicate that Dexrazoxane is cardioprotective but that it may also interfere with the anti-tumor activity of doxorubicin [52].

CONCLUSION

Extracellular reactivity and structural studies together with intracellular measurements of toxicity, uptake, targeting, and release of clinical anthracyclines and their synthetic, formaldehyde conjugates support a DNA covalent bonding mechanism for toxicity of the clinical anthracyclines. The mechanism involves drug catalyzed production of formaldehyde through induction of oxidative stress, covalent bonding of formaldehyde to drug at its 3'-amino group, and covalent attachment of drug via the formaldehyde at the 2-amino group of a G-bases. The combination of covalent bonding, hydrogen bonding and hydrophobic interactions between the drug and DNA serve to *virtually crosslink* the DNA at NGC sites. The DNA lesions are unstable and hydrolyze in MCF-7/Adr cells at two different rates with the faster rate assigned to hydrolysis of lesions at isolated G-bases and the slower rate to hydrolysis of lesions at NGC sites. To exploit this mechanistic knowledge, we synthesized drug formaldehyde conjugates, which serve as prodrugs to the metabolites of the clinical drugs. As such, the conjugates are more toxic to all eight panels of the National Cancer Institute 60 human tumor cell screen than the clinical drugs with increased toxicity more dramatic in more resistant cancer cells.

ACKNOWLEDGMENT

We thank Dr. Anthony Mauger and his colleagues at the Developmental Therapeutics Program of NCI for testing Epidoxoform in the human tumor cell screen. This work was supported by Grants CA78756 from NIH, RPG-98-110-01-ROG from the American Cancer Society, and DAMD17-98-1-8298 from the U.S. Army Breast Cancer Program, and a predoctoral fellowship to D.J.T. from the Division of Medicinal Chemistry of the American Chemical Society and Wyeth-Ayerst, Inc. We thank Vinchem, Inc. and Gensia-Sicor (Milan, Italy) for samples of epidoxorubicin.

LIST OF ABBREVIATIONS

C = Deoxycytosine

DAU = Daunorubicin (Daunomycin)

DAUF = Daunoform (daunorubicin-formaldehyde conjugate)

DOX = Doxorubicin (Adriamycin)

DOXF = Doxoform (doxorubicin-formaldehyde conjugate)

EPI = Epidoxorubicin (Epirubicin)

EPIF = Epidoxoform (epidoxorubicin-formaldehyde conjugate)

G = Deoxyguanosine

LRP = Lung resistance-related protein

MDR = Multidrug resistance

NCI = National Cancer Institute

MRP = Multidrug resistance protein

Pgp = 170 glycoprotein

REFERENCES

[1] Taatjes, D.J.; Fenick, D.J.; Gaudiano, G.; Koch, T.H. *Current Pharmaceutical Design* **1998**, *4*, 203.

[2] Cullinane, C.; van Rosmalen, A.; Phillips, D.R. *Biochemistry* **1994**, *33*, 4632.

[3] Cullinane, C.; Cutts, S.M.; van Rosmalen, A.; Phillips, D.R. *Nucleic Acids Res.* **1994**, *22*, 2296.

[4] Cutts, S.M.; Phillips, D.R. *Nucleic Acids Res.* **1995**, *23*, 2450.

[5] Cutts, S.M.; Parsons, P.G.; Sturm, R.A.; Phillips, D.R. *J. Biol. Chem.* **1996**, *271*, 5422.

[6] van Rosmalen, A.; Cullinane, C.; Cutts, S.M.; Phillips, D.R. *Nucleic Acids Res.* **1995**, *23*, 42.

[7] Olson, R.D.; Mushlin, P.S. *FASEB J* **1990**, *4*, 3076.

[8] Doroshow, J.H. In *Cancer Chemotherapy and Biotherapy*; Chabner, B. A.; Longo, D. L., Eds.; Lippincott-Raven; Philadelphia, **1996**; pp. 409.

[9] Myers, C. *Semin. Oncol.* **1998**, *25*, 10.

[10] Skladanowski, A.; Konopa, J. *Biochem. Pharmacol.* **1994**, *47*, 2279.

[11] Skladanowski, A.; Konopa, J. *Biochem. Pharmacol.* **1994**, *47*, 2269.

[12] Bartoszek, A.; Wolf, C.R. *Biochem. Pharmacol.* **1992**, *43*, 1449.

[13] Taatjes, D.J.; Gaudiano, G.; Resing, K.; Koch, T.H. *J. Med. Chem.* **1996**, *39*, 4135.

[14] Taatjes, D.J.; Gaudiano, G.; Resing, K.; Koch, T. *J. Med. Chem.* **1997**, *40*, 1276.

[15] Taatjes, D.J.; Gaudiano, G.; Koch, T.H. *Chem. Res. Toxicol.* **1997**, *10*, 953.

[16] Wang, A.H.J.; Gao, Y.G.; Liaw, Y.C.; Li, Y.K. *Biochemistry* **1991**, *30*, 3812.

[17] Bagchi, D.; Bagchi, M.; Hassoun, E.A.; Kelly, J.; Stohs, S.J. *Toxicology* **1995**, *95*, 1.

[18] Sinha, B.K.; Mimnaugh, E.G. *Free Rad. Biol. Med.* **1990**, *8*, 567.

[19] Mimnaugh, E.G.; Fairchild, C.R.; Fruehauf, J.P.; Sinha, B.K. *Biochem. Pharmacol.* **1991**, *42*, 391.

[20] Fenick, D.J.; Taatjes, D.J.; Koch, T.H. *J. Med. Chem.* **1997**, *40*, 2452.

[21] Taatjes, D.J.; Fenick, D.J.; Koch, T.H. *J. Med. Chem.* **1998**, *41*, 1306.

[22] Gewirtz, D.A. *Biochem. Pharmacol.* **1999**, *57*, 727.

[23] Zhang, H.; Gao, Y.G.; van der Marel, G.A.; van Boom, J.H.; Wang, A.H. *J. Biol. Chem.* **1993**, *268*, 10095.

[24] Podell, E.R.; Harrington, D.J.; Taatjes, D.J.; Koch, T.H. *Acta Cryst.* **1999**, *D55*, 1516.

[25] Williams, L.D.; Frederick, C.A.; Ughetto, G.; Rich, A. *Nucleic Acids Res.* **1990**, *18*, 5533.

[26] Chaires, J.B.; Satyanarayana, S.; Suh, D.; Fokt, I.; Przewloka, T.; Priebe, W. *Biochemistry* **1996**, *35*, 2047.

[27] Zeman, S.M.; Phillips, D.R.; Crothers, D.M. *Proc. Natl. Acad. Sci. USA* **1998**, *95*, 11561.

[28] Mross, K.; Maessen, P.; vanderVijgh, W.J.F.; Gall, H.; Boven, E.; Pinedo, H.M. *J. Clin. Oncol.* **1988**, *6*, 517.

[29] Taatjes, D.J.; Fenick, D.J.; Koch, T.H. *Chem. Res. Toxicol.* **1999**, *12*, 588.

[30] Crooke, S.T.; DuVernay, V.H. In *Anthracyclines Current Status and New Developments*; Crooke, S. T.; Reich, S. D., Eds.; Academic Press; New York, **1980**; pp. 151.

[31] Serafino, A.; Sinibaldi-Vallebona, P.; Gaudiano, G.; Koch, T.H.; Rasi, G.; Garaci, E.; Ravagnan, G. *Anticancer Res.* **1998**, *18*, 1159.

[32] Luce, R.A.; Sigurdsson, S.T.; Hopkins, P.B. *Biochemistry* **1999**, *38*, 8682.

[33] Schweitzer, B.A.; Egholm, M.; Koch, T.H. *J. Am. Chem. Soc.* **1992**, *114*, 242.

[34] Mahler, C.; Denis, L. *Cancer* **1992**, *70*, 329.

[35] Slack, N.H.; Murphy, G.P. *Urology* **1983**, *22*, 1.

[36] Francini, G.; Petrioli, R.; Manganelli, A.; Cintorino, M.; Marsili, S.; Aquino, A.; Mondillo, S. *Br. J. Cancer* **1993**, *67*, 1430.

[37] Kaighn, M.E.; Narayan, K.S.; Ohuki, Y.; Lechner, J.F.; Jones, L.W. *Invest. Urol.* **1979**, *17*, 16.

[38] Stone, K.R.; Mickey, D.D.; Wunderli, H.; Mickey, G.H.; Paulson, D.F. *Int. J. Cancer* **1978**, *21*, 274.

[39] Horoszewicz, J.S.; Leong, S.S.; Kawinski, E.; Karr, J.P.; Rosenthal, H.; Chu, T.M.; Mirand, E.A.; Murphy, G.P. *Cancer Res.* **1983**, *43*, 1809.

[40] Taatjes, D.J.; Koch, T.H. *Anticancer Res.* **1999**, *19*, 1201.

[41] Lampidis, T.J.; Kolonias, D.; Podona, T.; Israel, M.; Safa, A.R.; Lothstein, L.; Savaraj, N.; Tapiero, H.; Priebe, W. *Biochemistry* **1997**, *36*, 2679.

[42] Leier, I.; Jedlitschky, G.; Buchholz, U.; Cole, S.P.C.; Deeley, R.G.; Keppler, D. *J. Biol. Chem.* **1994**, *269*, 27807.

[43] Scheffer, G.L.; Wijngaard, P.L.; Flens, M.J.; Izquierdo, M.A.; Slovak, M.L.; Pinedo, H.M.; Meijer, C.J.; Clevers, H.C.; Scheper, R.J. *Nature Med.* **1995**, *1*, 578.

[44] Kreis, W.; Budman, D.R.; Broome, J.; Cowan, K.; Calabro, A.; Akerman, S. *Cell Pharmacol.* **1995**, *2*, 229.

[45] Weinstein, J.N.; Myers, T.G.; O'Connor, P.M.; Friend, S.H.; A. J. Fornace, J.; Kohn, K.K.; Fojo, T.; Bates, S.E.; Rubinstein, L.V.; Anderson, N.L.; Buolamwini, J.K.; vanOsdol, W.W.; Monks, A.P.; Scudiero, D.A.; Sausville, E.A.; Zaharevitz, D.W.; Bunow, B.; Viswanadhan, V.N.; Johnson, G.S.; Wittes, R.E.; Paull, K.D. *Science* **1997**, *275*, 343.

[46] Goormaghtigh, E.; Chatelain, P.; Caspers, J.; Ruysschaert, J.M. *Biochem. Pharmacol.* **1980**, *29*, 3003.

[47] Leng, F.; Savkur, R.; Fokt, I.; Przewloka, T.; Priebe, W.; Chaires, J.B. *J. Am. Chem. Soc.* **1996**, *118*, 4731.

[48] Weenen, H.; Maanen, J.M.v.; Planque, M.M.d.; McVie, J.G.; Pinedo, H.M. *Eur. J. Cancer Clin. Oncol.* **1984**, *20*, 919.

[49] Fiallo, M.M.L.; Drechsel, H.; Garnier-Suillerot, A.; Matzanke, B.F.; Kozlowski, H. *J. Med. Chem.* **1999**, *42*, 2844.

[50] Gelvan, E.; Samuni, A. *Cancer Res.* **1988**, *48*, 5645.

[51] Minotti, G.; Recalcati, S.; Mordente, A.; Liberi, G.; Calafiore, A.M.; Mancuso, C.; Preziosi, P.; Cairo, G. *FASEB J* **1998**, *12*, 541.

[52] Abbott, B.D.; Ippolitti, C.M. *J. Pharm. Technol.* **1998**, *14*, 182.

Formaldehyde in Human Cancer Cells: Detection by Preconcentration-Chemical Ionization Mass Spectrometry

Shuji Kato, Patrick J. Burke, Tad H. Koch, and Veronica M. Bierbaum

Department of Chemistry and Biochemistry, University of Colorado, Boulder, Colorado 80309, and University of Colorado Cancer Center, Denver, Colorado 80262

ANALYTICAL® CHEMISTRY

Reprinted from
Volume 73, Number 13, Pages 2992–2997

Anal. Chem. **2001**, *73*, 2992–2997

Formaldehyde in Human Cancer Cells: Detection by Preconcentration-Chemical Ionization Mass Spectrometry

Shuji Kato, Patrick J. Burke, Tad H. Koch, and Veronica M. Bierbaum*

Department of Chemistry and Biochemistry, University of Colorado, Boulder, Colorado 80309, and University of Colorado Cancer Center, Denver, Colorado 80262

A rapid and highly sensitive method for the detection of formaldehyde utilizing selected ion flow tube-chemical ionization mass spectrometry is reported. Formaldehyde in aqueous biological samples is preconcentrated by distillation and directly analyzed using gas-phase thermal energy proton transfer from H_3O^+; this procedure can be performed in 30 min. The method detection limit for formaldehyde based on seven replicate measurements of reference water samples (2.5 mL) is 80 nM at the 99% confidence level. Detection is linear up to 130 μM. This technique allows the first measurement of natural formaldehyde levels in human cancer cells in vitro. Elevated levels of formaldehyde relative to the reference water are observed for doxorubicin-sensitive cells (MCF-7 breast cancer, K562 leukemia, HeLa S3 cervical cancer) with estimated intracellular formaldehyde concentrations ranging from 1.5 to 4.0 μM, whereas formaldehyde in doxorubicin-resistant MCF-7/Adr breast cancer cells is essentially at reference level. This trend is inverted for prostate cancer cells LNCaP (sensitive) and DU-145 (resistant). Correlation of natural formaldehyde level with doxorubicin cytotoxicity is a function of the expression of enzymes that neutralize oxidative stress and the drug efflux pump, P-170 glycoprotein.

Formaldehyde is ubiquitous in the environment and is commonly found in air, water, and industrial products. The compound is known to be mutagenic and carcinogenic. Because of the adverse health effects, ambient, occupational, and consumer exposures to formaldehyde have been an issue of serious concern. Analytical chemistry and toxicology of this specific compound have been extensively discussed.[1] Formaldehyde and other carbonyls are also a biological consequence of lipid peroxidation following oxidative stress,[2-4] both physiological and chemically induced. Recently, biological assay of formaldehyde has been of considerable interest as the compound reflects the physiological state of tumor-bearing mice and human subjects,[5-7] as well as oxidative stress in rats induced by treatment with xenobiotics[3] and an antitumor drug.[4] In our laboratory, formaldehyde levels were recently measured in human breast cancer cells in vitro, after treatment with various anthracycline antitumor drugs.[8] Low-molecular-weight carbonyls, including formaldehyde, are highly volatile and reactive. Furthermore, many of these compounds do not possess a chromophore. Analytical derivatization has thus been a common and lengthy step in their detection. Quantification of trace levels of formaldehyde in biological samples is probably the most challenging of these as contamination of solvents is a common problem.[9] Large concentrations of background formaldehyde can easily degrade the actual limit of quantitation even when the intrinsic detection limit pertinent to the instrument noise is extremely small.

A conventional formaldehyde determination with the Hantzsch reaction utilizes derivatization with the Nash reagent followed by colorimetry.[10] An advantage of this reaction is the specificity to formaldehyde; interference is significant only when there are large amounts (~100-fold excess) of acetaldehyde. The detection, however, is not exceedingly sensitive; a minimum detectable concentration is reported to be ~50 μM,[11] although ~5 μM might be inferred from the absorbance data alone.[10] Many other derivatization methods involve separation of derivatives before detection. Ebeler et al. used derivatization to thiazolidines followed by gas chromatographic (GC) separation in determining the concentrations of small aldehydes in various tissues of mice[5] and in expired air from mice and human subjects.[6] With the nitrogen phosphorus detector, the limit of quantitation for formaldehyde was 22 μM (0.67 of formaldehyde/mL of homogenate).[5] Two current standard methods employ derivatizations of carbonyls with

(1) *Formaldehyde: Analytical Chemistry and Toxicology*; Turoski, V., Ed.; Advances in Chemistry Series 210; American Chemical Society: Washington, DC, 1985.
(2) Tamura, H.; Kitta, K.; Shibamoto, T. *J. Agric. Food Chem.* **1991**, *39*, 439–442.
(3) Shara, M. A.; Dickson, P. H.; Bagchi, D.; Stohs, S. J. *J. Chromatogr.* **1992**, *576*, 221–233.
(4) Bagchi, D.; Bagchi, M.; Hassoun, E. A.; Kelly, J.; Stohs, S. J. *Toxicology* **1995**, *95*, 1–9.
(5) Ebeler, S. E.; Hinrichs, S.; Clifford, A. J.; Shibamoto, T. *J. Chromatogr., B* **1994**, *654*, 9–18.
(6) Ebeler, S. E.; Clifford, A. J.; Shibamoto, T. *J. Chromatogr., B* **1997**, *702*, 211–215.
(7) Spanel, P.; Smith, D.; Holland, T. A.; Singary, W. A.; Elder, J. B. *Rapid Commun. Mass Spectrom.* **1999**, *13*, 1354–1359.
(8) Kato, S.; Burke, P. J.; Fenick, D. J.; Taatjes, D. J.; Bierbaum, V. M.; Koch, T. H. *Chem. Res. Toxicol.* **2000**, *13*, 509–516.
(9) Cancilla, D. A.; Que Hee, S. S. *J. Chromatogr.* **1992**, *627*, 1–16.
(10) Nash, T. *Biochem. J.* **1953**, *55*, 416–421.
(11) Kottes-Andrews, B. A.; Reinhardt, R. M. In *Formaldehyde: Analytical Chemistry and Toxicology*; Turoski, V., Ed.; Advances in Chemistry Series 210; American Chemical Society: Washington, DC, 1985; Chapter 7.

10.1021/ac001498q CCC: $20.00
Published on Web 05/24/2001

2,4-dinitrophenylhydrazine (DNPH) and *O*-(2,3,4,5,6-pentafluorophenyl)methylhydroxylamine hydrochloride (PFBHA). The hydrazone and oxime derivatives are separated typically by high-performance liquid chromatography (HPLC) and by GC, respectively. Shara et al. first applied the DNPH derivatization of formaldehyde to a biological sample, i.e., enhanced excretion of formaldehyde in the urine of xenobiotic-exposed rats.[3] The limit of detection from the standard addition technique was exceptionally low: 0.5 pmol of formaldehyde hydrazone in a 20-μL aliquot injected (0.025 μM).[3] The PFBHA method is relatively new and reviewed extensively by Cancilla and Que Hee.[9] This method takes advantage of mass spectrometric (MS) detection, which provides additional information on the molecular weight for identifying unknown carbonyls.[12] The PFBHA derivatization has been widely used for detection of formaldehyde and other carbonyls in environmental samples.[9,13,14] For biological samples, however, contamination of solvents by short-chain aldehydes has limited the application of this method to larger aldehydes.[9,15] For both derivatization methods, a technique based on simultaneous sorption and derivatization on a resin has recently been reported to simplify and expedite sample preparation procedures.[16]

More recently, proton transfer-chemical ionization mass spectrometry (PT-CIMS) has been shown to be a powerful approach for the on-line, simultaneous detection of volatile organic compounds from a variety of samples, ranging from environmental and biological samples to consumer products.[17,18] Volatile species are continuously removed from liquid or solid samples, extracted into the gas phase, and immediately analyzed without the need for derivatization or preseparation. As a consequence, sampling and analysis are executed very rapidly in a matter of seconds. In addition, the PT-CIMS method is highly sensitive and easily quantified. The capability for detection without preseparation results from the mild and universal mode of chemical ionization. When hydronium ion H_3O^+, the most commonly used precursor reagent, collides with formaldehyde, the ion−molecule reaction proceeds very rapidly ($k = 3 \times 10^{-9}$ cm^3 s^{-1})[19,20] to produce exclusively protonated formaldehyde. The proton-transfer reaction is exothermic by 5.2 kcal/mol[21] and has been comprehensively explored by Hansel et al.[22] Many organic compounds can be similarly detected as corresponding protonated ions since most organics including carbonyls have greater proton affinities than water. Spanel et al. coupled the selected ion flow tube (SIFT) technique with the CIMS detection to measure formaldehyde in the headspace of urine samples from prostate and bladder cancer patients.[7] The reported detection sensitivity of 10 ppb in the gas phase can be converted to ~20 μM in urine by using the Henry's law constant.[23] We recently used a similar SIFT-CIMS approach to measure formaldehyde in the headspace of aqueous lysates of breast cancer cells, both sensitive and resistant, which had been cultured and treated with the anthracycline antitumor drugs, doxorubicin and daunorubicin.[8] The instrument stability and extremely low noise signal at the m/z of CH_2OH^+ allowed the limit of quantitation to be as low as 5 μM in the lysate solution.

These in vitro measurements of formaldehyde have contributed to understanding of anthracycline antitumor drug mechanisms and tumor cell resistance mechanisms. While formaldehyde levels for untreated cells were at background within the detection limits, elevation of formaldehyde was observed for drug-treated sensitive cells but not for resistant cells.[8] The elevation of formaldehyde in sensitive cells is consistent with a mechanism of drug cytotoxicity that involves induction of oxidative stress culminating in the production of formaldehyde among other products; the drug-sensitive cancer cells are known to have lower levels of enzymes that neutralize oxidative stress.[24] The formaldehyde that is produced then binds the drug molecule to the cell DNA, most likely leading to strand breaks in conjunction with topoisomerase II.[25] An alternative explanation for the observed lower levels of formaldehyde in drug-treated resistant cells is the overexpression of an active drug efflux pump, the multidrug resistance protein P-170 glycoprotein.[24,26] We now hypothesize that formaldehyde levels in untreated cancer cells can be a prognostic indicator of response to anthracycline antitumor drugs. Higher levels may indicate a fertile environment for drug-induced formaldehyde production. However, despite the highly sensitive detection with the SIFT-CIMS, natural levels of formaldehyde in cancer cells were too low to be determined in vitro.[8]

The above hypothesis can be examined by using techniques with significantly improved detection sensitivities. In the present paper, we describe a highly sensitive method, i.e., preconcentration-SIFT-CIMS, by which formaldehyde in liquid samples is distilled and collected before CIMS analysis. This method removes limitations inherent in the headspace sampling mode of formaldehyde detection (as discussed below) and proves to be one of the most sensitive methods for directly measuring formaldehyde levels in biological samples. We apply this technique to the determination of natural formaldehyde levels in several types of human cancer cells with varied drug resistance, and we explore the correlation between anthracycline toxicity and natural formaldehyde levels.

EXPERIMENTAL SECTION

Materials. MCF-7 human breast adenocarcinoma cells and HeLa S3 human cervical adenocarcinoma cells were obtained from

(12) Yu, J.; Jeffries, H. E.; Le Lacheur, R. M. *Environ. Sci. Technol.* **1995**, *29*, 1923−1932.
(13) Glaze, W. H.; Koga, M.; Cancilla, D. *Environ. Sci. Technol.* **1989**, *23*, 838−847.
(14) Bao, M.-l.; Pantani, F.; Griffini, O.; Burrini, D.; Santianni, D.; Barbieri, K. *J. Chromatogr., A* **1998**, *809*, 75−87.
(15) Yazdanpanah, M.; Luo, X.; Lau, R.; Greenberg, M.; Fisher, L. J.; Lehotay, D. C. *Free Radical Biol. Med.* **1997**, *23*, 870−878.
(16) Breckenridge, S. M.; Yin, X.; Rosenfeld, J. M.; Yu, Y. H. *J. Chromatogr., B* **1997**, *694*, 289−296.
(17) Lindinger, W.; Hansel, A.; Jordan, A. *Int. J. Mass Spectrom. Ion Processes* **1998**, *173*, 191−241.
(18) Smith, D.; Spanel, P. *Int. Rev. Phys. Chem.* **1996**, *15*, 231−271.
(19) Adams, N. G.; Smith, D.; Grief, D. *Int. J. Mass Spectrom. Ion Phys.* **1978**, *26*, 405−415.
(20) Mackay, G. I.; Tanner, S. D.; Hopkinson, A. C.; Bohme, D. K. *Can. J. Chem.* **1979**, *57*, 1518−1523.
(21) (a) Lias, S. G.; Bartmess, J. E.; Liebman, J. F.; Holmes, J. L.; Levin, R. D.; Mallard, W. G. *J. Phys. Chem. Ref. Data* **1988**, *17* (Suppl. 1). (b) *NIST Negative Ion Energetics Database* (Version 3.01); NIST Standard Reference Database 19B, 1993. (c) *NIST Chemistry WebBook*, NIST Standard Reference Database Number 69, November 1998 release.
(22) Hansel, A.; Singer, W.; Wisthaler, A.; Schwarzmann, M.; Lindinger, W. *Int. J. Mass Spectrom. Ion Processes* **1997**, *167/168*, 697−703.
(23) *CRC Handbook of Chemistry and Physics*, 75 ed.; Lide, D. R., Ed.; CRC Press: Boca Raton, FL, 1994.
(24) Sinha, B. K.; Mimnaugh, E. G. *Free Radical Biol. Med.* **1990**, *8*, 567−581.
(25) Taatjes, D. J.; Fenick, D. J.; Gaudiano, G.; Koch, T. H. *Curr. Pharm. Des.* **1998**, *4*, 203−218.
(26) Gottesmann, M. M.; Pastam, I. *Annu. Rev. Biochem.* **1993**, *62*, 385−427.

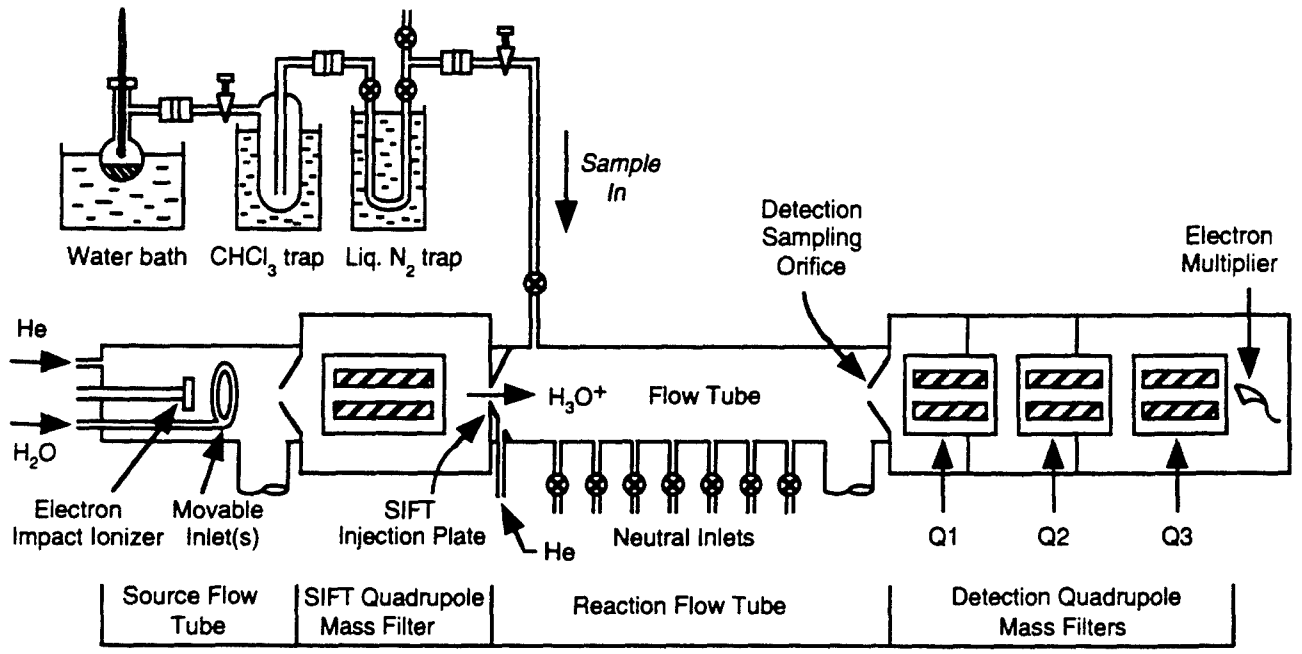

Figure 1. Preconcentration-SIFT-CIMS apparatus.

American Type Culture Collection (Rockville, Maryland). MCF-7/Adr, an Adriamycin-resistant subline, were provided by Dr. William W. Wells (Michigan State University, East Lansing, MI). K562 human chronic myeloid leukemia cells were provided by Prof. Natalie Ahn (University of Colorado, Boulder, CO). LNCaP human metastatic prostate adenocarcinoma cells and DU-145 human metastatic prostate carcinoma cells were provided by Dr. Andrew Kraft (University of Colorado Health Sciences Center, Denver, CO). All tissue culture materials were obtained from Gibco Life Technologies (Grand Island, NY). Millipore water is defined as distilled water further purified with a Milli-Q UF Plus water purification system to 18.2 MΩ cm resistivity. Complete, Mini protease inhibitor cocktail tablets were obtained from Boehringer Mannheim (Indianapolis, IN).

Cancer Cell Samples. Six human cancer cell lines were maintained in vitro: MCF-7, MCF-7/Adr, K562, HeLa S3, LNCaP, and DU-145. Reagents and procedures in the cell culture and processing have been described previously.[8] Except for K562 leukemia cells, which grow in suspension, cultured adherent cells were dissociated from culture flasks by trypsinization for 5 min at 37 °C. The average diameters of cancer cells after release with trypsin were determined under a microscope to be 23 (±2), 23 (±2), 21 (±2), 18 (±2), 17 (±2), and 14 (±2) μm, respectively. Cells from several flasks were collected, counted, and pelleted by centrifugation at 300*g* for 8 min at 20 °C. The supernatant was removed and cells were subjected to formaldehyde assay; the previous study found higher concentrations of formaldehyde inside the cells compared to the cell culture media. Cells were resuspended in 5 mL of buffered saline and centrifugation was repeated. This cycle of saline wash was conducted twice. The pellet was then resuspended in 2.6 mL of Millipore water, and protease inhibitors in 0.4 mL of Millipore water were added to quench enzymatic reactions following cell lysis. The cells were mechanically lysed at 1200 psi with a French press. The lysed solution was adjusted to pH 2.9–3.0 by adding ~30 μL of hydrochloric acid (1.2 M), and the resultant mixture was allowed to stand at room temperature for 30 min. In contrast to the previous study in which the overall lysate was directly analyzed, the lysed sample was centrifuged at 3000*g* for 8 min at 20 °C to separate out solid residue, and the supernatant solution in 2.5 mL was subjected to preconcentration-SIFT-CIMS for the assay of formaldehyde. The supernatant solution is designated as the "lysate" sample in the present study. For a control, the solid residue comprising macromolecules such as proteins and nucleic acids was resuspended in Millipore water (2.5 mL), adjusted to pH 2.9–3.0, and allowed to stand at room temperature for ~5 h, and formaldehyde was analyzed similarly with preconcentration-SIFT-CIMS.

SIFT-CIMS Apparatus. A schematic diagram of the preconcentration-SIFT-CIMS apparatus is shown in Figure 1. Details of the SIFT-CIMS instrument and operation have been described elsewhere.[8,27] In the source flow tube, electron impact on helium (0.25 Torr) generated He^+ and metastable He*, which then reacted with water vapor added downstream in a series of reactions to form primarily H_3O^+ ions. The source ions were extracted into the SIFT quadrupole mass filter to allow mass selection of H_3O^+, which was then injected into the second reaction flow tube containing helium carrier gas (0.5 Torr) at 300 K. The injected ions are quickly thermalized by collisions with helium buffer, and only thermal energy ion–molecule reactions take place in the reaction flow tube region between the injected ions and gaseous analyte from the distillation sampler (Figure 1). Reactant and product ions were extracted through the detection sampling orifice into the detection mass filters consisting of triple quadrupoles (Q1–Q3). In the present study, Q3 was used for mass selection while Q1 and Q2 provided efficient ion transport. Mass-resolved ions were detected with the electron multiplier. Count rates for H_3O^+ ions were typically 75 000 counts/s. The ion signal at m/z 31 (CH_2OH^+) indicated the presence of formaldehyde.

Measurement Procedure. A cell sample solution (2.5 mL) was contained in a vacuum-tight flask (~40 mL) immersed in a

(27) Van Doren, J. M.; Barlow, S. E.; DePuy, C. H.; Bierbaum, V. M. *Int. J. Mass Spectrom. Ion Processes* **1987**, *81*, 85–100.

water bath at 50 °C and slowly distilled under vacuum to dryness over ~20 min while being vigorously agitated with magnetic stirring (Figure 1). Water vapor was condensed in a trap cooled to −63.6 °C with a chloroform slush bath while formaldehyde was condensed in a small U-trap (Pyrex, ~7 cm^3 in volume) cooled to −196 °C with liquid nitrogen. The stainless steel transfer line and valves between the flask and chloroform-cooled trap were kept at 60 °C to prevent condensation. The U-trap was warmed to room temperature, the inlet valve on the trap was opened, and formaldehyde was directly introduced into the reaction flow tube for SIFT-CIMS analysis. The formaldehyde signal was monitored with a dwell time of 1 s/channel while the detection quadrupole (Q3) was tuned to m/z 31 (CH_2OH^+). Before each measurement, the transfer line after the U-trap valve was passivated with water vapor to reduce the formaldehyde contaminant from the inlet surfaces[8] while being evacuated to the low-pressure flow tube. This procedure was employed to minimize the background signal of formaldehyde. Cell samples (lysate or solid residue) were measured between "reference" samples, i.e., fresh solutions of Millipore water plus protease inhibitors in 2.5 mL (pH 3.0, HCl), and elevation (or depletion) of formaldehyde was measured with respect to the reference. At least three reference samples were measured in a 1-day experiment. The calibration curve was constructed using freshly prepared dilute solutions of formalin (2.5 mL) of up to 130 μM. Complete measurements for all cell lines (some were repeatedly cultured and measured) required a few months, with the experiment cycle primarily determined by the cell culture step. Formaldehyde signals from each measurement were normalized to both the parent ion intensity for H_3O^+ and relative instrument sensitivity for CH_2OH^+, both of which were regularly monitored. For calibrating the relative sensitivity for formaldehyde, a 40-mL flask containing a fresh dilute solution of formalin (5 mL, 1300 μM) was directly attached to the flow tube inlet, in place of the distillation sampler, and the formaldehyde signal was measured via headspace sampling[8] in comparison with the parent H_3O^+ intensity.

RESULTS AND DISCUSSION

1. Limitations in Formaldehyde Detection with Headspace Sampling. Water vapor is inherently introduced into the flow tube by headspace sampling of aqueous solutions. This significantly reduces the detection sensitivity of formaldehyde. Protonated formaldehyde CH_2OH^+ readily binds with water, and this cluster $CH_2OH^+ \cdot H_2O$ reacts with a second water molecule to form formaldehyde and $H_3O^+ \cdot H_2O$.[22] Although a drift field can be employed to dissociate the $CH_2OH^+ \cdot H_2O$ cluster, back proton transfer from CH_2OH^+ to water becomes significant in a drift field in the presence of excess water vapor.[22] Therefore, the overall detection sensitivity for formaldehyde cannot be dramatically enhanced.

In an alternative approach, we used a cold trap (−63.6 °C) or a phosphorus pentoxide cartridge to selectively remove water vapor; passing the headspace gas through the trap or over the P_2O_5 bed was found to increase the detection sensitivity of formaldehyde by 1 order of magnitude (~0.5 μM). However, the resulting sensitivity enhancement was still insufficient for measuring natural formaldehyde levels in cell lysates. Formaldehyde is highly soluble in water and its extraction into the gas phase is the limiting step in headspace sampling, as reflected in the poor

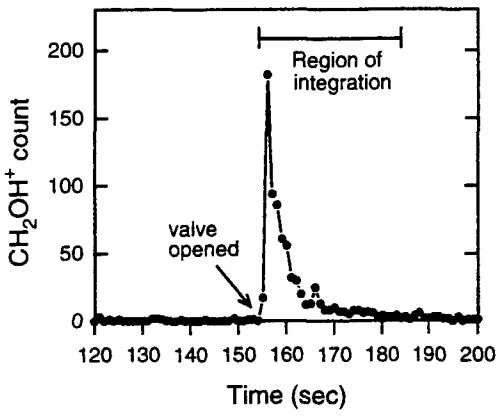

Figure 2. Formaldehyde signal (CH_2OH^+ ion count at m/z 31) obtained from preconcentration-SIFT-CIMS of a K562 leukemia cell lysate. Dwell time, 1 s; region of integration, 30 s.

Henry's law constant.[23] Rates for the extraction of formaldehyde into the gas phase become slower for more dilute samples; for very low levels of formaldehyde, the instrument noise becomes comparable to the ion signals.

2. Formaldehyde Detection with Preconcentration-SIFT-CIMS. Figure 2 shows an example of formaldehyde signal (CH_2OH^+ at m/z 31), obtained from distillation of a K562 leukemia cell lysate. The transfer line after the U-trap valve (Figure 1) was opened to the flow tube for a few minutes before sample introduction, during which time the background signal at m/z 31 was found to be very small (<1 count/s on average). When the U-trap valve was opened, ion counts due to formaldehyde increased immediately and then returned to the original level in a matter of seconds. The total formaldehyde counts were obtained by integrating the signal over the peak area with a region of interest of 30 s. The entire procedure is fairly simple and rapid; distillation takes ~20 min followed by the SIFT-CIMS measurement in 3 min as demonstrated above.

The calibration curve obtained from distillation of dilute formalin solutions was found to be linear over the concentration range studied (R^2 = 0.994 up to 130 μM). Total formaldehyde counts from cell lysate, solid residue, or reference samples are converted to aqueous formaldehyde concentrations by using the calibration curve. No difference was observed between the formaldehyde signals from Millipore water, Millipore water at pH 3.0 (HCl), and the reference sample, i.e., Millipore water plus protease inhibitors at pH 3.0 (HCl). This ensures that contamination or interference by hydrochloric acid or protease inhibitors is negligible. Formaldehyde detected from the reference samples ranged from 0.17 to 0.43 μM (250−650 counts of protonated formaldehyde). These values are compared to those determined in Millipore water using the PFBHA derivatization method (0.03−0.17 μM).[13]

The method detection limit (MDL), a performance criterion for chemical analysis, was estimated by the procedure described by Glaser et al.[28] Seven replicate reference samples of Millipore water plus protease inhibitors (pH 3.0, 2.5 mL), which are naturally loaded with trace formaldehyde (~0.4 μM), were analyzed by preconcentration-SIFT-CIMS. The MDL was calculated from

(28) Glaser, J. A.; Foerst, D. L.; McKee, G. D.; Quave, S. A.; Budde, W. L. *Environ. Sci. Technol.* **1981**, *15*, 1426−1435.

$3.143\sigma_{n-1}$ at the 99% confidence level to be 0.08 μM (~130 counts of protonated formaldehyde). This is a more conservative limit for the quantitation of formaldehyde than the limit of 0.007 μM (~10 counts of protonated formaldehyde), which is estimated from the background signal at m/z 31 (Figure 2). The limit of quantitation for the distillation sampling method exceeds that for headspace sampling (~5 μM) by nearly 2 orders of magnitude. The enhanced sensitivity benefits from both excellent separation of formaldehyde from water (vapor pressures of formaldehyde and water are 68 and 5.3 × 10^{-3} Torr, respectively, at −63 °C)[23] and formaldehyde being collected and measured in batch for a large signal, in contrast to the continuous headspace sampling.[8] In addition, the distillation method is direct and water is the only source of contamination. The MDL would be further improved by reducing formaldehyde in Millipore water. Preconcentration-SIFT-CIMS is one of the most sensitive methods for the quantitation of formaldehyde in biological tissues, as demonstrated below by the measurements of natural formaldehyde levels in cultured cancer cells.

3. Levels of Natural Formaldehyde inside Cancer Cells. Experimental results from several laboratories suggest that the toxicity of the clinically important anthracycline antitumor drugs, doxorubicin and daunorubicin, results in part from the ability of these drugs to induce production of formaldehyde, which is then used to covalently bind the drug to DNA.[25,29-33] Resistance to the anthracyclines can result from overexpression of enzymes that neutralize oxidative stress and overexpression of the drug efflux pump.[24,26] Natural levels of formaldehyde were measured here to determine whether the natural level is a prognosticator of tumor cell susceptibility to the anthracyclines. We reasoned that if natural levels were high, the cells may have lower levels of antioxidants and/or enzymes that neutralize oxidative stress.

The natural level of formaldehyde in cancer cells is determined from the elevation of the CH_2OH^+ signal with respect to the reference sample (Millipore water plus protease inhibitors at pH 3.0). Figure 3 shows the results on MCF-7 versus MCF-7/Adr breast cancer cells along with reference samples. An elevation of ~500 counts of CH_2OH^+ relative to reference was observed for MCF-7-sensitive cell lysate, whereas formaldehyde in MCF-7/Adr-resistant cell lysate was essentially at the reference level. The elevation observed for MCF-7 is converted to the formaldehyde concentration in lysate of 0.33 μM, significantly below the sensitivity with the headspace sampling but well within the capability of this method. The formaldehyde concentration inside cells is calculated from the diameter and number of cells as 1.5 μM, more than 2 orders of magnitude smaller than those (0.3−1 mM)[8] following drug treatment with physiological levels of daunorubicin.

Sample solutions were adjusted to pH 3 after cell lysis to reverse Schiff base chemistry to release carbonyls that are bound

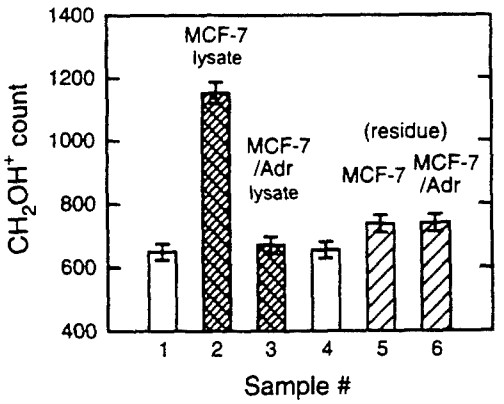

Figure 3. Measurement of natural formaldehyde levels in breast cancer cells without drug treatment. Key: 2, MCF-7 lysate; 3, MCF-7/Adr lysate; 5, MCF-7 residue; 6, MCF-7/Adr residue; 1 and 4, reference samples (Millipore water + protease inhibitors). All samples at pH 2.9−3.0. Error bars represent ion counting statistics (one standard deviation).

to cellular nucleophiles such as proteins, nucleic acids, and cell membrane lipids. Formaldehyde also binds with glutathione to form an adduct, *S*-(hydroxymethyl)glutathione, in aqueous solution.[34,35] The adduct and free formaldehyde (primarily as methylene glycol) are in equilibrium,[34,35] from which formaldehyde is removed upon distillation. The acidic condition also prevents the adduct from slowly rearranging to a variety of more complex structures.[34,35] Recovery of formaldehyde under the acidic condition was also examined by measuring formaldehyde in the solid residues after centrifugation. The MCF-7 and MCF-7/Adr residues, resuspended at pH 3, were allowed to stand at room temperature for an extended period of ~5 h in an attempt to extract remaining formaldehyde (entries 5 and 6, Figure 3). Elevation of CH_2OH^+ signal was insignificant for those samples (<90 counts), considerably less than the elevation observed for the MCF-7 lysate. Similar measurements were conducted for solid residues of LNCaP and DU-145 cells, and the formaldehyde levels were found to be essentially at reference level. These results confirm that natural formaldehyde is recovered in lysate samples under the acidic condition and that chemical reactions of solid residues to produce formaldehyde are negligible.

Results from all cell lines are summarized in Table 1 along with the IC_{50} values for the antitumor drug doxorubicin (DOX). The IC_{50} value is a measure of drug toxicity, representing the concentration of drug that inhibits half the growth of tumor cells. The observation of elevated formaldehyde levels in MCF-7-sensitive cells and not in MCF-7/Adr-resistant cells is consistent with the observed lower levels of enzymes that neutralize oxidative stress in sensitive MCF-7 cells.[24] Sensitive K562 and HeLa S3 cells also displayed substantial elevations of CH_2OH^+ signal (400−500 counts) and have natural formaldehyde levels similar to those of MCF-7 cells. This correlation between drug toxicity and natural formaldehyde levels was not detectable within the sensitivity of the previous headspace sampling method.[8] Formaldehyde levels in the prostate cancer cells, LNCaP (sensitive) and DU-145

(29) Wang, A. H. J.; Gao, Y. G.; Liaw, Y. C.; Li, Y. K. *Biochemistry* **1991**, *30*, 3812−3815.
(30) Cullinane, C.; van Rosmalen, A.; Phillips, D. R. *Biochemistry* **1994**, *33*, 4632−4638.
(31) Taatjes, D. J.; Gaudiano, G.; Resing, K.; Koch, T. H. *J. Med. Chem.* **1997**, *40*, 1276−1286.
(32) Zeman, S. M.; Phillips, D. R.; Crothers, D. M. *Proc. Natl. Acad. Sci. U.S.A.* **1998**, *95*, 11561−11565.
(33) Cullinane, C.; Cutts, S. M.; Panousis, C.; Phillips, D. R. *Nucleic Acids Res.* **2000**, *28*, 1019−1025.
(34) Mason, R. P.; Sanders, J. K. M.; Crawford, A.; Hunter, B. K. *Biochemistry* **1986**, *25*, 4504−4507.
(35) Naylor, S.; Mason, R. P.; Sanders, J. K. M.; Williams, D. H.; Moneti, G. *Biochem. J.* **1988**, *249*, 573−579.

Table 1. Natural Formaldehyde Levels in Lysates of Tumor Cells without Drug Treatment and Calculated Concentrations Inside Cells

entry	cell	no. of cells ($\times 10^6$)	Δ[HCHO][a] (μM)	[HCHO] (μM) inside cells[b]	IC_{50} (nM) DOX (3 h)[c]
1	MCF-7	86	0.33 ± 0.03[d]	1.5 ± 0.4	300[f]
2	MCF-7/Adr	29	0.01 ± 0.02	0.1 ± 0.3	10000[f]
3	K562	89	0.34 ± 0.03	1.9 ± 0.6	–[g]
4	HeLa S3	55	0.27 ± 0.02	4.0 ± 1.4	35[h]
5	LNCaP	78	-0.01 ± 0.01[e]	-0.1 ± 0.2[e]	25[i]
6	DU-145	94	0.06 ± 0.02[e]	1.1 ± 0.6[e]	240[i]

[a] Elevated formaldehyde in lysates relative to the reference sample. [b] Calculated from cell diameters of 23, 23, 21, 18, 17, and 14 μm for entries 1–6, respectively. [c] IC_{50} values for doxorubicin (DOX) representing the concentration of drug that inhibits half the growth of tumor cells with a 3-h drug treatment period. [d] Error bars represent one standard deviation of the ion counting statistics. [e] Weighted average of two experiments (see the text). [f] Reference 36. [g] The IC_{50} values for K562 are 275 [37] and 10 nM[38] for 1- and 72-h treatments, respectively. [h] Reference 39. [i] Reference 40.

(resistant), are inverted relative to DOX cytotoxicity. Resistant DU-145 cells exhibited a small elevation of ~100 counts of CH_2OH^+, whereas sensitive LNCaP cells showed no elevation above reference. A repeated cell culture/CIMS measurement essentially duplicated the subtle difference. Therefore, a weighted average over the two measurements is shown in Table 1. The inverted formaldehyde abundance, however, is consistent with LNCaP cells showing significantly higher catalase, glutathione peroxidase, and glutathione reductase activity than DU-145 cells.[41] These enzymes play central roles in detoxification of hydrogen peroxide, an intracellular precursor to formaldehyde.[24,42] Drug toxicity to the prostate cancer cells appears to be more strongly correlated with the expression of P-170 glycoprotein drug efflux pump; DU-145 cells overexpress the pump and LNCaP cells do not.[43] Drug cytotoxicity is clearly a complex function of multiple factors, and natural levels of formaldehyde may be an indicator of one factor, a favorable environment for doxorubicin induction of oxidative stress.

These experiments are the first demonstration of measuring natural formaldehyde levels in tumor cells in vitro. Previous studies measured formaldehyde levels in various tissues of mice with nerve sheath tumors,[5] expired air from tumor-bearing mice and breast cancer patients,[6] and urine of bladder and prostate cancer patients.[7] Elevation of formaldehyde was not conclusive for breast cancer patients prior to chemotherapy, at least in part because of the limits of quantitation with the derivatization method, although mice with significantly heavier tumor burden showed excess formaldehyde.[6] Urine of cancer patients exhibited elevation of formaldehyde, but prior or current treatment with DOX was not addressed.[7] Our improved method of detection provides direct access to the natural formaldehyde levels in tumor cells.

CONCLUSION

A sensitive technique for the determination of formaldehyde in biological samples is demonstrated. Formaldehyde is distilled and collected from aqueous solutions of cancer cell lysates and directly subjected to analysis with CIMS detection under thermal energy conditions. The sensitivity is calibrated by standard dilute solutions of formalin. Preconcentration by distillation significantly improves the limit of quantitation over headspace sampling, which inherently introduces interfering water vapor. Preconcentration-SIFT-CIMS is one of the most sensitive approaches for formaldehyde detection including the derivatization methods, while being considerably more rapid. Natural formaldehyde levels in human cancer cell lines are measured in vitro. A correlation is observed between the formaldehyde levels and drug cytotoxicity for breast cancer, leukemia, and cervical cancer cells while the toxicity for prostate cancer cells appears to be more complex in origin; however, in all cases, the levels of formaldehyde are consistent with the levels of antioxidants.

ACKNOWLEDGMENT

This work was supported by Grants CA78756 from the National Cancer Institute of the NIH and DAMD 17-98-1-8298 from the U.S. Army Research and Materiel Command. P.J.B. thanks the Colorado Institute for Research in Biotechnology (CIRB) and the U.S. Army Breast Cancer Research Program (DAMD 17-01-1-0213) for predoctoral fellowships. We thank William W. Wells for MCF-7/Adr cells, Natalie Ahn for K562 cells, and Andrew Kraft for LNCaP and DU-145 cells.

Received for review December 19, 2000. Accepted April 16, 2001.

AC001498Q

(36) Fenick, D. J.; Taatjes, D. J.; Koch, T. H. *J. Med. Chem.* **1997**, *40*, 2452–2461.
(37) Palyi, I. *Cancer Treat. Rep.* **1986**, *70*, 279–284.
(38) Marbeuf-Gueye, C.; Ettori, D.; Priebe, W.; Kozlowski, H.; Garnier-Suillerot, A. *Biochim. Biophys. Acta* **1999**, *1450*, 374–384.
(39) Burke, P. J.; Koch, T. H., submitted to *Anticancer Res.*
(40) Taatjes, D. J.; Koch, T. H. *Anticancer Res.* **1999**, *19*, 1201–1208.
(41) Jung, K.; Seidel, B.; Rudolph, B.; Lein, M.; Cronauer, M. V.; Henke, W.; Hampel, G.; Schnorr, D.; Loening, S. A. *Free Radical Biol. Med.* **1997**, *23*, 127–133.
(42) Taatjes, D. J.; Gaudiano, G.; Koch, T. H. *Chem. Res. Toxicol.* **1997**, *10*, 953–961.
(43) Theyer, G.; Schirmböck, M.; Thalhammer, T.; Sherwood, E. R.; Baumgartner, G.; Hamilton, G. *J. Urol.* **1993**, *150*, 1544–1547.

DEPARTMENT OF THE ARMY
US ARMY MEDICAL RESEARCH AND MATERIEL COMMAND
504 SCOTT STREET
FORT DETRICK, MARYLAND 21702-5012

REPLY TO
ATTENTION OF:

MCMR-RMI-S (70-1y) 8 Jan 2003

MEMORANDUM FOR Administrator, Defense Technical Information Center (DTIC-OCA), 8725 John J. Kingman Road, Fort Belvoir, VA 22060-6218

SUBJECT: Request Change in Distribution Statement

1. The U.S. Army Medical Research and Materiel Command has reexamined the need for the limitation assigned to the enclosed. Request the limited distribution statement for the enclosed be changed to "Approved for public release; distribution unlimited." These reports should be released to the National Technical Information Service.

2. Point of contact for this request is Ms. Judy Pawlus at DSN 343-7322 or by e-mail at judy.pawlus@det.amedd.army.mil.

FOR THE COMMANDER:

PHYLLIS M. RINEHART
Deputy Chief of Staff for
Information Management

Encl

ADB265840

ADB266633

ADB282069

ADB279138	ADB251763	ADB265386
ADB264578	ADB281601	ADB282057
ADB281679	ADB258874	ADB258251
ADB281645	ADB281773	ADB264541
ADB261128	ADB281660	ADB241630
ADB261339	ADB259064	ADB281924
ADB273096	ADB266141	ADB281663
ADB281681	ADB281664	ADB281659
ADB259637	ADB258830	
ADB256645	ADB266029	
ADB262441	ADB281668	
ADB281674	ADB259834	
ADB281771	ADB266075	
ADB281612	ADB281661	